UNIVERSIDAD NACIONAL DE COLOMBIA

PARAMETRIC ANALYSIS IN DEEP URBAN EXCAVATIONS USING FULLY COUPLED FLOW-DEFORMATION ANALYSIS

Camilo Antonio Ballesteros Luna

Universidad Nacional de Colombia

Facultad de Minas, Departamento de Ingeniería Civil

Medellin, Colombia

2019

PARAMETRIC ANALYSIS IN DEEP URBAN EXCAVATIONS USING FULLY COUPLED FLOW-DEFORMATION ANALYSIS

Camilo Antonio Ballesteros Luna

Research thesis presented as partial requirement to obtain the title of:

Magister en Ingeniería Geotécnica

Director:

David G. Zapata-Medina, Ph.D.

Codirector:

Luis G. Arboleda-Monsalve, Ph.D.

Research line:

Urban excavations

Universidad Nacional de Colombia

Facultad de Minas, Departamento de Ingeniería Civil

Medellín, Colombia

2019

A mi amada Madre, Lilia Luna Remolina a quien le debo todo lo que soy.

Acknowledgments

First I would like to thank my family, specially my beloved mom, Lilia Luna, without her unconditional love and support this achievement would have not been possible, my dad, Rodolfo, my mom Teresa, my aunt Mercedes, and all and each one of the Lunas, all of them have been the most important support through these years of preparation and one of the reasons that keeps me going every day during these time away from home.

I would like to express my deepest gratitude to my Professor, David Zapata, for his support, mentoring, patience and guidance through this Masters, without his advice this would be an impossible task, thanks for believing in me. Also I would like to specially thank Professor Luis Arboleda, for his priceless orientation and providing the necessary resources that make possible this research.

I also want to thank my friends and classmates that always supported and helped me countless times, and made me feel like home, Alejandro, John, Diego, Eliana, Luis, Maria, Cristina, Jaime, Carellys, Andres, Alejandra, Leon, the list is very large and it continues, I will always be grateful for your company, I admire and value all of you. Also my colleagues in Construsuelos, closest friends, and all the people I have in my heart back at home, thanks for your support and patience, Laura V, John, Laura, Jas, Fabio, Paola, Miguel and to all of those who accompanied me from the distance during this process.

Abstract

Currently, the implementation of advanced methods for the analysis of deep urban excavations such as the Fully coupled flow-deformation analysis that enables to simultaneously calculate stress, deformations and pore water pressures in a time dependent process and can take into account partially drained conditions are easily available in several programs for numerical simulation, however, there is not a clear definition about the necessary conditions for its correct implementation. This research work present a method to define the drainage condition that most likely will take place during an excavation process. Guidelines to define the applicability of fully drained and undrained cases are presented. Special focus is given to define the cases were the implementation of fully coupled flow-deformation analyses is essential for an accurate modeling of excavation in soft to medium fully saturated clays. This research work is believed to be the first attempt to employed advanced finite element modeling of a generalized excavation where soil consolidation and non-linear soil behavior were simulated via fully couple flow-deformations analyses along with the advanced hypoplasticity clay model that accounts for stress history and small strain behavior. The proposed design charts are based on a parametric study conducted to evaluate the effects on excess pore pressures and ground surface settlements of variations in excavation rates, hydraulic conductivity of the soil, excavation geometry and support system stiffness. The proposed method is validated against field performance data (i.e. ground surface settlements and excess pore water pressures) collected from 11 different excavation case histories around the world.

Keywords: Excavations, Fully coupled flow-deformation analysis, excess pore water pressures, alpha parameter, hydraulic conductivity, excavation rate, excavation geometry, partially drained conditions, deformations, numerical modeling.

Resumen

Actualmente, la implementación de métodos avanzados para el análisis de excavaciones urbanas, como el análisis completamente acoplado de flujo-deformación que permite calcular simultáneamente los esfuerzos, las deformaciones y las presiones de poros durante procesos tiempo-dependiente y además puede tener en cuenta las condiciones parcialmente drenadas, se encuentran fácilmente disponibles en varios programas de simulación numérica, sin embargo no existe una definición clara sobre las condiciones necesarias para su correcta implementación. Este trabajo de investigación presenta un método para definir las condiciones de drenaje que probablemente tendrán lugar durante un proceso de excavación. Se establecen pautas para definir la aplicabilidad de los casos totalmente drenado y no drenado. Se prestó especial atención a definir los casos en los que la implementación del análisis completamente acoplado de flujo-deformación es esencial para un modelado preciso de excavaciones en arcillas completamente saturadas. Se cree que este trabajo de investigación es el primer intento de emplear un proceso de modelamiento avanzado mediante el método de elementos finitos de una excavación generalizada en la que se modelo la consolidación del suelo y el comportamiento no lineal de este, mediante análisis acoplado de flujo-deformación junto con el modelo constitutivo avanzado de hipoplasticidad para arcillas que captura la historia de esfuerzos y el comportamiento a pequeñas deformaciones del suelo. Las gráficas de diseño propuestos se basaron en un estudio paramétrico realizado para evaluar los efectos sobre la presión de poros en exceso y los asentamientos del suelo variando las tasas de excavación, la conductividad hidráulica del suelo, la geometría de la excavación y la rigidez del sistema de soporte. El método propuesto se validó con los datos de mediciones de datos en campo (asentamientos y presiones de poros) recopilados de 11 casos diferentes de excavaciones urbanas profundas en todo el mundo

Palabras Clave: excavación, análisis completamente acoplado de flujo-deformación, presiones de poros en exceso, conductividad hidráulica, tasa de avance de excavación, geometría de la excavación, condiciones parcialmente drenadas, deformaciones, modelación numérica.

Table of Contents

Pág.

Table of Contents ..... **VII**
List of figures ..... **IX**
List of tables ..... **XIII**
1. INTRODUCTION **15**
1.1 Statement of the Problem 15
1.2 Relevance of Research 17
1.3 Objectives of the Research 18
1.4 Content of Thesis 19
2. TECHNICAL BACKGROUND **20**
2.1 Fully coupled flow-deformation analysis 20
2.1.1 Generalities 20
2.1.2 Biot´s theory of consolidation in Plaxis 23
2.1.3 Plaxis finite element discretization of Biot´s theory 27
2.1.4 Elastoplastic consolidation 29
2.2 Constitutive Models and Material Behavior 29
2.2.1 Hypoplasticity Model 29
2.3 Fully coupled flow-deformation analysis in Excavation cases histories 34
3. FULLY COUPLED ANALYSIS FOR A GENERALIZED EXCAVATION **41**
3.1 Finite Element Base Model 41
3.2 Typical results of the base model 48
4. PARAMETRIC STUDY **54**
4.1 Influence of hydraulic conductivity, excavation rate and excavation width 56
4.2 Excess pore water pressure ratio (alpha) 66
4.3 Influence of wall stiffness 71
4.4 Data synthesis and proposed method 72
5. VALIDATION WITH EXCAVATION CASE HISTORIES **76**

6. CONCLUSIONS AND RECOMMENDATIONS 82
6.1 Summary 82
6.2 Conclusions 82
6.3 Recommendations 84
APPENDIX A 85
A.1 Allston Science Complex, Boston (Rouainia et al., 2017) – Case 1 85
A.2 Enterprise Center Project, Taipei (Liao and Ou, 1997) – Case 2 87
A.3 Sun Yat-Sen Memorial Hall Station, Taipei (Hsiung, 2002) – Case 3 89
A.4 Post Office Square Garage, Boston (Whittle et al., 1993) – Case 4 91
A.5 Lion Yard Development, Cambridge (Ng, 1992) – Case 5 93
A.6 New England Medical Center Subway Station, Boston (Jaworsky, 1973) – Case 6 95
A.7 Yishan Road Station, Shanghai (Liu et al., 2005) – Case 7 97
A.8 HDR-4 Subway Project, Chicago (Finno et al., 1991) – Case 8 99
A.9 Central Artery Tunnel Project, Boston (Whelan, 1995) – Case 9a and 9b 101
A.10 Geotechnical centrifuge model, Cambridge (Lam et al., 2014) – Case 10 104
A.11 Geotechnical centrifuge model, Tokyo (Takemura et al., 1999) – Case 11 106
APPENDIX B 109
B.1 Homoscedasticity and test for normality 111
B.2 Confidence interval 112
7. -REFERENCES 115

List of figures

Pág.

Figure 2-1. a) Relation between consolidation and FCFDA b). Relation between semi-Coupled and FCFDA (Bae et al. 2016). 22
Figure 2-2. Definition of parameters: N, λ*, κ*, taken from (Mašín 2005) 30
Figure 2-3. Parameters for basic model: (a) position of isotropic normal compression line (N); (b) slope of isotropic normal compression line (λ*); (c) ratio isotropic loading and unloading line (λ*/κ*); (d) friction angle at constant volume (*φ*'). 32
Figure 2-4. Calibration of constitutive parameters for HC model with intergranular strains: (a) size of the elastic range, R, (b) degradation rate parameter, β, (c) degradation rate parameter, χ, (d) parameters for different soils (Mašín 2015). 34
Figure 2-5. Time dependent deformation of an excavation in Singapore (Yong et al. 1989) 36
Figure 2-6. Variation of excess pore pressure and excavation rate for different hydraulic conductivities (after Nogueira, et al. 2009) 37
Figure 2-7. Coupled consolidation results: a). comparison of predictions with measured pore water pressures; b). comparison predictions with ground movements measurements (after Rouainia, et al. 2017) 38
Figure 2-8. Vertical soil movements in the center of the excavation site (after Ng, et al. 1992).... 38
Figure 2-9. Pore pressure response around the site at the end of excavation (after Ng, et al. 1992) 39
Figure 2-10. Contours lines of the excess pore pressure ratio α for two different values of the width in undrained conditions (after Callisto, et al. 2014)..... 40
Figure 2-11. Decrease of the average values of the α parameter for increasing time factor *T* (after Callisto, et al. 2014)..... 40
Figure 3-1. a) Plane strain conditions scheme and b) Indication of positive stress components (after Brinkgreve et al. 2011). 41

Figure 3-2. a) Position of points and stress nodes in soil elements b) Position of points and stress nodes in plate elements (after Brinkgreve et al. 2011). 42
Figure 3-3. Plane strain model illustrating soil stratigraphy, internal strutting, water table position and sheet pile wall. 44
Figure 3-4. Finite element mesh used in the numerical model. 44
Figure 3-5. a) Interpolation in groundwater flow at calculation phase 17 and b) Active pore pressure after the interpolation and consolidation phases at calculation phase 17. 47
Figure 3-6. Construction sequence, phases 0-17. 48
Figure 3-7. Computed horizontal displacements contours. 49
Figure 3-8. Lateral wall movements at different phase of the excavation. 50
Figure 3-9. Computed vertical displacements contours. 51
Figure 3-10. Ground surface settlements at different phase of the excavation 52
Figure 3-11. Computed Excess pore water pressure contours. 53
Figure 4-1 Variation of excess pore pressure and excavation rate for different hydraulic conductivities for excavation width of 10.0m 57
Figure 4-2 Variation of excess pore pressure and excavation rate for different hydraulic conductivities for excavation width of 20.0m 58
Figure 4-3 Variation of excess pore pressure and excavation rate for different hydraulic conductivities excavation width of 30.0m 58
Figure 4-4 Surface settlement profile excavation width 10.0 m 61
Figure 4-5 Surface settlement profile excavation width 20.0 m 61
Figure 4-6 Surface settlement profile excavation width 30.0 m 62
Figure 4-7 Comparison between final ground water level fully drained analysis and fully coupled analysis using a ratio ER/k = 10^1 62
Figure 4-8 Lateral wall movements: (s) excavation width 10.0m; (b) excavation width 20.0m; (c) excavation width 30.0m 64
Figure 4-9 Ground surface settlements for an excavation width of 20.0 m: (a) ER/k=10^1; (b) ER/k=10^2; (c) ER/k=10^3; (d) ER/k=10^4 65
Figure 4-10 Normalized maximum lateral deformation vs Normalized maximum vertical surface 66
Figure 4-11 Zones of excess pore water pressure used in the alpha values computed for all the numerical models. 67
Figure 4-12 values of α versus the ratio b/h: (a) fully undrained; (b) ER/k=10^5; (c) ER/k=10^4; (d) ER/k=10^3 68

Figure 4-13 values of α versus the ratio b/h: (a) ER/k=600; (b); ER/k=200 (c) ER/k=100; (d) ER/k=60 69
Figure 4-14 values of α versus the ratio b/h: (a) ER/k=30; (b); ER/k=20 (c) ER/k=15; (d) ER/k=10 70
Figure 4-15 Normalized maximum vertical surface settlement vs alpha (α) parameter: (a) normal scale; (b); logarithmic scale 72
Figure 4-16 Flow chart for prediction excess pore water pressures at bottom of the excavation, behind the retaining wall, maximum surface ground settlements and selection for correct drainage analysis 74
Figure 5-1 Performance of the proposed method for the Excess pore water pressures prediction, and bounds of 95% prediction interval. 78
Figure 5-2 Performance of the proposed method for the maximum ground surface settlements prediction a). All case histories. b). Similar conditions cases histories 81
Figure A-1 Characteristics of the excavation support system, soil profile and excavation stages for the Allston Science Complex (Rouainia et al., 2017) 86
Figure A-2 Characteristics of the excavation support system, soil profile, monitoring system and excavation stages for the National Enterprise Center Project (Liao and Ou, 1997). 88
Figure A-3 Characteristics of the excavation support system, monitoring system and excavation stages for the Sun Yat-Sen Memorial Hall Station (Chin et al., 1994) 90
Figure A-4 Characteristics of the excavation support system, excavation stages and the stratified soil profile for the Post Office Square (Whittle et al., 1993) 92
Figure A-5 Characteristics of the excavation support system, excavation levels and the stratified soil profile for the Lion Yard Project (Ng, 1992) 94
Figure A-6 Characteristics of the excavation support system, excavation levels and the stratified soil profile for the New England Medical Center Subway Station (Jaworsky, 1973) 96
Figure A-7 Characteristics of the excavation support system, excavation levels and the stratified soil profile for the Yishan Road Station, Shanghai (Liu et al., 2005) 98
Figure A-8 Characteristics of the excavation support system, excavation levels and the stratified soil profile for the HDR-4 Subway Station, Chicago (Finno et al., 1989) 100
Figure A-9 Characteristics of the excavation support system, excavation levels and the stratified soil profile for the Central Artery Tunnel Project North Side, Boston (Whelan, 1995) 102
Figure A-10 Characteristics of the excavation support system, excavation levels and the stratified soil profile for the HDR-4 Subway Station, Chicago (Finno et al., 1989) 103

Figure A-11 Characteristics of the excavation support system, excavation levels and the stratified soil profile for the centrifuge model, Cambridge (Lam et al., 2014) 105
Figure A-12 Characteristics of the excavation support system, excavation levels and the stratified soil profile for the centrifuge model, Tokyo (Takemura et al., 1999)..... 107
Figure B-1 Linear fit between the observed and predicted Excess pore water pressures..... 110
Figure B-2 Standardized Residuals according to the adjusted values, $y = x$..... 111
Figure B-3 Normal probability graph and Shapiro-Wilk test results 112
Figure B-4 prediction confidence bands of 95% level of confidence 113

List of tables

Pág.

Table 2-1. Basic and advanced Hypoplasticity parameters. 31
Table 3-1. Soil parameters used for base model 45
Table 3-2. Structural parameters used for base model 45
Table 3-3. Construction sequence followed in the numerical simulation 46
Table 4-1. Values of hydraulic conductivity and excavation for models 1-25 55
Table 4-2. Additional ratios between excavation rate and hydraulic conductivity analyzed 55
Table 4-3. Wall retaining system parameters for models 100 to 138 56
Table 5-1. Excavation case histories: geometry, soil properties, support system and excavation characteristics 76
Table 5-2. Excavation case histories: estimated parameters for the implementation of the proposed method 77
Table 5-3. Excavation case histories: measured and predicted excess pore water pressures and settlements 77
Table A-1. Resume of input data and results for the proposed method at the ASC case 87
Table A-2. Resume of input data and results for the proposed method at the NECP case 89
Table A-3. Resume of input data and results for the proposed method at the BL-12 case 91
Table A-4. Resume of input data and results for the proposed method at the POS case 93
Table A-5. Resume of input data and results for the proposed method at the LYP case 95
Table A-6. Resume of input data and results for the proposed method at the NEMCS case 97
Table A-7. Resume of input data and results for the proposed method at the YRS case 99
Table A-8. Resume of input data and results for the proposed method at the HDR-4 case 101
Table A-9. Resume of input data and results for the proposed method at the North side of the CATP case 103

Table A-10. Resume of input data and results for the proposed method at the South side of the CATP case..... 104
Table A-11. Resume of input data and results for the proposed method at the South side of the centrifuge model in Cambridge 106
Table A-12. Resume of input data and results for the proposed method at the South side of the centrifuge model in Tokyo. 108
Table B-1. Values for Confidence Interval of 95%..... 112
Table B-2. Uncertainty of the model expressed by the Bias factor "BF"..... 114

1. INTRODUCTION

The exponential growth of the world's population during the past decades, and especially its demographic concentration in urban areas, expect that 70 percent of the world population will be urban by 2050 (United Nations 2007). It is a remarkable and unsettling fact, also most of the big cities have reached or are reaching their geographical limits to expand, whereby the lack of available land is becoming an imperative problem to solve. It is necessary to adopt a model of urban development that allow us to provide an effective solution for the basic demands such us real state and transportation. Construction of vertical and underground infrastructure such us high raise buildings, tunnels and subway stations has increased in urban areas to satisfy these demands. The design and construction of these projects are complex as they involve deep excavations that can induce excessive ground movements and affect adjacent buildings and utility lines. Then, reliable predictions of ground movements play a major role in the design of effective and successful excavation support systems.

The interaction between the excavation support system, specific site and underground conditions, construction sequence and adjacent infrastructure is a highly complex problem. It requires taking into account a large number of geotechnical and geometrical boundary conditions and influential factors that are interdependent at different degrees. Some of them are: type and stiffness of the support system, constitutive soil response, subsurface stratigraphy, sequencing and construction times, workmanship and weather among others. This research focuses on the correct determination of the drainage condition that can cause changes in effective stress and consequently induced larger ground deformations.

1.1 Statement of the Problem

The stress field and drainage boundaries continuously change as the excavation is advanced. One example is the change in the drainage paths due to the installation of the support walls. Under this

condition, ground movements arising from consolidation process take place. Then, accurate predictions of excavation-induced ground movements require to take into account the coupled effects of the excavation activities that generate deformations and the specific sub-surface water conditions. When the construction of an excavation occurs over an extended period of time, soils behave in a fully drained manner (Lambe, 1970). The assumption of undrained conditions and total stress approach in the design of excavations, even in clay materials, demands careful analysis since pore water pressure dissipation is very likely to occur during the construction process. Osaimi and Clough (1979) used a finite element formulation in which deformation and pore water pressure were coupled to show that the perfectly undrained behavior, in which zero percent of consolidation is expected, is very unlikely to exist even for the case of excavations in very thick clay deposits.

The conventional analysis and design of deep excavations are framed under these drainage limits conditions, fully drained or fully undrained. Different authors have studied the transition states between these two conditions. Holt and Griffiths (1992) studied the progression among states of drained and undrained behavior in the analysis of excavations. It was shown that slower excavations rates produced an almost drained behavior even for very low values of soil permeability. Whittle et al (1993) presented the analysis of an excavation in Boston using a coupled flow and finite element formulation for describing partial drainage conditions during construction. The correct drainage conditions during the excavation process is essential for accurate predictions of ground movements. Yong et al. (1989) compare a fully undrained, fully drained and a coupled analysis of a braced excavation in Singapore. They concluded that the undrained analysis underestimated the sheet pile wall movements as opposed to a fully coupled consolidation analysis that accurately estimated the time dependent progressive movement of the sheet pile.

The hydraulic conductivity of the soil is one the most important parameters associated with establishing the drainage conditions under which the excavation is advanced. Chen and Wang (2013) conducted a parametric study to evaluate the influence of the so call soil permeability on the ground settlements. They showed that ground settlements increase with increasing the permeability coefficient. However, the shape of the settlement profile is similar regardless of the soil permeability employed. Other researches have investigated the influence of the hydraulic conductivity in the drainage condition. Nogueira et al. (2009) presented the variation of excess pore water pressure with the rate of excavation and hydraulic conductivity. They concluded that a drained response was obtained only for excavations rates of the same order of magnitude as the hydraulic conductivity of the soil. Contrary, the excavation rate would have to be three orders of magnitude larger than the

hydraulic conductivity to reach an undrained response. For intermediate conditions, partially drained conditions usually prevail in excavation processes and consequently, a fully coupled analysis of deformations and pore pressures is required.

1.2 Relevance of Research

The numerical analysis of deep excavations is a complex structure-soil-fluid interaction problem that demands careful consideration of all variables involved. Among them are correct construction and sequencing stages; advanced constitutive soil models capable of capturing the main features of soil behavior for different stress paths and at different shear strain levels; site specific groundwater; hydraulic conductivity; excavation rate and subsurface conditions. Limited research has been performed in the analysis of deep excavations using advance constitutive soil models and fully coupled finite element formulations to study these effects on the ground movement's predictions. This work proposes a new design methodology in order to overcome the deficiencies of the current methods.

Previous works that have investigated the use of fully coupled flow deformation analyses have not defined clearly and directly the relationship between the implementation of this method and the impact on ground deformations that arise due to the excavation process and their dependency on the drainage conditions under which the analysis is carried out. This research intends to define under which circumstances prevail partially drained conditions, which require the implementation of fully coupled analyses. This work also aims at relating excess pore water pressures to excavation-induced ground deformations as pore pressure measurements are relatively simple and inexpensive procedures during construction.

It is well known that in the construction industry there are few projects in which economic efforts are made in order to install a sufficient geotechnical monitoring system (i.e. control settlement points, inclinometer and vibrating wire piezometers). It allows us to know in real time the behavior of the most important variables that control the design and the performance of an excavation process (i.e. generation and dissipation of pore water pressures, horizontal and vertical ground deformations). This research proposes a new methodology based on a parametric analysis through an extensive program of numerical simulations made in the software Plaxis 2D that includes the influences of the geometry of the excavation, stiffness of support system, and basic properties of the underground soil

and rate of excavation to predict excavation-induced excess pore water pressures and ground deformations.

Excavation performance analyses and geotechnical modeling by means of finite element including a fully coupled flow deformation formulation are a very scarce. For future excavation projects with similar conditions that not include a complete geotechnical monitoring system, this research will allow to obtain an idea of the magnitude of the excess pore water pressure and the maximum ground deformations that may arise due to the excavation process. It will also allowed to understand under which circumstances prevail partially drained conditions and the correct implementation of a fully coupled flow deformation analysis.

1.3 Objectives of the Research

The main objective of this research is to define under which conditions the fully coupled flow deformation analysis is required for a correct numerical simulation of a deep excavation in saturated soil and develop a methodology that allows the designer to estimate the magnitude of excess pore water pressures and ground deformations.

The specific objectives of this work include:

- Create a base numerical model of a deep urban excavation under plane strain conditions in the software Plaxis 2D including the fully coupled flow deformation analysis and soil non-linearity.
- Understand under which circumstances the implementation of the fully coupled flow deformation analysis is required and partially drained conditions prevail.
- Developed a method for the prediction of the magnitude of the developed excess pore water pressures and the maximum ground deformations that arise due to the soil unloading process.
- Developing design flow charts that will guide the engineer thorough the entire process of the prediction method.
- Developed a data base of cases histories that document the field performance (i.e. pore water pressures and ground surface settlements) of a variety of specific site conditions.
- Conduct a validation process of the method proposed using the developed data base of different cases histories.

1.4 Content of Thesis

Chapter 2 of this document presents technical background related to the fully coupled flow deformation analysis and the constitutive soil model. Initially, the fully coupled flow-deformation analysis definition, the difference with a consolidation analysis and fundamental concepts are presented (i.e. Biot's theory and basics equation for the coupled analysis implementation). Then, the theoretical principles and controlling parameters of the constitutive models used in this research to represent the non-linear behavior of the soil. Finally, a complete review of the technical literature for the implementation of the fully coupled analysis in the specific case for deep urban excavations is included.

Chapter 3 presents, in a detailed manner, the numerical base model, the assumed geotechnical characteristics, construction sequence and typical results

Chapter 4 presents the results of the parametric study completed to isolate the effects of the geometry of the excavation (i.e. depth and width), the hydraulic conductivity of the underground soil, the rate of the excavation process and the stiffness of the excavation support system. Also, the parametric analysis implemented for the construction of the new methodology is described.

Chapter 5 validates the proposed prediction method with performance data extracted from different excavation case histories worldwide.

Chapter 6 summarizes this research and presents conclusions and recommendations.

2. TECHNICAL BACKGROUND

2.1 Fully coupled flow-deformation analysis

2.1.1 Generalities

In order to analyze in a proper manner the mechanical behavior of saturated soils submitted under time dependent changes of the hydraulic boundary conditions, it is necessary to take into account both phases in the water-soil mixture, this types of scenario leads to a mixed equations of displacements and pore pressures that needs to be solve simultaneously (i.e. fully coupled flow deformation analysis that for simplicity we can called "FCFDA"), meaning a two way coupled analysis between a seepage analysis and stress analysis is reached. For some cases which involve a horizontal phreatic level, the problem can be simplified by breaking down the total pore pressures into a constant component (steady state pore pressures) and a time dependent component (excess pore water pressures) (Galavi, 2010), but in many practical cases the assumption that steady state pore water pressure is maintained is not accomplish and therefore a more general formulation according to Biot's theory of coupled consolidation (Biot, 1956) is required due to enables to simultaneously calculate stress, deformation and pore water pressures that changes with time. Some practical examples where this method is required include the drawdown of the reservoir level behind a dam, embankments dam subjected to tidal waves, partially drained excavations and dewatering of a building site (Brinkgreve et al. 2011). It should be noted that the solution for the case of partially saturated soil is more complex due to the elastoplastic behavior of soil skeleton and suction dependency of the degree of saturation and relative hydraulic conductivity, all coefficients of the global stiffness matrix in the finite element formulation of Biot theory are non-linear, instead the equations from saturated soil where only the elastoplastic stiffness matrix is non-linear, is worth to be noticed that in this research only fully saturated soils where used in all the numerical simulations, the analysis of these effects in partially saturated soils are out of the scope of this work.

It is important to remark the difference of the approach between the consolidation analysis, the semi-coupled analysis and the fully coupled flow – deformation analysis in Plaxis 2D due both methods are fairly similar and one can get easily confused, here we present the major similarities and differences between the methods mention above mainly focus into the PLAXIS 2D finite element implementation.

In the first place one have to understand that in Plaxis total stresses are composed by the effective stresses, σ´, and active pore pressures, $P_{active,}$ and the so called active pore pressures is defined as the pore water pressure, $P_{water,}$ times the effective saturation, $S_{eff.,}$ as follows:

$$\sigma = \sigma' + P_{active} \quad (1)$$

$$P_{active} = S_{eff} P_{water} \quad (2)$$

One can see that when the degree of saturation is set to one (i.e. fully saturated soil) the pore water pressure is exactly the same to the active pore pressure, as mention before in this research, regardless of the Plaxis capability for model partially saturated soil behavior, only fully saturated soil numerical simulations were made. Regarding the pore water pressures, a further division is made between steady state pore pressures, $P_{steady,}$ and the excess pore pressure, $P_{excess.}$

$$P_{water} = P_{steady} + P_{excess} \quad (3)$$

In Plaxis, the steady state pore pressures are not supposed to change during a deformation analysis, are considered input data, and are generated by means of the pore pressure calculation type parameter in the phases window (i.e. phreatic, groundwater flow and pressures from previous phase), an importance difference with the rest of the deformation calculation types, in the fully coupled flow-deformation analysis does not allow for the selection of pore pressure calculation type due in this case the total pore pressures are calculated together with displacements. To enable the above mention distinction between the steady state pressures and the excess pore pressures, the steady state pore pressures are automatically calculated on the basis of a preliminary steady state groundwater flow calculation using the hydraulic boundary conditions at the end of each calculation phase. On the other hand, excess pore water pressures are pore pressures that are generated as a an outcome from stress changes in undrained materials, is worth to be mention that in both, a consolidation analysis

and in the fully coupled flow deformation analysis, excess pore pressures can occur in any material and its depending on the hydraulic conductivity of the material.

The consolidation analysis begins with the assumption that steady state pore water pressure can be maintained, and is usually conducted in order to understand the development and dissipation of excess pore water pressure in a saturated cohesive soil as a function of time, as mention above, this analysis is used to simulate the phenomenon of how excess pore water pressures changes with the variations in load and/or boundary conditions. In contrast, the fully coupled flow deformation analysis doesn't follow the assumption that steady state pore pressure is maintained, and unlike the consolidation analysis it is possible to define the changes is seepage boundary conditions with time, and principally allow us to calculate the simultaneously development of deformations and pore pressures as a result of time-dependent changes of the hydraulic conditions.

The semi-coupled or sequential analysis is the simplest way to consider the pore water pressure distribution by conducting a ground water flow calculation type beforehand, and reflecting it in the stress analysis conducting in the following step, but since deformation due to stress analysis doesn't influence the seepage phenomenon, there is no two-way coupling. **Figure 2-1** shows graphically the differences of approach between the semi-coupled analysis, the consolidation analysis and the fully coupled flow-deformation analysis.

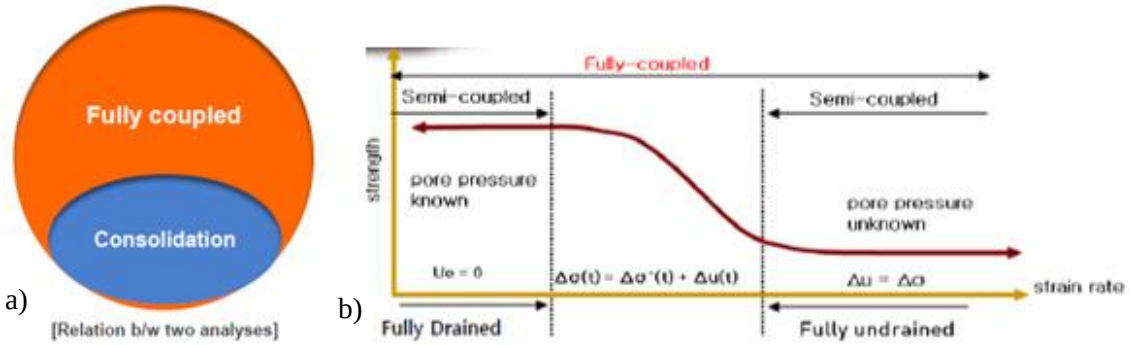

Figure 2-1. a) Relation between consolidation and FCFDA b). Relation between semi-Coupled and FCFDA (Bae et al. 2016).

2.1.2 Biot´s theory of consolidation in Plaxis

Plaxis follow the general theory of three dimensional coupled consolidation first exposed by Biot, (1941) in order to implement the fully coupled flow-deformation analysis, here is presented a general description of Biot´s coupled consolidation theory.

Biot´s assume the following basic properties of the soil for its formulation theory:

- Material isotropy
- Reversibility of stress-strain relations under final equilibrium conditions
- Linearity of stress-strain relationships
- Small strains
- Water incompressibility
- The water flows thorough the soil according Darcy´s law

In resume the combinations of the fluid mass conservation with Darcy´s law for laminar flow (i.e. continuity equation), equilibrium conditions of a stress field (i.e. equilibrium equation) and the momentum of balance equations with Hooke´s law for elastic deformation results in the Biot flow-deformation model of poro-elasticity.

The first approach proposed by Biot consist in excluding the pore pressures (i.e. changes in pore water pressures occur at sufficiently slow rate) and the variation in the water content so the strain in the soil skeleton is only function of the six stress components and by assuming isotropic properties the stress-strain relationships can be reduced to Hook´s law for an elastic body. The equation denote the normal and shear stress respectively as, σi, τi and the normal and shear strain respectively as, εi, γi; so we have:

$$\varepsilon_x = \frac{\sigma_x}{E} - \frac{\upsilon}{E}(\sigma_Y + \sigma_Z)$$
$$\varepsilon_y = \frac{\sigma_y}{E} - \frac{\upsilon}{E}(\sigma_z + \sigma_x)$$
$$\varepsilon_z = \frac{\sigma_z}{E} - \frac{\upsilon}{E}(\sigma_x + \sigma_y) \qquad (4)$$
$$\gamma_x = \frac{\tau_x}{G}$$
$$\gamma_y = \frac{\tau_y}{G}$$
$$\gamma_z = \frac{\tau_z}{G}$$

In previous formulation the constants, E, G and υ are respectively the Young´s modulus, the shear modulus and the Poisson´s ratio for the solid skeleton, due to the relation between this three values there are only two different constants to know at the time.

Now is presented the general poro-elasticity concepts for Biot´s theory, for the case of an isotropic fluid-fill porous medium, this are contain in two linear constitutive equations for the case of an isotropic applied stress field. In addition to the stress field, σ, and the fluid pore pressure, ρ, the other field quantities to have into account are the volumetric strain, ξ, and the increment of fluid content, θ. The constitutive equations simply express the volumetric strain (ξ) and the increment of fluid content (θ) as a linear combination of the stress field and the fluid pore pressure, as follow:

$$\xi = a_{11}\sigma + a_{12}\rho \tag{5}$$

$$\theta = a_{21}\sigma + a_{22}\rho \tag{6}$$

Equation (5) is a statement of observation that changes in applied stress and/or pore pressures produced a fractional volume change. Equation (6) shows that any changes in applied stress and/or pore pressure required fluid to be added to or remove from storage. The generic coefficients denoted as,a_{ij} are the poro-elastic constants defined as ratios of field variables while maintaining various constraints on the elementary control volume. The physical meaning of each coefficient is found by taking the ratio of the change in a dependent variable (ξ, θ) relative to the change in an independent variable (σ, ρ), while holding the remaining independent variable constant, expressed as:

$$a_{11} = {}^{\delta\xi}/_{\delta\sigma}\,|\rho_{=0} = \frac{1}{K} = \beta_b \tag{7}$$

$$a_{12} = {}^{\delta\xi}/_{\delta\rho}\,|\sigma_{=0} = \frac{1}{H} = \beta_P \tag{8}$$

$$a_{22} = {}^{\delta\theta}/_{\delta\rho}\,|\sigma_{=0} = \frac{1}{R} = S_\sigma \tag{9}$$

The coefficient obtained in equation (7) denoted as,β_b, is obtained by measuring the volumetric strain due to changes in the applied stress while holding the pore pressure constant (i.e. drained condition), hence this coefficient is known as drained compressibility and k is the drained bulk modulus. The coefficient obtained in equation (8) denoted as,β_p, it described how much the bulk volume changes due to a pore pressure change while holding the applied stress constant, and is known as the poro-elastic expansion coefficient. The coefficient obtained in equation (9) denoted as,S_σ, it described the variation in water content for a given change in water pressure and is known

as the unconstrained specific storage coefficient. This three coefficients completely characterizes the poroelastic response for an isotropic applied stress.

Other important constants have been derived from these, for instance Biot introduce the constrained specific storage coefficient noted as, S_ε, is a measured of the amount of water which can be forced into the soil under pressure while the volume of the soil is kept constant, and is defined as follow:

$$S_\varepsilon = \frac{1}{Q} = \frac{1}{R} - \frac{\alpha}{H} \tag{10}$$

The ratio of the pore compressibility to the bulk compressibility, is known as the Biot´s coefficient and represents the ratio of the water volume squeeze out to the volume change of the soil if the latter is compressed while allowing the water to scape (i.e. water pore pressure ρ=0). One can notice that values for constants α and Q will be significantly important in partially saturated soils, due to its values will be depending on the degree of saturation of the soil.

Now Biot incorporated the effect of the pore water pressure (ρ) in equation (4), and introduce the dependence effect of the increment of water content (θ) on these same variables. Now because isotropy of the material was assumed the water pressure cannot produce any shearing strain and its effect is the same on all three components of the strain ($\varepsilon_x, \varepsilon_y, \varepsilon_z$). Now as mentioned before introducing the effects of ρ and θ in equation (4) and expressing the stresses as functions of the strain and the water pressure (ρ), we find:

$$\begin{aligned}
\sigma_x &= 2G\left(\varepsilon_x + \frac{\upsilon\xi}{1-2\upsilon}\right) - \alpha\rho \\
\sigma_y &= 2G\left(\varepsilon_y + \frac{\upsilon\xi}{1-2\upsilon}\right) - \alpha\rho \\
\sigma_z &= 2G\left(\varepsilon_z + \frac{\upsilon\xi}{1-2\upsilon}\right) - \alpha\rho \\
\tau_x &= G\gamma_x \\
\tau_y &= G\gamma_y \\
\tau_z &= G\gamma_z
\end{aligned} \tag{11}$$

The physical constants considered above refer to the properties of the soil for the state of equilibrium when the water pressure is uniform throughout. Now due to the intention is to study the transient

state we must add to the four distinct constants above (E, υ, α, Q) the so-called hydraulic conductivity of the soil (k)

Biot now present the differential equations for the transient phenomenon of consolidation, and applying the equilibrium conditions into equation (11) we obtain:

$$\begin{aligned} &G\nabla^2 u + \frac{G}{1-2v}\frac{\delta\xi}{\delta x} - \alpha\frac{\delta\rho}{\delta x} = 0 \\ &G\nabla^2 v + \frac{G}{1-2v}\frac{\delta\xi}{\delta y} - \alpha\frac{\delta\rho}{\delta y} = 0 \\ &G\nabla^2 w + \frac{G}{1-2v}\frac{\delta\xi}{\delta z} - \alpha\frac{\delta\rho}{\delta z} = 0 \end{aligned} \quad (12)$$

Due to there are four unknowns and only three equations, to complete the system Biot introduced the Darcy´s law equation for water flow in a porous medium. According to Darcy´s law the rate of water flow through a soil mass is proportional to the hydraulic head gradient, and using the continuity equation that states that the water outflow from a volume is equal to the changes in the mass concentration, and assuming the water to be incompressible, the rate of water content of an element of soil must be equal to the volume of water entering per second through the surface of the element, so we find:

$$V_x = -k\,\frac{\delta V_x}{\delta x};\; V_y = -k\,\frac{\delta V_y}{\delta y};\; V_z = -k\,\frac{\delta V_z}{\delta z} \quad (13)$$

$$\frac{\delta\theta}{\delta t} = -\frac{\delta V_x}{\delta x} - \frac{\delta V_y}{\delta y} - \frac{\delta V_z}{\delta z} \quad (14)$$

And combining equations (4) (13) and (14) we have

$$K\nabla^2\rho = \alpha\frac{\delta\xi}{\delta t} + \frac{1}{Q}\frac{\delta\rho}{\delta t} \quad (15)$$

Now the four differential equations (12) and (15) are the basics equations satisfied by the four unknowns. Under partially saturated circumstances the following is implied

$$Q = \infty\,;\; \alpha = 1 \quad (16)$$

And the general differential equations can be simplified, expressed as:

$$\begin{aligned} &\mathrm{G}\nabla^2 u + \frac{G}{1-2v}\frac{\delta\xi}{\delta x} - \frac{\delta\rho}{\delta x} = 0 \\ &\mathrm{G}\nabla^2 v + \frac{G}{1-2v}\frac{\delta\xi}{\delta y} - \frac{\delta\rho}{\delta y} = 0 \\ &\mathrm{G}\nabla^2 w + \frac{G}{1-2v}\frac{\delta\xi}{\delta z} - \frac{\delta\rho}{\delta z} = 0 \\ &K\nabla^2\rho = \frac{\delta\xi}{\delta t} \end{aligned} \qquad (17)$$

2.1.3 Plaxis finite element discretization of Biot´s theory

In Plaxis, the finite element implementation of the Biot´s theory of consolidation use the following standard notation:

$$\underline{U} = \underline{\underline{N}}\,\underline{v} \qquad \underline{p} = \underline{\underline{N}}\,\underline{p_n} \qquad \underline{\epsilon} = \underline{\underline{B}}\,\underline{v} \qquad (18)$$

Where $\underline{U}$ is the continuous displacement vector within an element, $\underline{v}$ is the nodal displacement vector, $\underline{p}$ is the water pore pressure, $\underline{p_n}$ is the excess pore pressure vector, the matrix $\underline{\underline{N}}$ contains the interpolation functions and $\underline{\underline{B}}$ is the strain interpolation matrix. As one can noticed, in Plaxis the same interpolation functions are used for displacements and pore pressures.

As mention before Biot´s theory use the equilibrium equation and applying the above finite element approximation we obtain:

$$\int \underline{\underline{B^T}}\, d\underline{\sigma}\, dV = \int \underline{\underline{N^T}}\, d\underline{b}\, dV + \int \underline{\underline{N^T}}\, d\underline{t}\, dS + r_0 \qquad (19)$$

Where $\underline{b}$ is a body force due to self-weight, $\underline{t}$ represents the surface tractions, r_0 is the residual vector force that usually is equal to zero, however by adding the residual force vector the computational procedure solve the inaccurate of previous loads steps problem. The term dV indicates integration over the volume body considered and dS indicates the surface integral.

Now, the nodal equilibrium equation is obtained by dividing the total stresses into pore pressures and effective stresses, and is expressed as:

$$\underline{\underline{K}}\,d\underline{v} + \underline{\underline{L}}\,d\underline{p_n} = d\underline{f_n} \tag{20}$$

Where $\underline{\underline{K}}$ is the stiffness matrix, $\underline{\underline{L}}$ is the coupling matrix and $d\underline{f_n}$ is the incremental load vector.

Now to continue the process in the Biot´s theory of consolidation, the continuity equation is adopted in the following form:

$$\frac{\nabla^T \underline{\underline{R}} \nabla(\gamma_w y - p_{steady} - p)}{\gamma_w} - \underline{m}^T \frac{\delta \underline{\varepsilon}}{\delta t} + \frac{n}{k_w}\frac{\delta p}{\delta t} = 0 \tag{21}$$

Where $\underline{\underline{R}}$ is the permeability matrix, n is the porosity, K_w is the bulk modulus of the pore fluid and γ_w is the unit weight of the pore fluid. As one can noticed the pore pressures are considered positive for tension.

The equilibrium and continuity equations can be compressed into a block matrix equation, and using an integration procedure to solve the equation, the integration is expressed as:

$$\begin{bmatrix} \underline{\underline{K}} & \underline{\underline{L}} \\ \underline{\underline{L}}^T & -\underline{\underline{S}}^* \end{bmatrix} \begin{bmatrix} \Delta\underline{V} \\ \Delta\underline{p_n} \end{bmatrix} = \begin{bmatrix} 0 & 0 \\ 0 & \Delta t\underline{\underline{H}} \end{bmatrix} \begin{bmatrix} \underline{V_0} \\ \underline{p_{n0}} \end{bmatrix} + \begin{bmatrix} \Delta\underline{f_n} \\ \Delta t\underline{q_n^*} \end{bmatrix} \tag{22}$$

Where:

$$\underline{\underline{S}}^* = \alpha\Delta t\underline{\underline{H}} + \underline{\underline{S}} \qquad \underline{q_n^*} = \underline{q_{no}} + \alpha\Delta\underline{q_n} \tag{23}$$

The parameters $\underline{V_0}$ and $\underline{p_{n0}}$ denotes values at the beginning of a time step, the parameter α is the time integration coefficient.

As mention before, if the soil under analysis present partially saturated conditions all matrices and the external flux are nonlinear. Regarding the above mention the following topics have to be taken into account (Galavi, 2010):

- The stiffness matrix is usually stress-dependent
- The hydraulic conductivity is pressure dependent, due to dependency of relative permeability

- The coupling matrix as well as the compressibility matrix are suction dependent, the latter also depends on the derivate of saturation.
- Both equilibrium and conservation equations are non-linear terms for partially saturated soils, the first one is due to the weight of the soil which is a function of the degree of saturation and for the second equation this behavior is due to the suction dependency of the relative hydraulic conductivity.

2.1.4 Elastoplastic consolidation

Due to the constitutive material model used in this research (Hypoplasticity model) is capable of capture the nonlinear behavior of the soils, and the stress dependent stiffness behavior of the model, the equilibrium equations are not necessary satisfied using the procedure described in previous sections. Hence, the equilibrium equations is reviewed here, instead of Eq. (20), the equilibrium equation is rewritten in a sub-incremental form, expressed as:

$$\underline{\underline{K}}\,d\underline{v} + \underline{\underline{L}}\,d\underline{p_n} = \underline{r_n} \tag{24}$$

Where $\underline{r_n}$ is the global residual vector, the total displacement increment $\Delta\underline{v}$ is the summation of sub-increments $\delta\underline{v}$ from all iterations in the current step.

$$\underline{r_n} = \int \underline{\underline{N^T}}\,\underline{b}\,dV + \int \underline{\underline{N^T}}\,\underline{t}\,dS - \int \underline{\underline{B^T}}\,\underline{\sigma}\,dV \tag{25}$$

So in the first iteration is considered $\underline{\sigma} = \underline{\sigma_0}$ (i.e. the stress at the beginning of the step). Successive iterations are used on the current stresses that are computed according to the appropriate constitutive model.

2.2 Constitutive Models and Material Behavior

2.2.1 Hypoplasticity Model

Hypoplasticity is an advanced constitutive model captures the nonlinear behavior of fine grained soils at large strains under different stress paths, within the field of critical state soil mechanics. This

model does not consider conventional process of decomposing strains in elastic and plastic groups, so does not work with yield surface and plastic potential definitions.

This model is focused for clays, and was proposed by (Mašín 2005) (Mašín 2014)(Mašín 2015) but in its first versions proposed, it was focused on granular materials (Kolymbas et al. 1996) and (von Wolffersdorff 1996), later extended to fine grain soils also (Niemunis and Krieg 1996)(Niemunis and Herle 1997)(Niemunis 2002)(Niemunis 2003), but there was a lack of accuracy at predicting behavior under anisotropic stress states, and defining shear stiffness at small strains.
A new constitutive parameter that controls the ratio between initial bulk and shear modulus was included by (Herle and Kolymbas 2004) looking for improve last deficiency mentioned. When intergranular strain concept was included, soil behavior subjected to cyclic loads and small strains was better represented. This model was improved by (Mašín 2014) by considering small strain stiffness anisotropy by working with stiffness tensor. Isotropic loading/unloading tests (beyond the preconsolidation pressure) were used for the calibration of the main basic model parameters.

Five main soil parameters are the basis of the basic Hypoplasticity constitutive model: $N, \lambda^*, k^*, \upsilon_{pp}$ and φ'. These parameters are all determined from standard laboratory tests, which represents a great advantage. k^* parameter represents the slope of isotropic unloading line, while slope and position of the isotropic normal compression line are represented by N and λ^*parameters, typically obtained from isotropic compression tests, or even one-dimensional constraint compression test such as oedometer test, could be useful to obtain them.

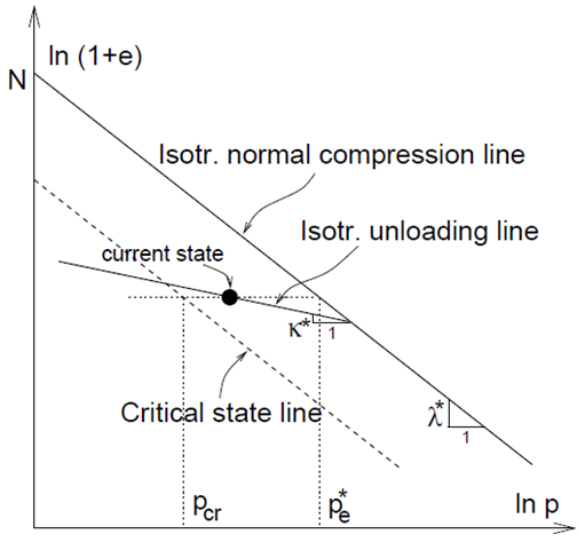

Figure 2-2. Definition of parameters: N, λ*, κ*, taken from (Mašín 2005)

Table 2-1. Basic and advanced Hypoplasticity parameters.

#	Symbol	Parameter name	unit
1	φc	Critical state friction angle	kN/m²
2	Pt	Shift of the mean stress due to cohesion	kN/m²
3	λ	Slope of the isotropic normal compression line	-
4	κ	Slope of isotropic unloading line	-
5	N	Position of the isotropic normal compression line	-
6	νpp	Control of the shear stiffness	-
7	αG	Ratio of horizontal and vertical shear modulus	-
8	Ag	Very small strain shear stiffness parameter	-
9	ηg		-
10	mrat	Intergranular strain concept parameter	-
11	R		-
12	βr	Intergranular strain concept parameters	-
13	χ		-

Relationships for the soft to medium stiff clays is marked for an almost constant variation with water content. For the stiff clays, the variation is almost linear with equations presented in **Figure 2-3**, in which is shown also a summary of N, λ^*, and / $\lambda^*/k^*$for stiff clays layers, obtained from One Museum Park West project (Arboleda-Monsalve 2014). Shear stiffness is related to the bulk-to-shear stiffness ratio r (Sarabia 2012) and it is controlled by parameter v_{pp}, obtained from parametric analysis. This parameter can be evaluated in terms of other basic model parameters calibrated from laboratory tests, as follows:

$$v_{pp} = \frac{3r(\lambda^*+k^*)-4k^*}{6r(\lambda^*+k^*)+4k^*} \quad (26)$$

Parametric analysis allowed this expression are based on stress-strain curves of undrained triaxial extension and compression tests. Considering a constant volume, friction angle φ' become a natural water content (w_n) and overconsolidation ratio (OCR) function, and for Blodgett and Deerfield layers, the K_0- consolidated triaxial compression tests become the basis for obtaining the normalized undrained shear strength against the vertical effective stress ($S_{uTXC}/\sigma_{v0}{}'$), which can be expressed as (Finno and Chung 1993).

$$\frac{S_{uc}}{\sigma_{v0}{}'} = 0.46(0.9 - w_n)OCR^{0.9} \quad (27)$$

The ratio $S_{uTXC}/\sigma_{v0}{}'$ proposed by (Wroth 1984) for isotropic compression triaxial tests was later modified by (Wroth 1984) and was given in terms of OCR and φ', as follows:

$$\frac{S_{uc}}{\sigma_{v0}{}'} = \frac{1}{6}M(1+2K_0)\left(\frac{\alpha_R OCR}{2}\right)^{\Lambda} \quad (28)$$

$$M = \frac{6\sin\varphi'}{3-sin\varphi'} \quad (29)$$

$$\alpha_R = \frac{9(1-K_{0nc})^2+M^2(1+2K_{0nc})^2}{M^2(1+2K_0)(1+2K_{0nc})} \quad (30)$$

$$K_0 = (1-sin\varphi')OCR^{sin\varphi'} \quad (31)$$

Where M is the critical state parameter M and Λ is the plastic volumetric ratio taken as 0.75 for most clays. **Figure 2-3** shows φ' input values for triaxial stress paths, and the relation for the OCR values from 1 to 2, which result in a difference of 2 degrees in φ' for these two states. Above equations are the ones allow to obtain the relationship between critical state frictional angle, natural water content, andOCR.

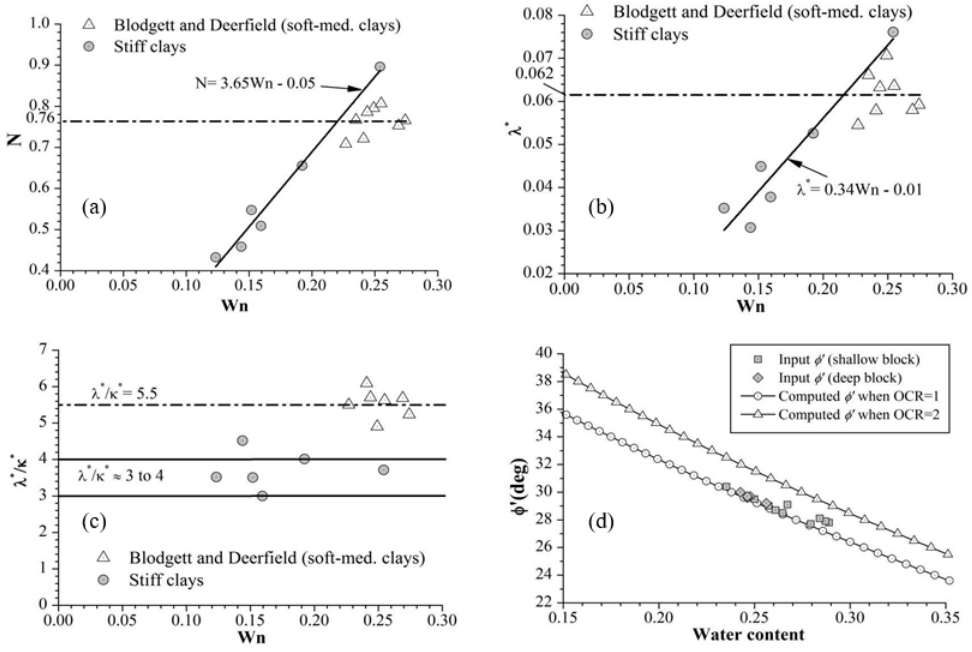

Figure 2-3. Parameters for basic model: (a) position of isotropic normal compression line (N); (b) slope of isotropic normal compression line (λ*); (c) ratio isotropic loading and unloading line (λ*/κ*); (d) friction angle at constant volume (φ').

Before Hypoplasticity constitutive model were enhanced to estimate soil behavior for strain levels lower than 0.1% with including intergranular strain concept, it was only useful for strains levels greater than that magnitude. With the new concept, a new variable which represents the deformation of the interface layers between soil particles was added, this parameter represents intergranular strain and is denoted as δ, which allowed to model stress history of the soil. Overall response comprises both particle rearrangement of soil skeleton and deformation of the intergranular interface layer between grains, when soil is subjected to continuous loads. Seven additional parameters are introduced in the constitutive model, as the intergranular strain concept considers small strain behavior of soil: $\alpha_G, A_G, n_g, m_{rat}, R, \beta_r$ and χ. The ratio of horizontal and vertical shear modulus under cross-anisotropic nature is represented by α_G. For Chicago clays, this parameter varies between 1.1 and 1.2 according to (Kim and Finno 2012). Very small strain shear stiffness (calibrated with bender elements in triaxial tests) are defined by A_G and n_g. Initial shear stiffness and effective mean normal stress are related between them, and that dependency can be expressed as:

$$G_{vh} = p_r A_g \left(\frac{p'}{p_r}\right)^{n_g} \quad (32)$$

G_{vh} is the shear stiffness and p_r is a reference pressure defined as 1 kPa.

Normal effective stress p' and deviatoric stress q are the stress invariants reported. Volumetric strain ε_{vol} and shear strain ε_{sh} represent the strain invariants. For axisymmetric conditions, these parameters can be defined as:

$$p' = (\sigma'_a + 2\sigma'_r)/3 \quad (33)$$

$$q = \sigma'_a - \sigma'_r \quad (34)$$

$$\varepsilon_{vol} = \varepsilon_a + 2\varepsilon_r \quad (35)$$

$$\varepsilon_{sh} = (2/3)\,(\varepsilon_a - \varepsilon_r) \quad (36)$$

Where σ'_a and σ'_r correspond to the axial and radial effective stresses, ε_{vol} and ε_{sh} correspond to the axial and radial strains, respectively. **Figure 2-4** shows enhanced model parameters, considering the addition of intergranular strain tensor. These parameters influence the stiffness degradation of soils, and this influence was analyzed under parametric studies by (Mašín 2015) who defined variation ranges for typical soils.

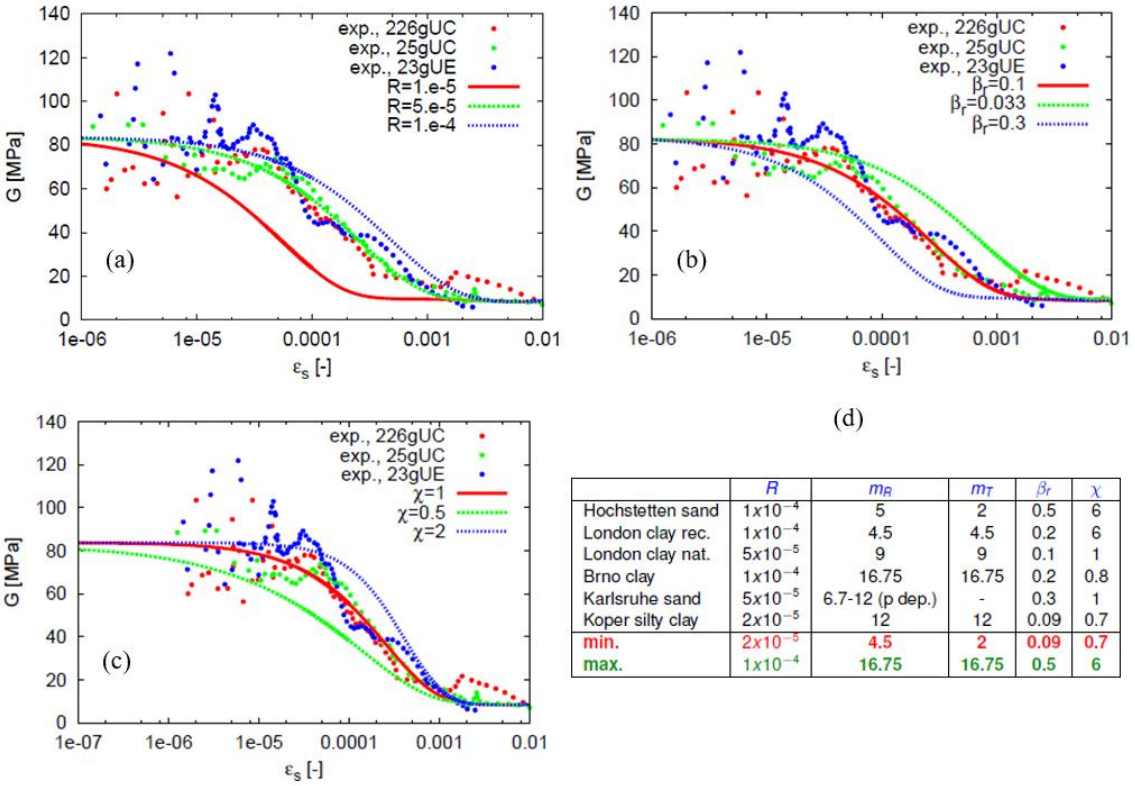

	R	m_R	m_T	β_r	χ
Hochstetten sand	$1x10^{-4}$	5	2	0.5	6
London clay rec.	$1x10^{-4}$	4.5	4.5	0.2	6
London clay nat.	$5x10^{-5}$	9	9	0.1	1
Brno clay	$1x10^{-4}$	16.75	16.75	0.2	0.8
Karlsruhe sand	$5x10^{-5}$	6.7-12 (p dep.)	-	0.3	1
Koper silty clay	$2x10^{-5}$	12	12	0.09	0.7
min.	$2x10^{-5}$	4.5	2	0.09	0.7
max.	$1x10^{-4}$	16.75	16.75	0.5	6

Figure 2-4. Calibration of constitutive parameters for HC model with intergranular strains: (a) size of the elastic range, R, (b) degradation rate parameter, β, (c) degradation rate parameter, χ, (d) parameters for different soils (Mašín 2015).

2.3 Fully coupled flow-deformation analysis in Excavation cases histories

There have been a few studies that had implemented the approach of partially drained analysis by using the coupled method during the study of the behavior of deep urban excavations in order to assess its contribution in respect of the accuracy in the predictions of the ground movements and the developed and dissipation of excess pore water pressures.

Yong et al. (1989) performed a coupled analysis of a braced excavation in Singapore and showed the importance of this type of analysis when estimating ground movements. As shown in **Figure 2-5**, an undrained analysis underestimated the sheet pile movements as opposed to a fully coupled consolidation analysis that accurately estimated the time dependent progressive movements of the sheet pile, providing a much better agreement between measured and computed performance. Other researches have also discussed the importance of analyzing the behavior of deep excavations using

fully coupled flow deformation analysis. Finno et al. (1991) study the behavior of the HDR-4 excavation using a coupled formulation of effective stress with fluid flow equations to track pore pressures generation and dissipations with time.

Holt et al. (1992) studied the transition between states of drained and undrained behavior in the analysis of excavations. It was shown as expected slower excavation rates produced an almost drained behavior even for very low values of soil permeability. For the particular case under study it was observed that the drained and undrained conditions were obtained by changing the hydraulic conductivity of the soil in approximately 3 orders of magnitude maintaining a constant rate of advance during the excavation.

Whittle et al. (1993) presented the analysis of an excavation in Boston using a mixed coupled flow and deformation finite element formulation for describing a partial drainage conditions during constructions, and concluded that interpretations based only on comparisons of lateral displacements are incomplete, lead to errors, and it is necessary to have measurements of vertical and lateral deformation as well as measurements of water pore pressures and the trends of the measured data obtained imply that small deformations is an important aspect of soil behavior and models capable of capturing the soil response at these levels must be adopted. Hsie and Small (1993) presented a method base on Biot´s theory that allow the computation of the displacements and pore pressures simultaneously, they identify the stress relief due to overburden removal and the drawdown of the groundwater surface as the two major factors responsible for ground movements, and conclude that if the drawdown is included in the numerical analysis, the surface settlement is predicted to be larger but the lateral movements of the side of the excavation is smaller than the case where no drawdown takes place, due to larger suctions give rise to smaller lateral defections of the side of the excavation.

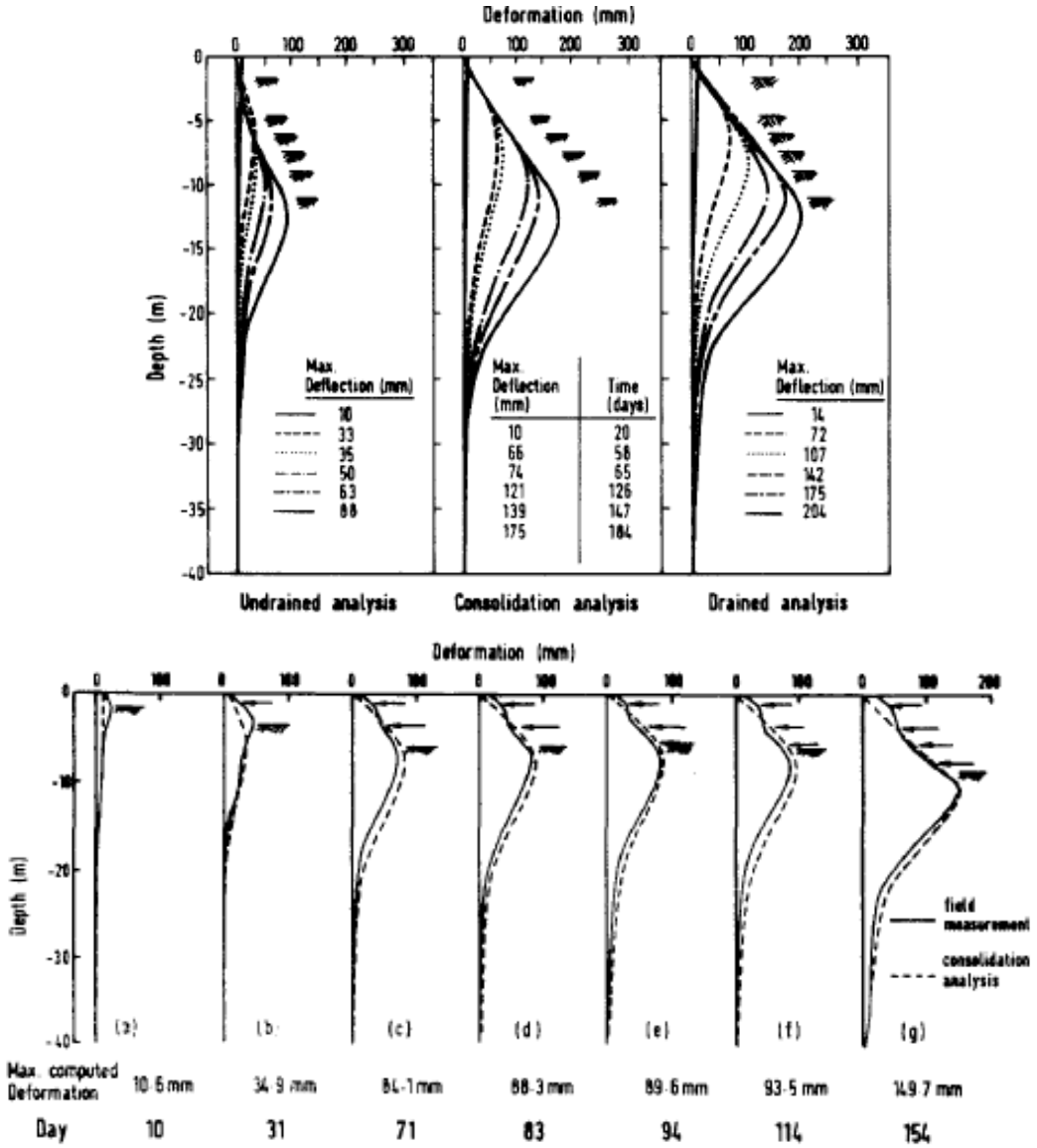

Figure 2-5. Time dependent deformation of an excavation in Singapore (Yong et al. 1989)

Nogueira et al. (2009) studied the variation of excess pore water pressure with the rate of excavation and hydraulic conductivity of the soil using a one-dimensional model with a fully coupled flow formulation, see **Figure 2-6.** They concluded that soil behavior can be characterized by drained conditions only for excavations rates of the same magnitude as the hydraulic conductivity of the soil. Conversely, the excavation rate would have to be three orders of magnitude larger than the hydraulic conductivity to achieve an undrained response. In the other hand Chin et al. (2014) studied the influence of the hydraulic conductivity in the ground settlements by performing a coupled consolidation analysis, and as expected show that the value of the ground settlements increases with

increasing the permeability coefficient, but the shape of the settlement profile are quite similar, but as the coefficient reduced below certain value the settlements not present any change (i.e. reached fully undrained conditions).

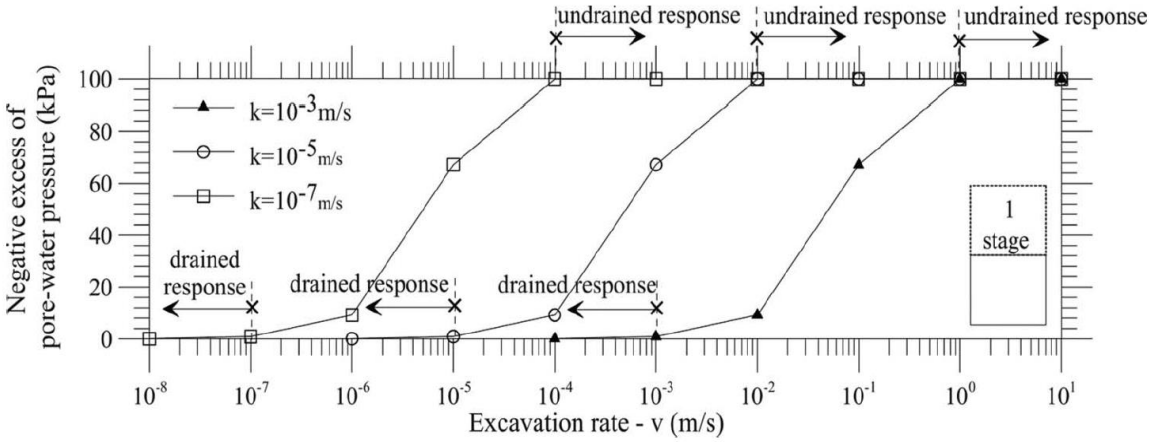

Figure 2-6. Variation of excess pore pressure and excavation rate for different hydraulic conductivities (after Nogueira, et al. 2009)

Rouainia et al. (2017) performed a fully undrained finite element model for the prediction of the behavior of a deep excavation in Boston, generally the numerical simulations provide a close match to field monitoring data for ground movements (i.e. lateral wall displacements and settlements), however the time dependent performance of the excavation was analyzed by performing a coupled consolidation analysis to study the accumulation of negative pore water pressures in the soil below the excavation base, and it concluded that the numerical analysis was very successful in predicting the magnitude and rate of change of pore pressures due to the unloading phase and the associated heave of the excavation base at three different investigated depths **Figure 2-7** According to their research although accurate predictions regarding soil deformations can be obtained from fully undrained analysis, only by performing a fully coupled flow deformation analysis the generation of excess pore water pressure can be correctly estimated. Ng (1992) support the previous statement, he performed a numerical analysis for a top-down excavation in Cambridge and shown a comparison between the observed vertical soil movements and the calculated swelling with depth, see ¡Error! No se encuentra el origen de la referencia.**8** , and concluded that using the undrained assumption inside the site, the analysis substantially under predicted the vertical sub-surface movements beneath the final excavated level unlike performing a coupled analysis that the calculated swelling corresponds accurately with the observed behavior, this is because the soil actually behaved like a partially drained material rather than in a truly drained manner.

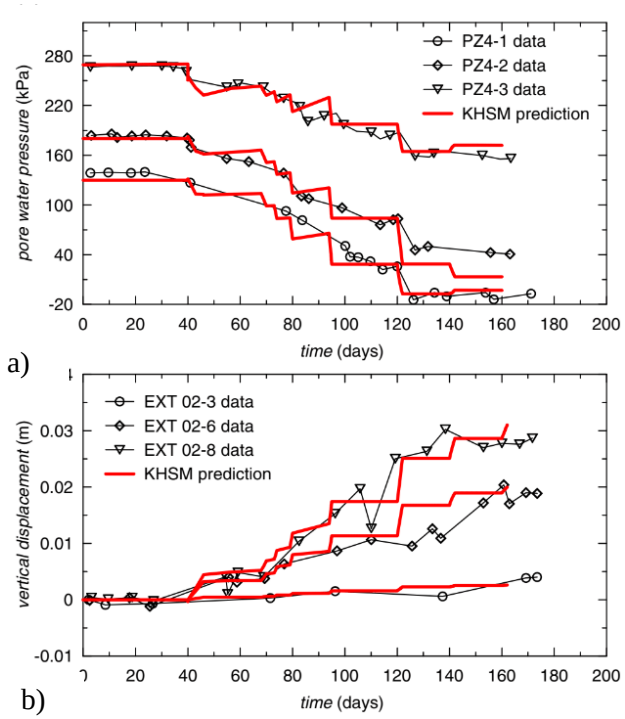

Figure 2-7. Coupled consolidation results: a). comparison of predictions with measured pore water pressures; b). comparison predictions with ground movements measurements (after Rouainia, et al. 2017)

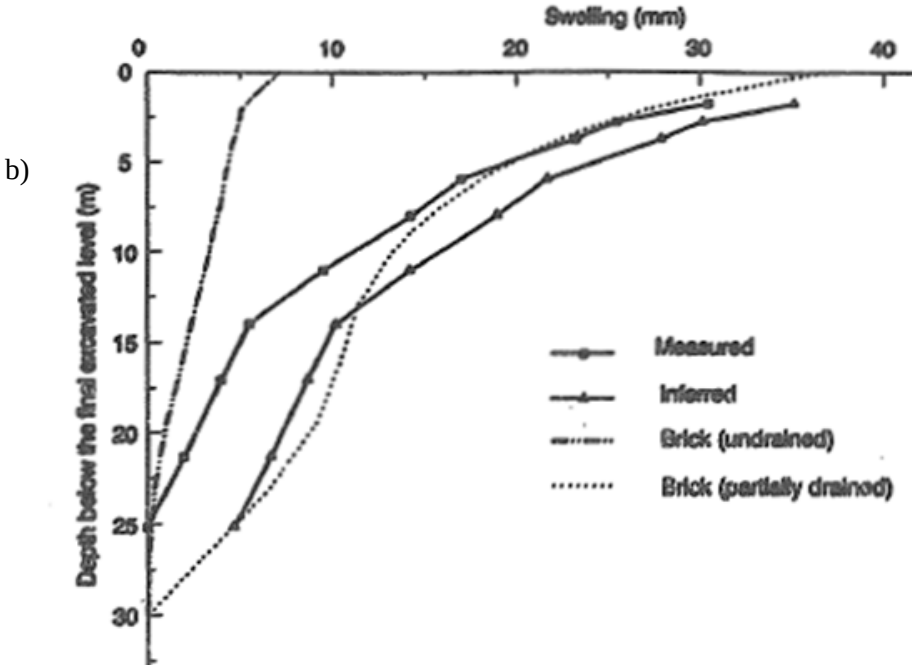

Figure 2-8. Vertical soil movements in the center of the excavation site (after Ng, et al. 1992)

Ng, (1992) introduce the so called excess pore water ratio (i.e. $\bar{B}$ and $\bar{H}$) defined it as the change of pore pressure that occur inside and outside the excavation site (i.e. ΔU_{IN} and ΔU_{OUT} respectively), due to the vertical stress relief inside the site (i.e.$\Delta\sigma_{IN}$) Equation (37) and (38)

$$\bar{B} = \frac{(\Delta U)_{IN}}{(\Delta\sigma_V)_{IN}} \tag{37}$$

$$\bar{H} = \frac{(\Delta U)_{OUT}}{(\Delta\sigma_V)_{IN}} \tag{38}$$

He presented the variation of $\bar{B}$ and $\bar{H}$ across the entire site during the last stage of the excavation **Figure 2-9**, it can be noticed that the response of pore water pressure to the vertical stress relief inside the site was greatest at the center of the excavation site and gradually decreases towards the retaining wall, meanwhile outside the site, in comparison with the results inside the excavation, the effects of the reduction of the stress relief on the pore water pressures were practically negligible.

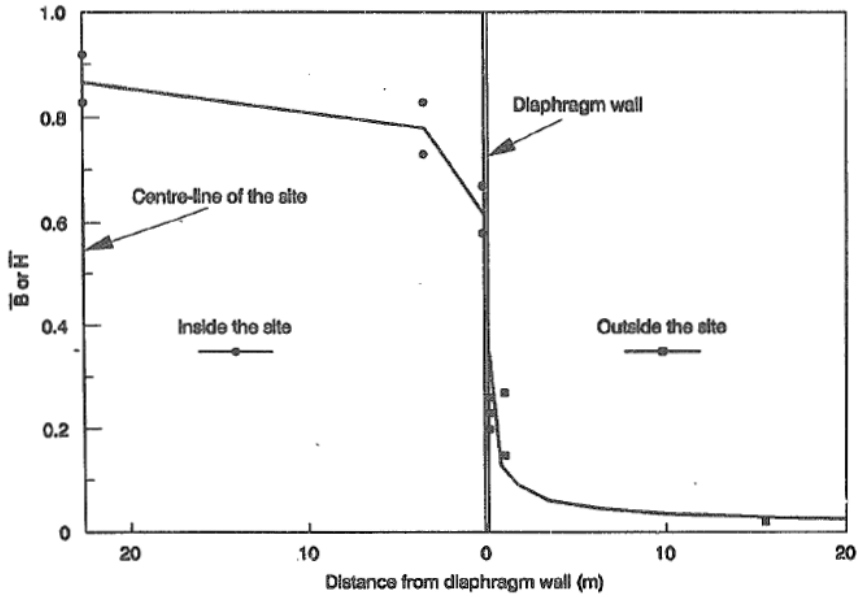

Figure 2-9. Pore pressure response around the site at the end of excavation (after Ng, et al. 1992)

Callisto et al. (2014) rewrite the excess pore water ratio using a new notation called it as the Alpha parameter, they plot the contours lines for the alpha parameter at the final stage of an undrained excavation for two different width **Figure 2-10** and in accordance with Ng (1992) it shows that the Alpha parameter is grater at the middle of the excavation and tends to be constant towards the retaining wall, also the alpha values calculated outside de site of the excavation are at the same range

from previous research. They also performed a coupled consolidation analysis but only starting from the final stage of the excavation to assess the progressive dissipation of the excess pore water pressure, and as expected show the decrease of the average values of Alpha at parameter at both locations, below the excavation and behind the retaining wall, against the time factor T , see **Figure 2-11** showing that for most of the time partially drained conditions prevail and a fully coupled flow deformation analysis must be implemented for accurately predictions.

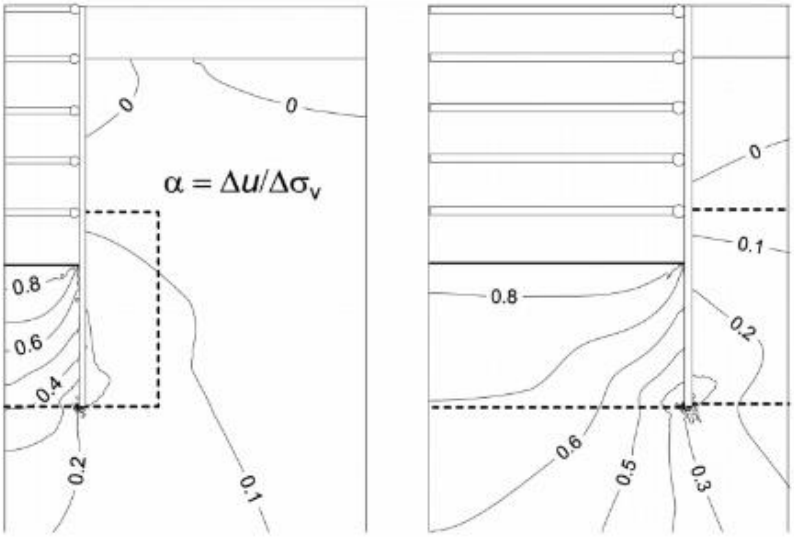

Figure 2-10. Contours lines of the excess pore pressure ratio α for two different values of the width in undrained conditions (after Callisto, et al. 2014)

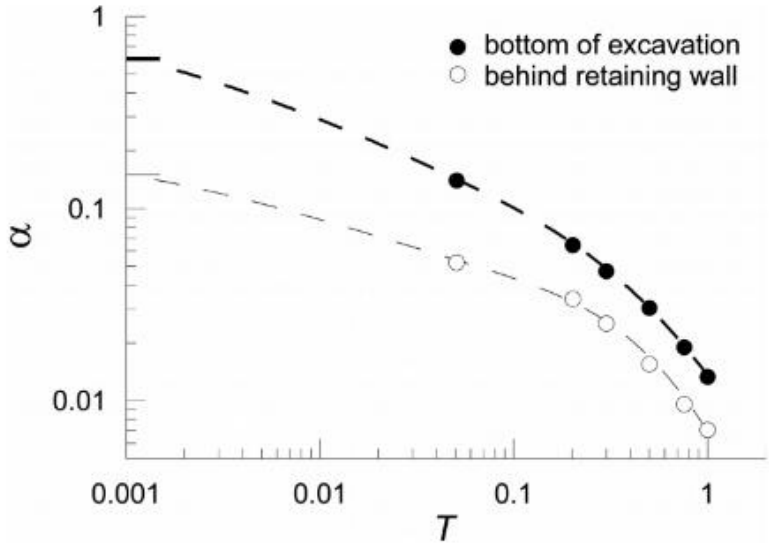

Figure 2-11. Decrease of the average values of the α parameter for increasing time factor T (after Callisto, et al. 2014)

3. FULLY COUPLED ANALYSIS FOR A GENERALIZED EXCAVATION

This chapter presents the details of a finite element base model carried out to define when it is necessary to implement a fully coupled flow-deformation analysis in the simulation of a deep excavation in soft to medium soil. Two-dimensional finite element models under plane strain conditions were implemented in the software Plaxis 2D (2016). The advanced constitutive soil model clay hypoplasticity was used to capture the small-strain response of the soil. In this section features and modeling assumptions made in the finite element model are presented.

3.1 Finite Element Base Model

In this research, a total of 138 models of a hypothetical two-dimensional (2D) fully coupled flow-deformation finite element simulation of a braced excavation were conducted under plane strain conditions using the software package Plaxis 2D (2016). Under plane strain conditions, displacements and strains in the out of plane direction (z-direction) are assume to be zero. However, normal stresses in this direction are fully taken into account (see **Figure 3-1**).

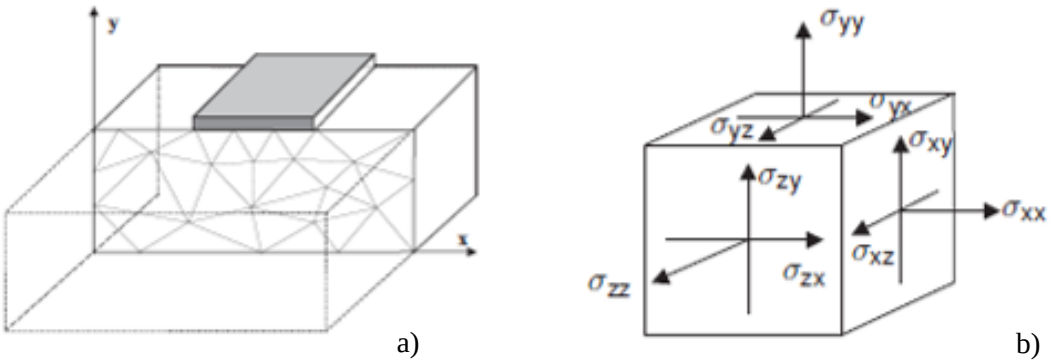

a) b)

Figure 3-1. a) Plane strain conditions scheme and b) Indication of positive stress components (after Brinkgreve et al. 2011).

In Plaxis 2D (2016), simulations, the soil elements were modeled by triangle elements. These elements are composed by 15 nodes and 12 internal stress points. This type of element uses a fourth order interpolation for displacement calculations, a characteristic that gives better precision and yields results of high quality stress in difficult geotechnical problems (Brinkgreve et al. 2011). The retaining wall was assumed ¨wished into place.¨ it mean that no stress changes or displacements in the surrounding soil were generated during wall installation. 5 node plate elements containing four pairs of stress points were used to model the wall. This type of element has three degrees of freedom per node, two translational (Ux, Uy) and one rotational (rotation in the x-y plane: $\emptyset_z$); and allows deflections due to shearing, bending and axial forces. The forces are evaluated from the stresses at the stress points and extrapolated to the element nodes. **Figure 3-2** shows the type of element use to model the soil and wall element indicating the nodes and stress points. Finally the sign convention used by Plaxis software defined all the compressive stresses and forces, including pore pressures, are taking to be negative, whereas tensile stresses and forces are taking to be positive.

The struts elements were modeled with a fixed-end anchor point element that is attached at one side and fixed at the other side. This element can be used to simulate anchors or props to support retaining walls (Brinkgreve et al. 2011). Soil-structure interaction was simulated by the inclusion of 10-node interface elements. These elements consist of five pair of nodes, compatible with the 5 nodal triangle side of a soil element. Interface elements were implemented in order to properly simulate the thin zone of intensely shearing material at the contact between the plate element (retaining wall) and the surrounding soil.

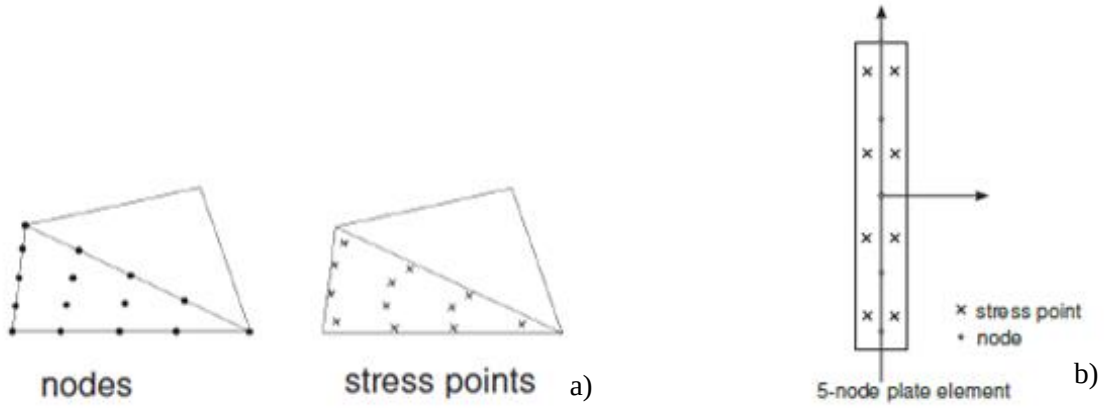

Figure 3-2. a) Position of points and stress nodes in soil elements b) Position of points and stress nodes in plate elements (after Brinkgreve et al. 2011).

Figure 3-3 presents a basic model scheme of the geometry for the braced excavation. The excavation zone was assumed 8-m-high and 20-m-wide. The retaining system was ¨wished into placed¨ at a depth of 12m and is propped by 4 levels of internal strutting. The groundwater table was located 1 m below the ground surface and extend uniformly to the model limits. Only half of the excavation was modeled taking advantage of the line of symmetry improving the calculation times. The boundaries of the finite element model were extended beyond the settlement zone of influenced induced by the excavation (Hsie and Ou, 1998). Boundary conditions were set as follows:

- Boundary X Minimum: Normally fixed and pervious
- Boundary X Maximum: Normally fixed and impervious
- Boundary Y Minimum: Fully fixed and impervious
- Boundary Y Maximum: Free and pervious

The mesh was considered with a higher degree of refining around the excavation zone. The opacity scale in the finite element mesh shown in **Figure 3-4** indicates the quality of the mesh. It increases as the sides of the triangles of 15 nodes become equal. In the numerical model 18026 nodes and 26424 stress points were implemented.

The soil profile in the numerical base model consist of 3 different types of clays increased stiffness with depth (soft, medium and hard clays). Although the specific excavation evaluated in this research is simplified and hypothetical, the employed soils represent Chicago clays whose properties have been extensively reported in the technical literature. The hypoplasticity clay model was used as the constitutive model for all the different soil types. This constitutive soil model is capable to capture the nonlinear behavior of soils at large strains in the framework of critical state soil mechanics as well as the small stress-strain response of the soils and the prediction of undrained stress paths. **Table 3-1** lists the hypoplasticity model parameters used in the analysis for each soil layer. These parameters were reported by (Sarabia, 2012; Arboleda-Monsalve, 2014) and were calibrated based on index properties and results oedometers and triaxial stress probes completed as part of the laboratory testing program of the One Museum Park West Excavation project located in the Chicago area.

The retaining wall system implemented in the base model represented a flexible retaining wall, specifically a sheet pile wall (PZ-27 section). The steel sheet pile geometric properties and the axial and flexural stiffness are listed in Table 2-1 define all the variables listed in Table 3-1

Table 2-1 define all the variables listed in table 3-1

Table 3-2.The retaining wall and all internal braced elements are assumed to behave as a linear elastic material.

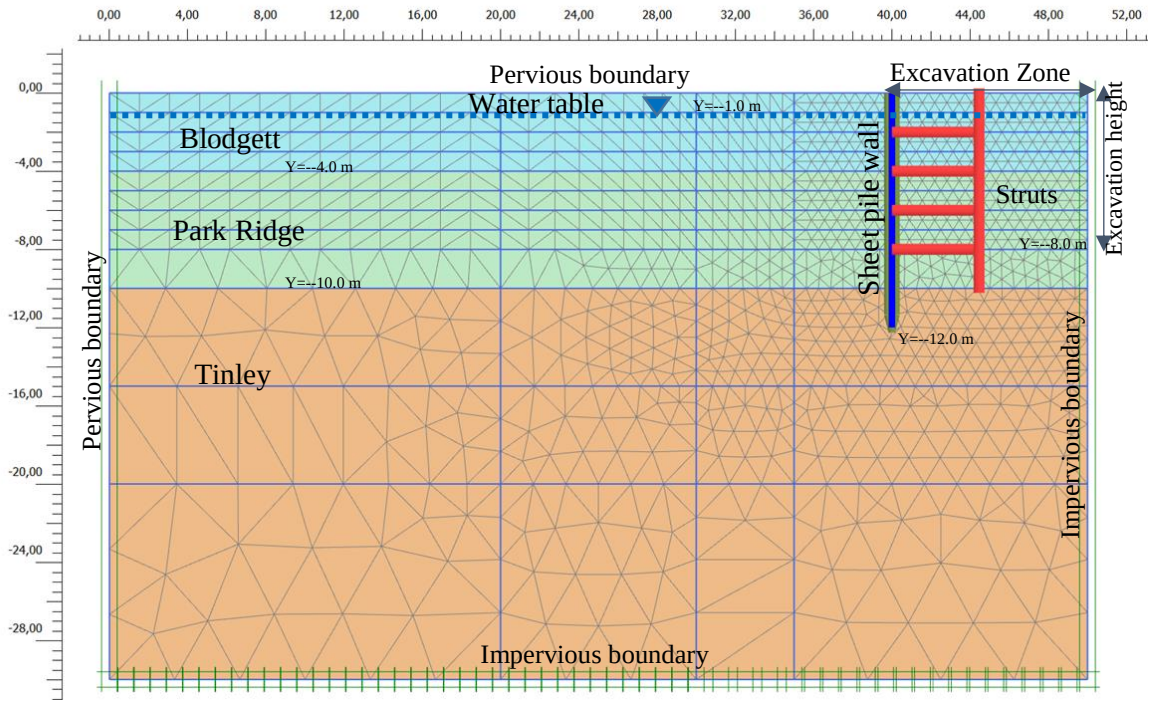

Figure 3-3. Plane strain model illustrating soil stratigraphy, internal strutting, water table position and sheet pile wall.

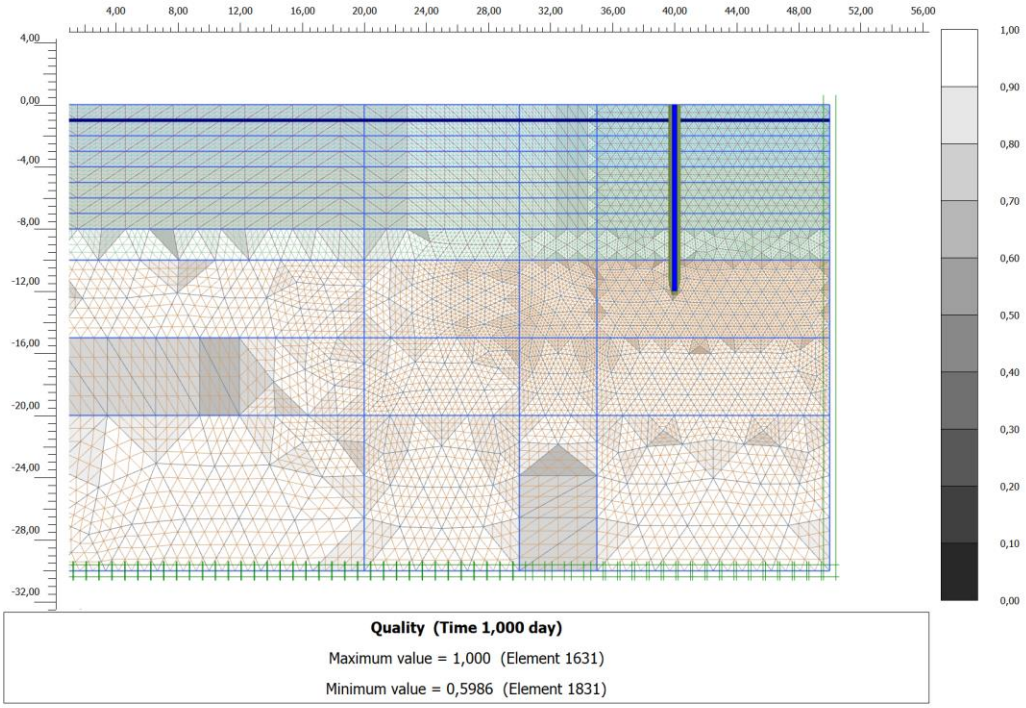

Figure 3-4. Finite element mesh used in the numerical model.

Table 3-1. Soil parameters used for base model

Name	**Blodgett**	**Park Ridge**	**Tinley**	**unit**
Model	Hypoplasticity	Hypoplasticity	Hypoplasticity	
Type	Undrained	Undrained	Undrained	
γ unsat	18.90	18.90	19.60	kN/m³
γ sat	18.90	18.90	19.60	kN/m³
e init	0.86	0.45	0.60	-
φc	24.2	30.3	36.7	kN/m²
Pt	25	25	25	kN/m²
λ	0.08200	0.05900	0.04000	-
κ	0.0230	0.01700	0.01100	-
N	1.0290	0.62000	0.53000	-
r	0.424	0.424	0.424	-
αG	1.10	1.10	1.10	-
Ag	4100	4100	4100	-
ηg	0.60	0.60	0.60	-
mrat	1.000	1.000	1.000	-
R	0.00005	0.00005	0.00005	-

βr	0.18	0.18	0.18	-
χ	1.30	1.30	1.30	-

Table 2-1 define all the variables listed in table 3-1

Table 3-2. Structural parameters used for base model

Name	**Sheet piles**	**Struts**	**unit**
EA1	28900000	$6.77x10^6$	kN/m
EA2	336000	-	kN/m
EI	50400	-	kN.m/m²
deq	0.1447	-	m
$L_{Spacing}$	-	1.0	m

Where EA, is the axial stiffness, EI is the flexural rigidity (beding stiffnes), deq is the equivalent plate thickness and $L_{Spacing}$ is the out plane spacing that help to calculate an equivalent stiffness per unit width. The soil excavation was simulated as dry conditions, meaning the dewatering of the excavation zone is included in the numerical models, i.e. excavation bottom free of water. The main construction activities were simulated by plastic calculations followed by ¨fully coupled flow deformation¨ phases to simulate construction times that allow a time dependent analysis of deformation and total pore water pressure, i.e., the sum of steady-state and excess pore water pressure. In order to address the simulation of the excavation bottom free of water at each plastic and fully coupled excavation phase, using a groundwater flow boundary condition, the hydraulic head at the bottom of the excavation was modified to the corresponding magnitude according to its elevation and the cluster of soil beneath the bottom of excavation were set to interpolate the pore water pressure, meanwhile the soil behind the sheet pile wall were set to calculate the pore pressures based on the phreatic level (See **Figure 3-5**).

The numerical simulation was used to model the excavation activities, installation of the retaining wall, supports and dewatering of the excavation is summarized in **Table 3-3**. The table lists phase number, type of analysis, construction time intervals (i.e. the time interval show in table 3.3. is only for the base model, ER/K ratio equal to $1x10^1$), and excavation elevations. The sequence followed in the numerical analysis for the base model to simulate the excavation process consisted in the generation of the initial state of stresses using the Ko procedure as recommended by Plaxis in cases with a horizontal surface and with all soil layers and phreatic levels parallel to the surface; followed by sheet pile installation, as mentioned before this procedure was considered ¨whish in to place.¨

The excavation process was a simplified sequence consisting in the uniform removal of 1.0 m of soil, until the final excavation level was reached(i.e., 8.0 meters). **Figure 3-6** illustrate the construction sequence followed in the numerical analysis.

Table 3-3. Construction sequence followed in the numerical simulation

	ID		Phase	Initial Elevation [CCD]	Final Elevation [CCD]	ΔH [m]	Calculation type	Time interval [days]
1		Initial phase	0				K0 procedure	0
2		Installation of sheeting	1				Plastic	0
3		L1 Excavation						
	3.1	Excavation-1	2	0.0	-1.0	1.0	Plastic	0
	3.2	FC analysis	3				Fully coupled flow-deformation	10
	3.3	Excavation-2 +Strut 1	4	-1.0	-2.0	1.0	Plastic	0
	3.4	FC analysis	5				Fully coupled flow-deformation	10
4		L2 Excavation						
	4.1	Excavation-3	6	-2.0	-3.0	1.0	Plastic	0
	4.2	FC analysis	7				Fully coupled flow-deformation	10
	4.3	Excavation-4 +Strut 2	8	-3.0	-4.0	1.0	Plastic	0
	4.4	FC analysis	9				Fully coupled flow-deformation	10
5		L3 Excavation						
	4.1	Excavation-5	10	-4.0	-5.0	1.0	Plastic	0
	4.2	FC analysis	11				Fully coupled flow-deformation	10
	4.3	Excavation-6 +Strut 3	12	-5.0	-6.0	1.0	Plastic	0
	4.4	FC analysis	13				Fully coupled flow-deformation	10
6		L4 Excavation						
	4.1	Excavation-7	14	-6.0	-7.0	1.0	Plastic	0
	4.2	FC analysis	15				Fully coupled flow-deformation	10
	4.3	Excavation-8 +Strut 4	16	-7.0	-6.0	1.0	Plastic	0
	4.4	FC analysis	17				Fully coupled flow-deformation	10

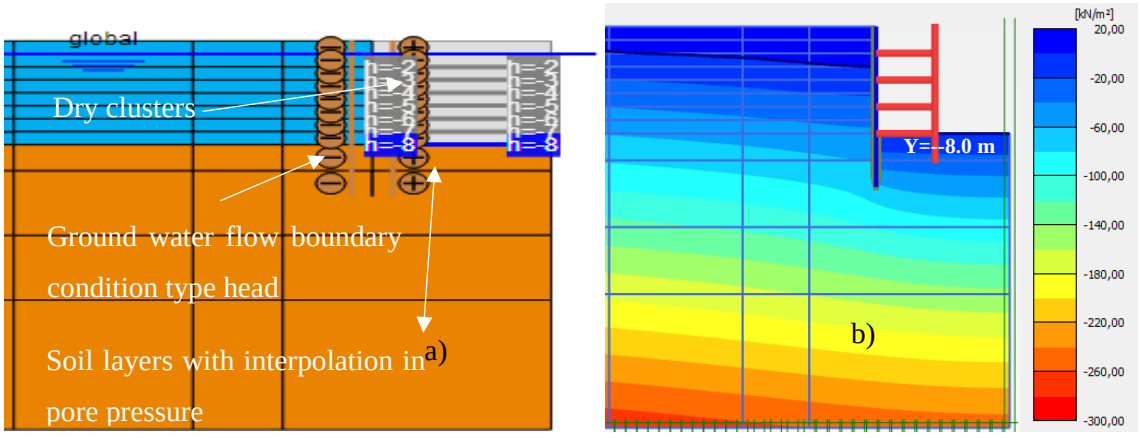

Figure 3-5. a) Interpolation in groundwater flow at calculation phase 17 and b) Active pore pressure after the interpolation and consolidation phases at calculation phase 17.

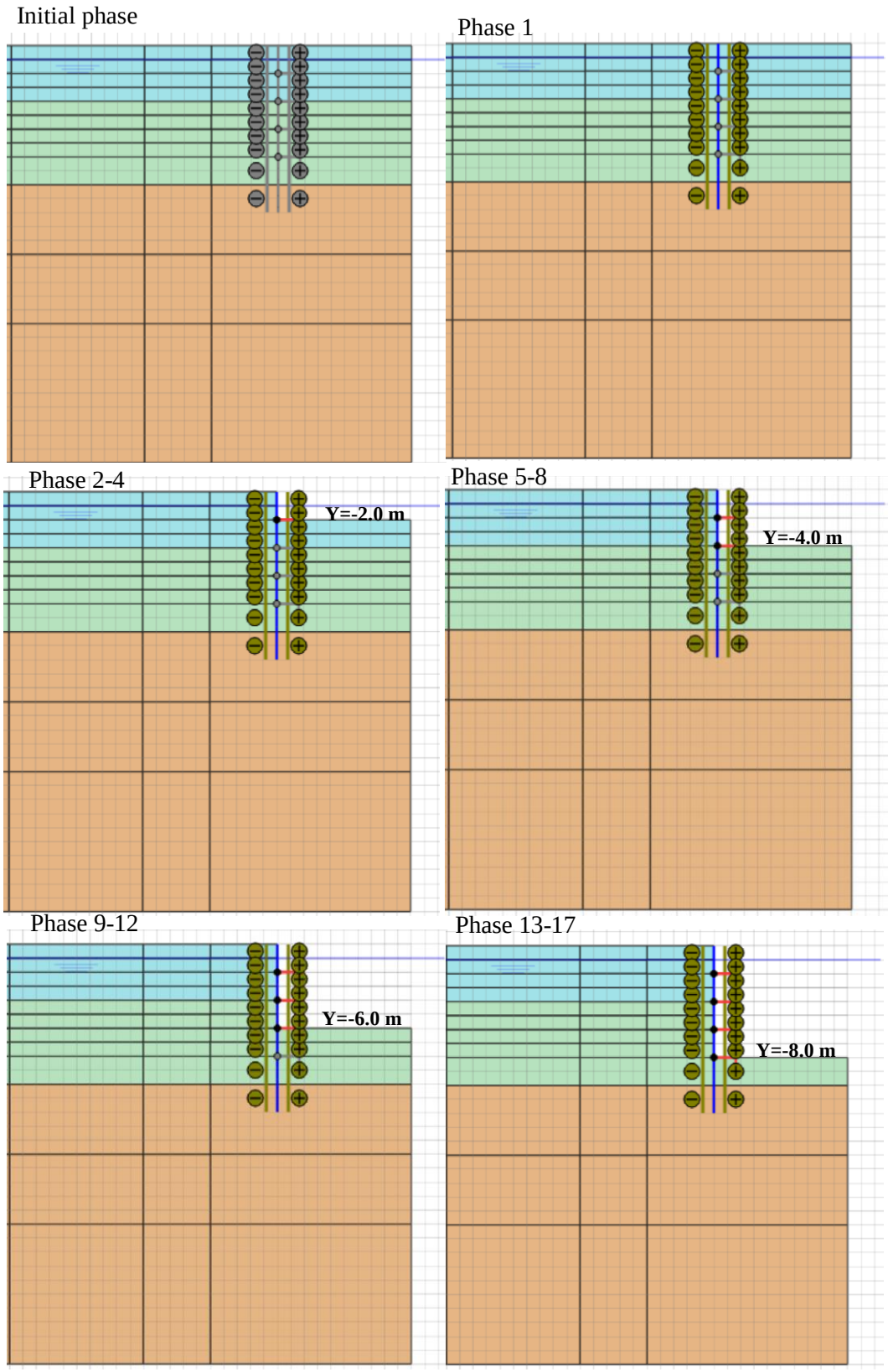

Figure 3-6. Construction sequence, phases 0-17.

3.2 Typical results of the base model

Figure 3-7 shows the horizontal displacement contours generated in Plaxis 2D for excavation stages corresponding to the elevations of the internal support. As expected, the maximum lateral displacement of the retaining wall is located at the same level of the bottom of the excavation.

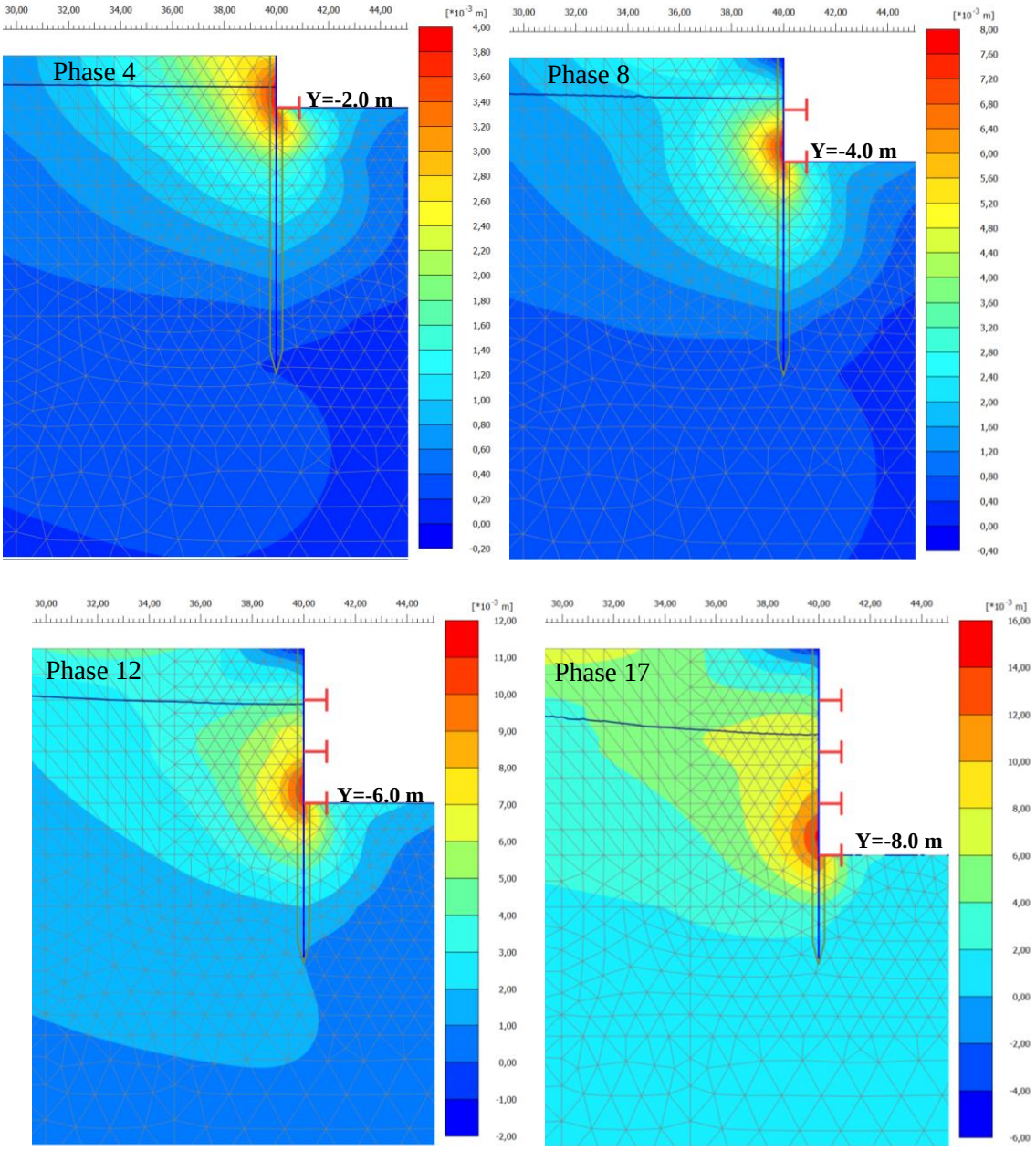

Figure 3-7. Computed horizontal displacements contours.

Figure 3-8 presents in the Y-axis the depth of the soil profile with respect to the ground surface and in the X-axis the lateral wall movements extracted at 0.5 m behind the retaining wall. The figure presents deformations for excavation stages corresponding to the elevations of the internal support. Note also that the maximum values for the horizontal displacements appears at the level at which the bottom of the excavation is located (i.e. -2.0m, -4.0m, -6.0m and -8.0m). Also note that the horizontal displacements rapidly decrease with depth until reaching the lower level of the retaining wall (i.e. -12.0m). Below this level, the lateral displacements became negligible. Considerable lateral displacements outward the excavation zone are presented near the ground surface at the end of the excavation process. This behavior is attributed to the major drawdown of the water table and the suction generated at these stage.

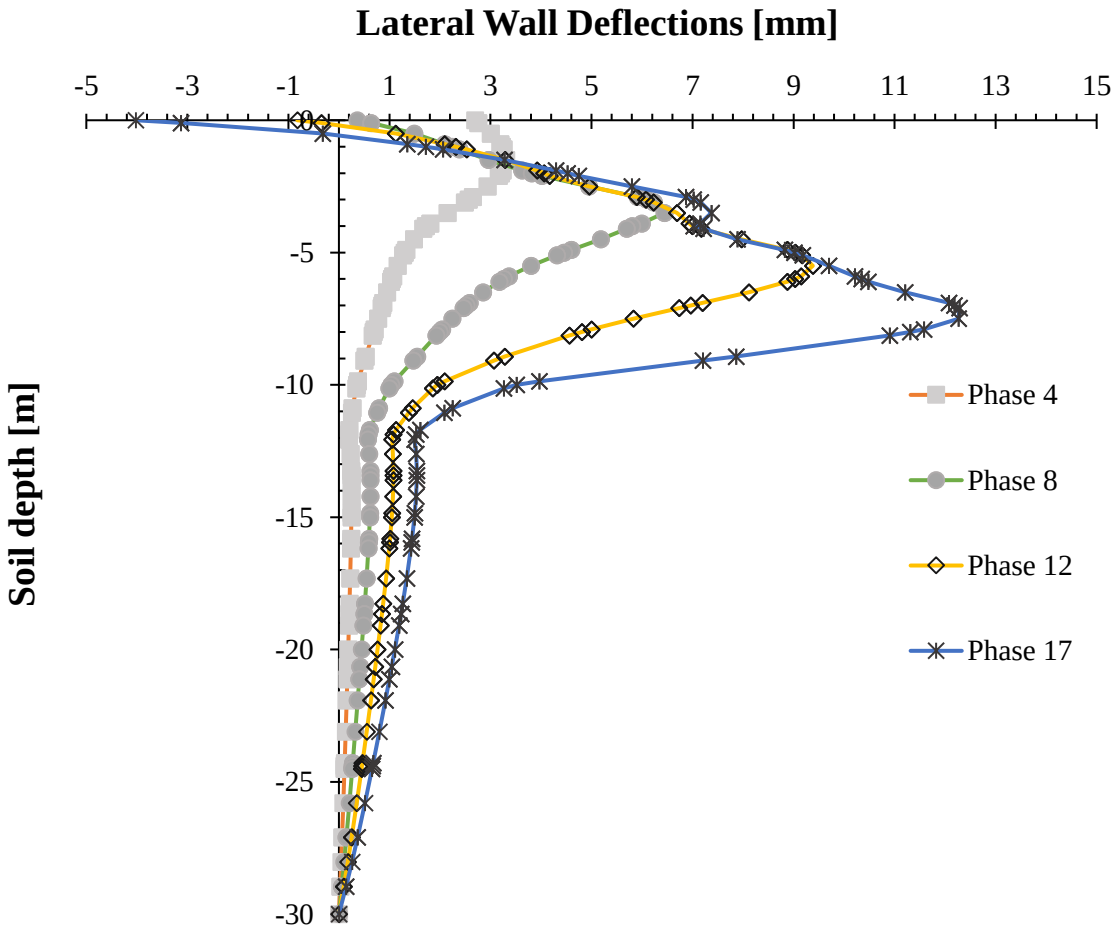

Figure 3-8. Lateral wall movements at different phase of the excavation.

Figure 3-9 shows the vertical displacement contours generated in Plaxis 2D for excavation stages corresponding to the elevations of the internal support. As expected, the maximum vertical displacement at the different stages is located close to the retaining wall and its magnitude decreases with the distance from the wall.

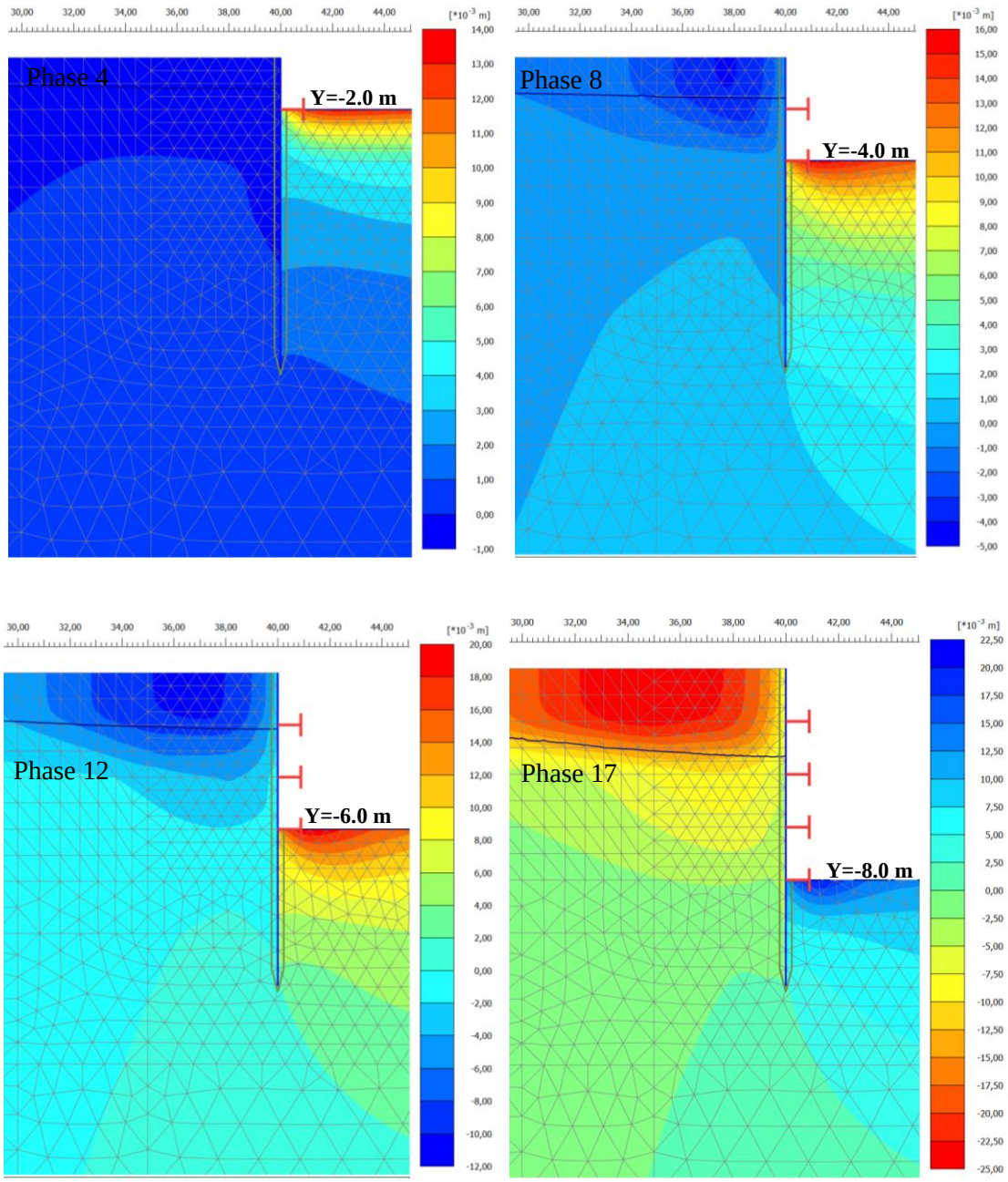

Figure 3-9. Computed vertical displacements contours.

Figure 3-10 presents the ground surface settlement profiles extracted 0.5m below the surface for excavation stages corresponding to the elevations of the internal support. As noticed before, the maximum values for the vertical displacements appears close to the wall. However, it can be establish that this distance is around half of the excavation height at each stage and the settlement zone of influence is 2 times the excavation height at each stage according with previous works (Hsie and Ou, 1998).

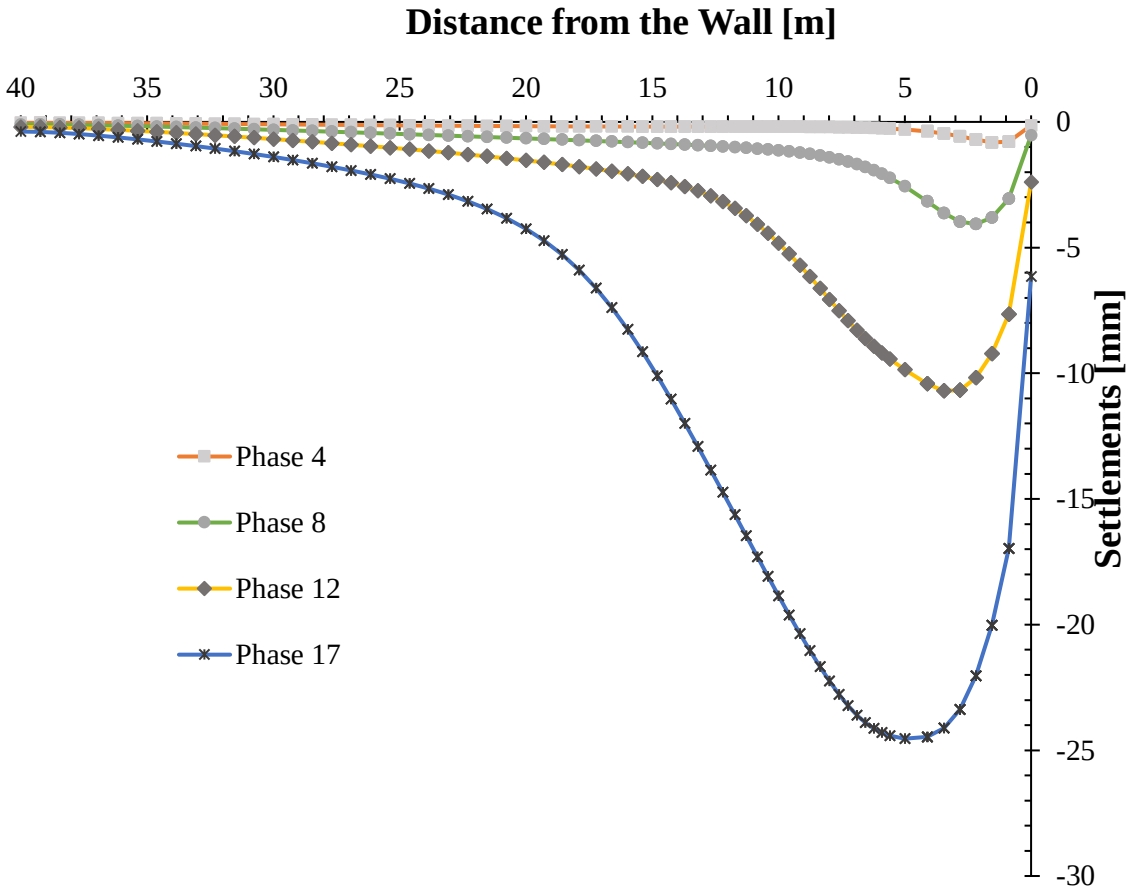

Figure 3-10. Ground surface settlements at different phase of the excavation

Figure 3-11 shows the excess pore water pressures generated in Plaxis 2D for excavation stages corresponding to the elevations of the internal support. It can be seen that the values of the excess pore water pressures generated at the bottom of the excavation remains constant throughout the width of the excavation, especially for deeper stages. As expected, only negative excess pore water pressures are generated at the soil immediately below the bottom of the excavation. For locations behind the wall, this parameter behaves in a similar way that to the ground surface settlements. The

largest value occur near the surface and at some distance away from the wall and tend to decrease as the distance from the wall increases.

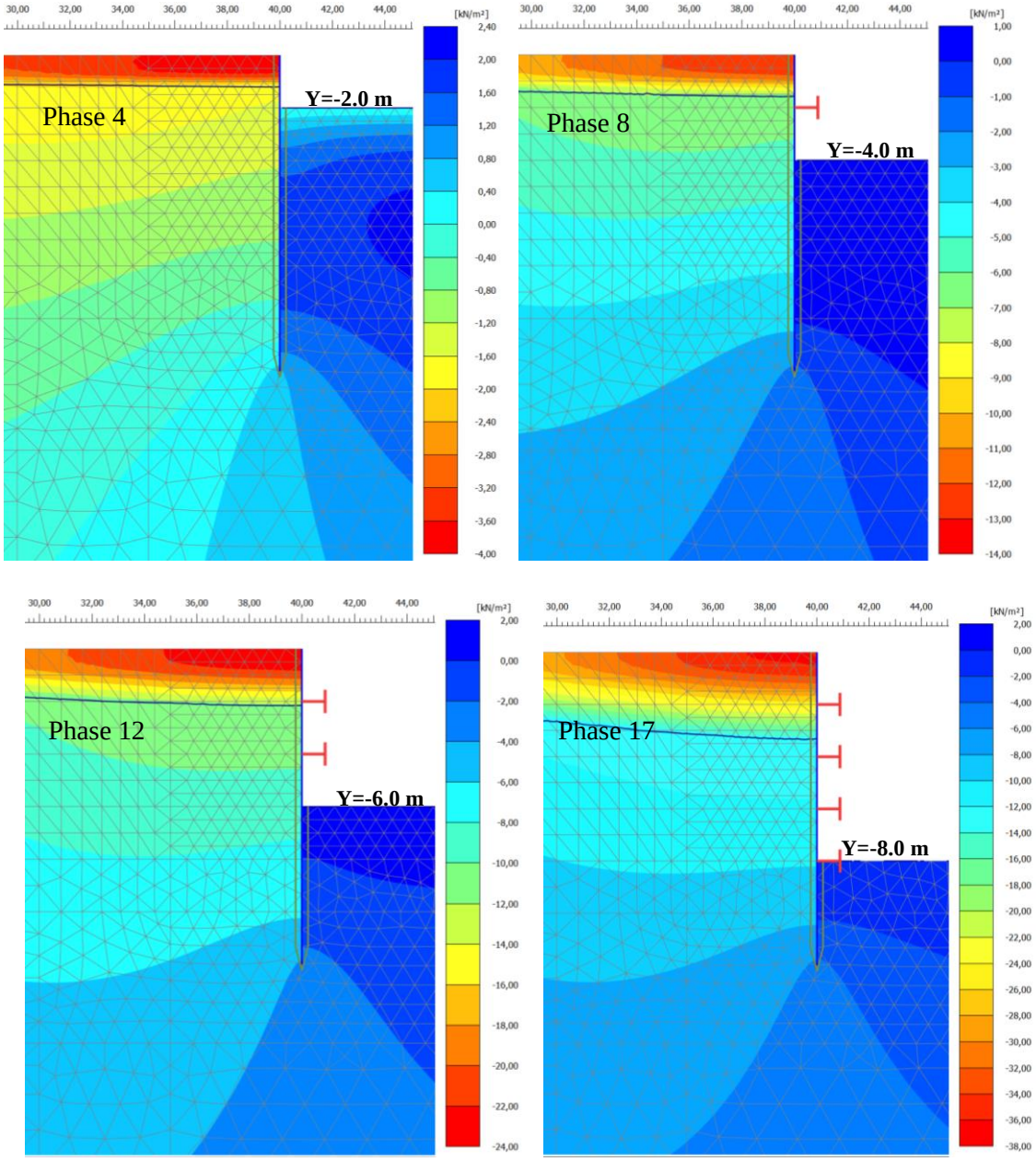

Figure 3-11. Computed Excess pore water pressure contours.

4. PARAMETRIC STUDY

The parametric study was conducted to investigate the effects of the hydraulic conductivity, excavation rate, support system stiffness, excavation width in the generation and dissipation of excess pore water pressure, which is directly related to the drainage conditions of the excavation. The parametric study is also used to evaluate the influence of the fully coupled analysis in the computed ground movements, specifically settlements behind the retaining wall are computed. The parametric study was designed to define when a fully coupled flow deformation analysis is required for the simulation of deep urban excavations in soft to medium clays. The goal is to develop design charts to predict the magnitude of excess pore water pressures generated at key locations, such us at the bottom of the excavation and behind the retaining wall. Excess pore water pressure plays a very important role in the stability and design of an excavation as it is directly related to the strength of the soil. This parametric study is also aimed at defining the drainage conditions in which the excavation is being carried out, i.e., fully drained, fully undrained or partially drained conditions. As mention in chapter 2, Nogueira et al. (2009) studied the variation of excess pore water pressure with the rate of excavation and soil hydraulic conductivity using a one-dimensional model with a fully coupled flow formulation. They concluded that soil behavior can be characterized by drained conditions only for excavations rates of the same magnitude as the hydraulic conductivity of the soil. Conversely, the excavation rate would have to be three orders of magnitude larger than the hydraulic conductivity to achieve an undrained response.

In order to define under which drainage condition the excavation is conducted, a parametric analysis, employing a full excavation and lateral support system model, was conducted to evaluate the generation and dissipation of excess pore water pressures. The parametric study takes into account the rate of the excavation (i.e. advance in depth of the excavation per unit of time) and the hydraulic conductivity of the soil. Variations between one and five orders of magnitude for different representative soil values of permeability were considered. The parametric study also varied the lateral system stiffness and the excavation width to determine its influence on the generation and

dissipation of excess pore pressures. Additionally, deformation data was obtained in order to generate settlement profiles and lateral wall deflections for each numerical model.

In models 1 to 25, the effects of varying the ratio between excavation rate and the hydraulic conductivity (i.e., ER/k) on the generation of excess pore water pressure was studied. **Table 4-1** shows the values and combination of excavation rate and soil permeability used in Models 1 to 25. In models 26 to 50, the width of the excavation was reduced by 50% (i.e., excavation width equal to 10.0 m); while in models 51 to 75 the width of the excavation was increased by 50% (i.e., excavation width equal to 30.0 m). Models 76 to 81 simulated the limit fully drained and fully undrained conditions to define the boundaries for each of the geometries and combinations of excavation rate and soil permeability previously analyzed.

Table 4-1. Values of hydraulic conductivity and excavation for models 1-25

Hydraulic conductivity		**Excavation Rate**				
(m/day)	**(cm/s)**	**(m/day)**				
1.0	$1.16x10^{-3}$	$1.0x10^{1}$	$1.0x10^{2}$	$1.0x10^{3}$	$1.0x10^{4}$	$1.0x10^{5}$
$1.0x10^{-1}$	$1.16x10^{-4}$	1.0	$1.0x10^{1}$	$1.0x10^{2}$	$1.0x10^{3}$	$1.0x10^{4}$
$1.0x10^{-2}$	$1.16x10^{-5}$	$1.0x10^{-1}$	1.0	$1.0x10^{1}$	$1.0x10^{2}$	$1.0x10^{3}$
$1.0x10^{-3}$	$1.16x10^{-6}$	$1.0x10^{-2}$	$1.0x10^{-1}$	1.0	$1.0x10^{1}$	$1.0x10^{2}$
$1.0x10^{-4}$	$1.16x10^{-7}$	$1.0x10^{-3}$	$1.0x10^{-2}$	$1.0x10^{-1}$	1.0	$1.0x10^{1}$

Additional ER/k ratios, especially in the most sensitive range of variation respect to the ground soil deformations, were considered in models 82 to 99. These cases represent the 3 previous excavation widths but varying the excavation rate and keeping constant the hydraulic conductivity. The additional ER/k ratios are presented in **Table 4-2**.

Table 4-2. Additional ratios between excavation rate and hydraulic conductivity analyzed

Excavation Rate / Hydraulic Conductivity (ER/k)										
10	15	20	30	60	100	200	600	1000	10000	100000

In models 100 to 132, the effect of a stiffer retaining wall on the generation of excess pore water pressure and ground deformations is evaluated. For these models, the hydraulic conductivity of model 82 was used and all of the ER/k ratios and excavations widths previously established were evaluated. Similarly, models 133 to 138 were created to define the limit fully drained and fully undrained conditions. It must be mentioned that the initial wall stiffness used in the based model

represents very flexible walls such as sheet pile walls. Models 100 to 138 represent medium stiff slurry walls such as tangent pile walls. **Table 4-3** shows the wall stiffness specified for Models 100 to 138.

Table 4-3. Wall retaining system parameters for models 100 to 138

Name	Tangent Pile walls	unit
EA1	14300000	kN/m
EI	274600	kN.m/m²
deq	0.48	m

4.1 Influence of hydraulic conductivity, excavation rate and excavation width

4.1.1. Effects on the excess pore water pressure

Figure 4-1, **Figure 4-2** and **Figure 4-3** shows the variation of the maximum excess pore water pressures with excavation rate and hydraulic conductivity for excavation widths of 10 m, 20 m, and 30 m, respectively. The plotted values correspond to maximum excess pore water pressures generated at the bottom of the excavation and are recorded at the final stage of the excavation. Also included in the figures are the simulation results corresponding to fully undrained and drained conditions (i.e. models 76-81). These models were created taking advantage of the capabilities offered by Plaxis (2016) which simplifies the modeling procedures and improves the performance of the calculations. As expected for the fully drained case, no excess pore water pressures are generated. For the cases calculated by the FCFDA as the excavation gets wider (100% increment), the magnitude of the excess pore water pressures generated show a significant increase (approximately 15% to 20%), especially for ER/k-ratios between 10^2 and 10^4. For larger ratios, the observed pore pressure increment was not significant, i.e., only 5%. In addition, for the fully undrained limit case, the magnitude of the excess pore water pressures increased larger than that calculated by the FCFDA. Increments between 25% and 30% were obtained as the width of the excavation duplicated. This behavior is attributed to the volume (weight) of the soil removed (Callisto et al. 2014).

In general, when the excavation rate is 4 orders of magnitude larger than the hydraulic conductivity of the soil, an undrained condition is reached with the excess pore pressure curve becoming

asymptotic as the excavation rate increases. This result is in agreement with previous research works (Griffiths et al. 1992) (Nogueira et al. 2009) where undrained behavior was obtained for excavation rates with 3 to 4 orders of magnitude larger than the hydraulic conductivity of the soil. Unlike previous works (Nogueira el at. 2009) where drained conditions were obtained for excavations rates around one order of magnitude smaller than the hydraulic conductivity of the soil, the results contained herein show that drained behavior can be achieved for excavation rates 1 order of magnitude larger than the hydraulic conductivity of the soil. Although as the excavation width increases, the magnitude of the excess pore water pressures marginally increases, especially for narrow excavations. It can be noticed that the width of the excavation does not have an important influence in the definition of the drainage limit conditions. It only slightly influences the distribution and dissipation rate of the excess pore water pressure.

Because of the slow or very fast excavation rates needed for achieving the drainage limit conditions, partially drained conditions prevail during standard excavation procedures in soft to medium clays. For a hydraulic conductivity of $1x10^{-4}$ m/day ($1.16x10^{-7}$ cm/s), the excavation rate should be approximately 1 m/day or 1mm/day for achieving fully undrained or fully drained conditions, respectively. It emphasizes the importance of fully coupled flow deformation analyses to properly estimate excavation-induced deformations.

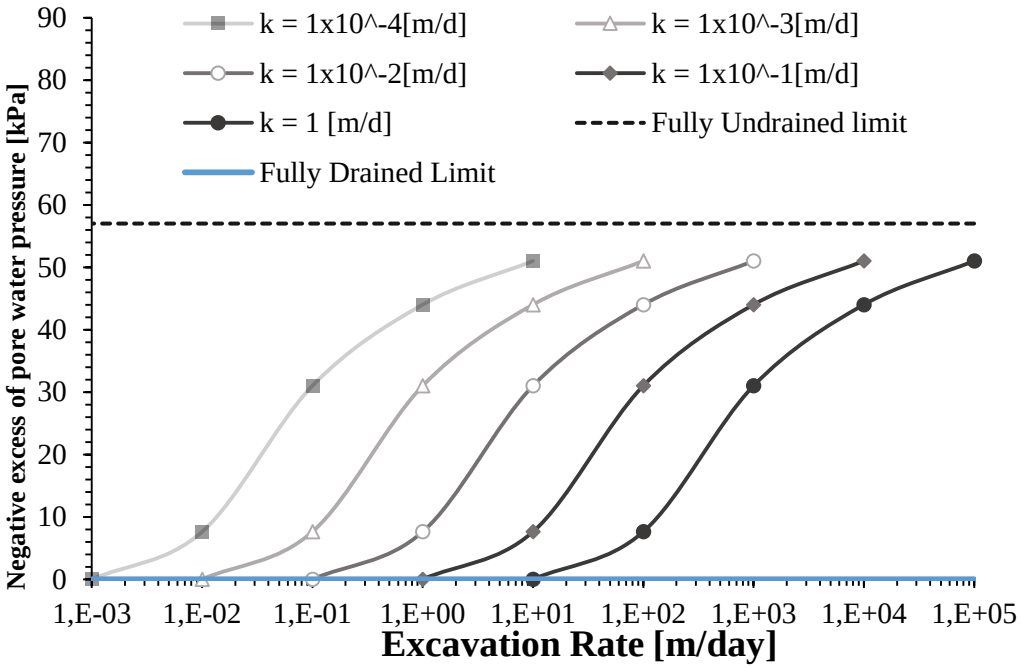

Figure 4-1 Variation of excess pore pressure and excavation rate for different hydraulic conductivities for excavation width of 10.0m

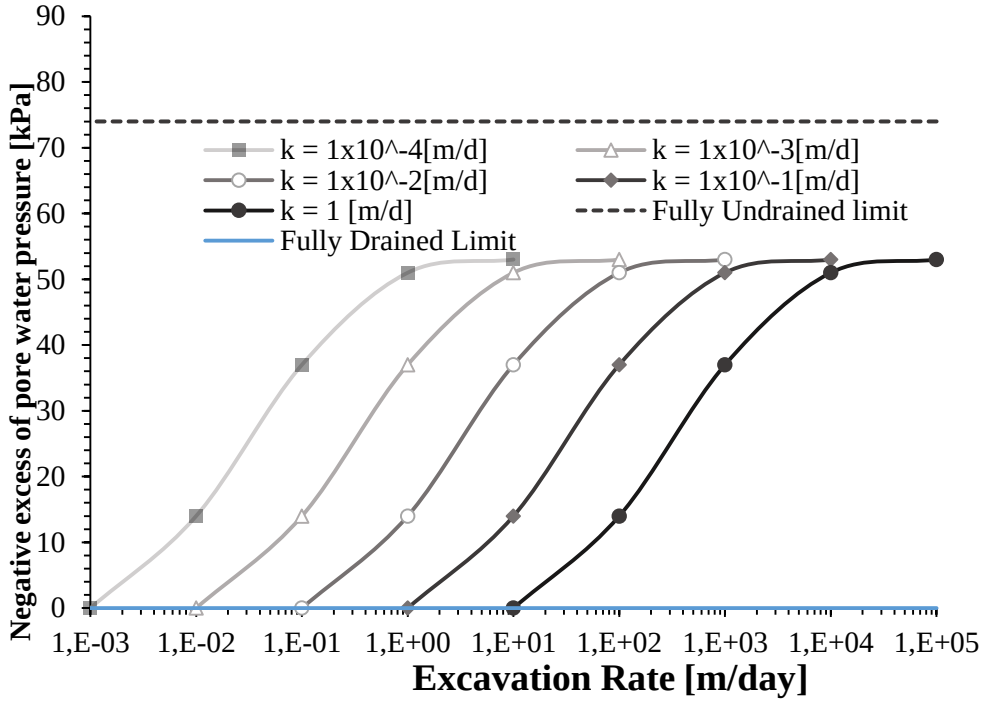

Figure 4-2 Variation of excess pore pressure and excavation rate for different hydraulic conductivities for excavation width of 20.0m

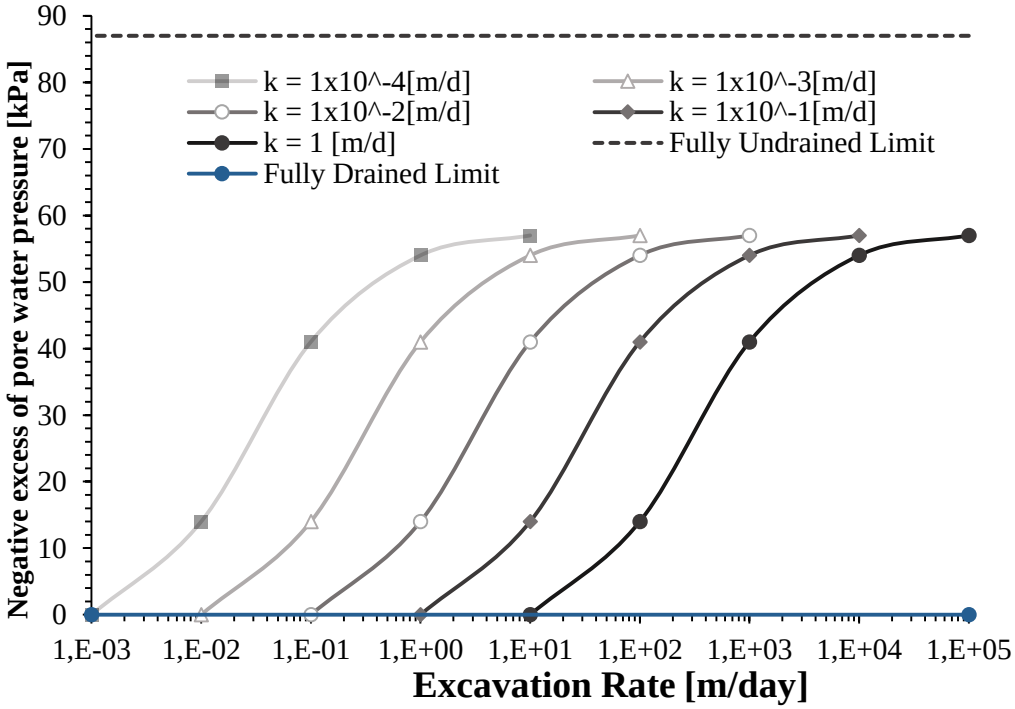

Figure 4-3 Variation of excess pore pressure and excavation rate for different hydraulic conductivities excavation width of 30.0m

4.1.2. Effects on ground deformations

Figure 4-4, **Figure 4-5** and **Figure 4-6** present distributions of surface ground settlements as a function of the distance from the wall based on fully coupled analyses for excavation widths of 10, 20 and 30 m, respectively. The figures include 7 different cases for a unique value of hydraulic conductivity, 5 different relations of ER/k varying from each other in one order of magnitude between 10^1 to 10^5, and the 2 limits for fully drained and undrained cases. As expected, the ground surface settlements are larger as the excavation rate decreases (i.e. tending to a drained behavior). The maximum settlement obtained for the case with an excavation rate of one order of magnitude larger than the hydraulic conductivity matches well the results for the limit drained models in wider excavations (i.e., cases where the excavation width is 20.0 and 30.0 m), unlike the narrower excavation models where differences of about 30% are obtained.

In spite of the agreement in the magnitude of the maximum ground surface settlements for fully drained conditions and models where the excavation rate was one order of magnitude larger than the soil hydraulic conductivity, larger discrepancies are observed in the shape of settlement profiles, especially for the location of the second inflexion point that defines the excavation zone of influence (Hsieh and Ou 1998). This can be explained by analyzing the water table position at the final stage of the excavation. The drawdown simulation of the water table considered in this work is in agreement with Small 1992; Nogueira et al. 2009; and Borges et al. 2013. It was shown that as the drawdown of the water table increases, i.e., achieving drained limit, larger surface settlements are predicted, but the lateral wall deflections are smaller than the cases where no drawdown is considered, i.e., undrained limit. As mention before, the drawdown of the water table directly affects the surface settlements. The discrepancy in the distribution or shape of the settlement profiles, based on fully drained and fully coupled analyses where $ER=10^1k$ is related with the differences observed in the water table drawdown process at the end of the excavation. For the fully drained model, the calculated drawdown is much larger than that the results obtained for FCFDA model which is considered to represent a more realistic prediction (see **Figure 4-7**). It is worth mentioning that the shape of the ground surface settlement obtained are in good agreement with typical concave settlement profiles reported by Hsieh and Ou (1998) based on worldwide excavation cases histories.

Note that for all the excavation widths modeled in this work, the settlement profiles present a significant reduction in the magnitude of maximum ground surface settlements when going from an

ER/k = 10^1 to 10^2. This effect is better observed in terms of the settlement magnitude where it is more significant for wider excavations (i.e. excavation widths of 20 and 30.0 m) and the reduction of the settlement profile is of such magnitude that for these cases the profile of settlements obtained is close to the settlement shape of the fully undrained case. Note that for ER/k ratios equal or larger than 10^2 or 10^3, very similar results are obtained in comparison with the fully undrained case, indicating that FCFDA are not required for ER/k ratios of 10^3 or larger and a fully undrained analysis will suffice to estimate ground deformations.

Figure 4-8 presents the lateral wall deformations as a function of the depth below the ground surface. Similar to **Figures 4-4** to 4-6, the same 7 cases are presented for the three different excavations widths modeled. It is noticed that the width of the excavation does not have a significant influence on the lateral wall deformations. On the other hand, as evidenced for the ground surface settlements behavior, the most remarkable changes in the magnitude of the lateral deflections is observed for ER/k ratios of 10^1 to 10^2, especially for wider excavations. Note that the lateral deformations decrease for lower excavation rates, unlike the behavior exhibited by the settlements. Also, the results obtained for the slowest excavation rate modeled, (i.e. ER=10^1k) show a major difference against the results for the fully drained case, which presented considerably smaller magnitudes for lateral wall deflections. It can be inferred that this type of analysis can underestimate the lateral movements of the wall for long-term conditions and more appropriate results seem to be obtained through the FCFDA implementation. Due to the numerical modeling performed assumed the retaining wall system as “wish in to place” and according with (Zapata-Medina, 2007) deformations associated with wall installation effects can comprise between 25 to 30 percent of the total excavation induced movements, the recommendation is that future research works with the FCFDA approach should be made incorporating this feature (i.e. wall installation effects) and accomplished an accurate prediction of the behavior of the lateral wall deflections.

It is worth mention that all the data plot in Figures 4-4, 4-5, 4-6 and 4-8 were obtain at phase 17 in the numerical models, i.e. after reaching the final level of the excavation, a time interval according to the ER/K ratio modeled in each case.

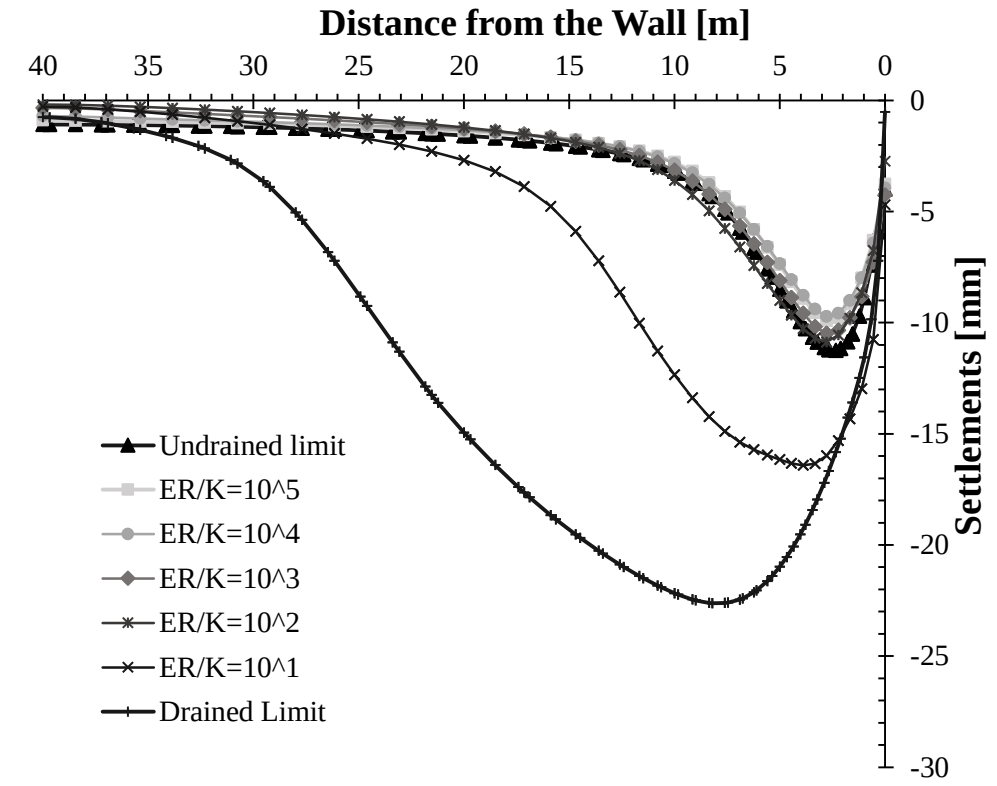

Figure 4-4 Surface settlement profile excavation width 10.0 m

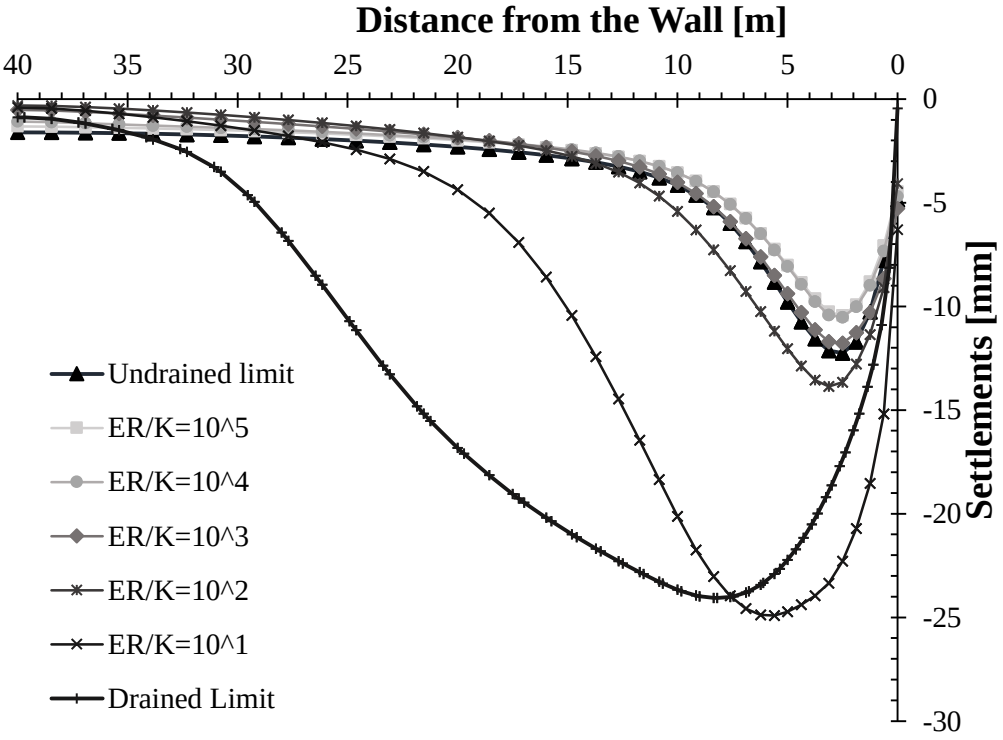

Figure 4-5 Surface settlement profile excavation width 20.0 m

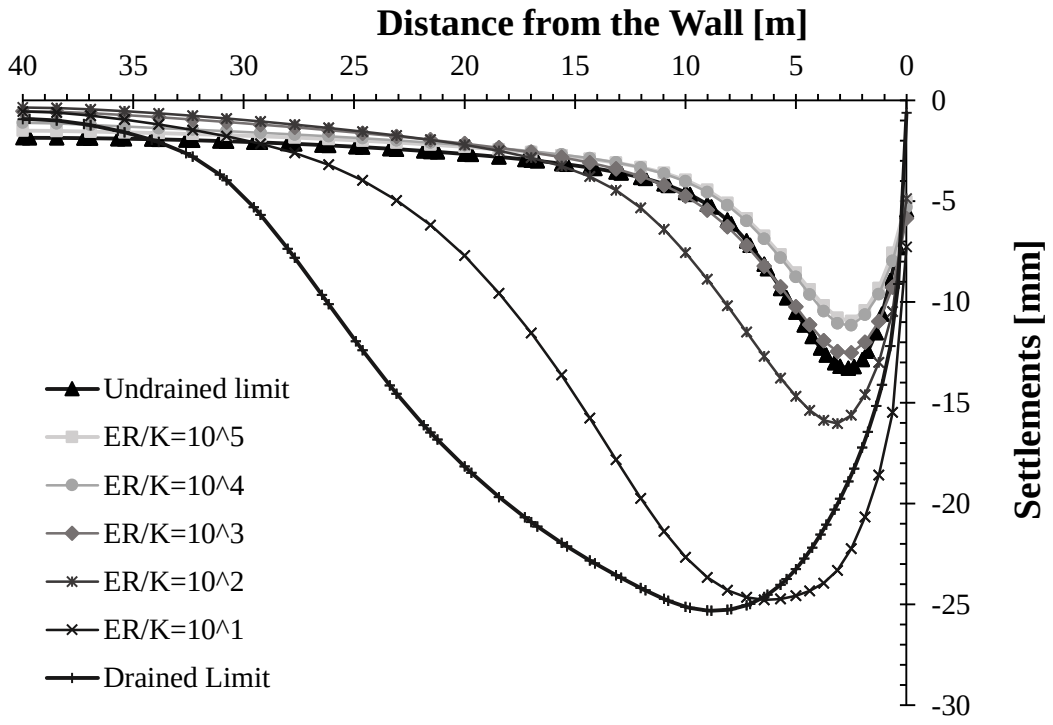

Figure 4-6 Surface settlement profile excavation width 30.0 m

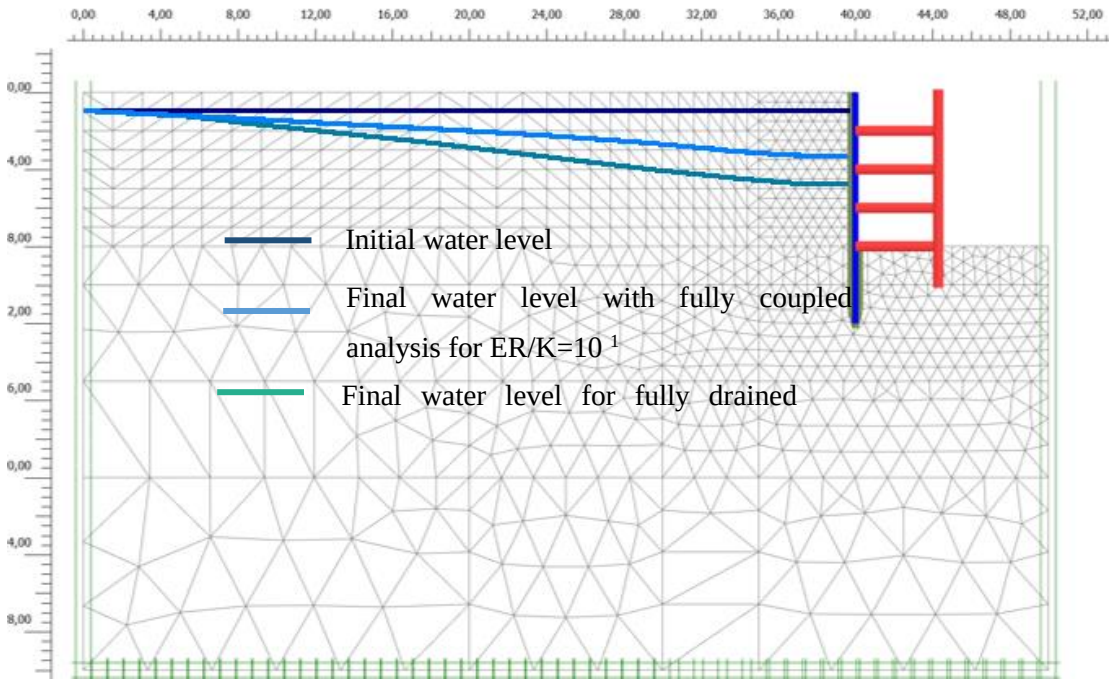

Figure 4-7 Comparison between final ground water level fully drained analysis and fully coupled analysis using a ratio ER/k = 10^1

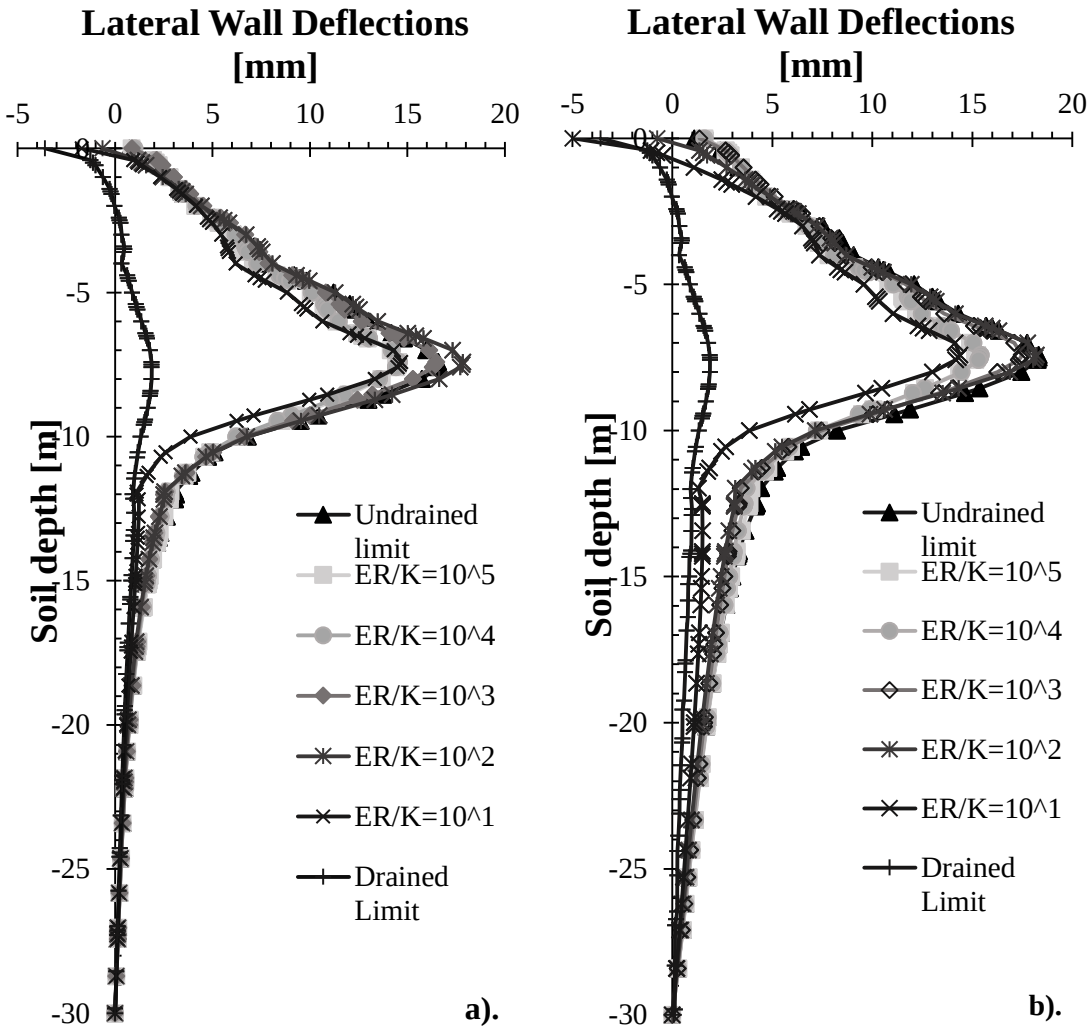
Lateral Wall Deflections [mm]
-5
0
5
10
15
20
0
-5
-10
-15
-20
-25
-30
Soil depth [m]
Undrained limit
ER/K=10^5
ER/K=10^4
ER/K=10^3
ER/K=10^2
ER/K=10^1
Drained Limit
a).
Lateral Wall Deflections [mm]
-5
0
5
10
15
20
0
-5
-10
-15
-20
-25
-30
Soil depth [m]
Undrained limit
ER/K=10^5
ER/K=10^4
ER/K=10^3
ER/K=10^2
ER/K=10^1
Drained Limit
b).

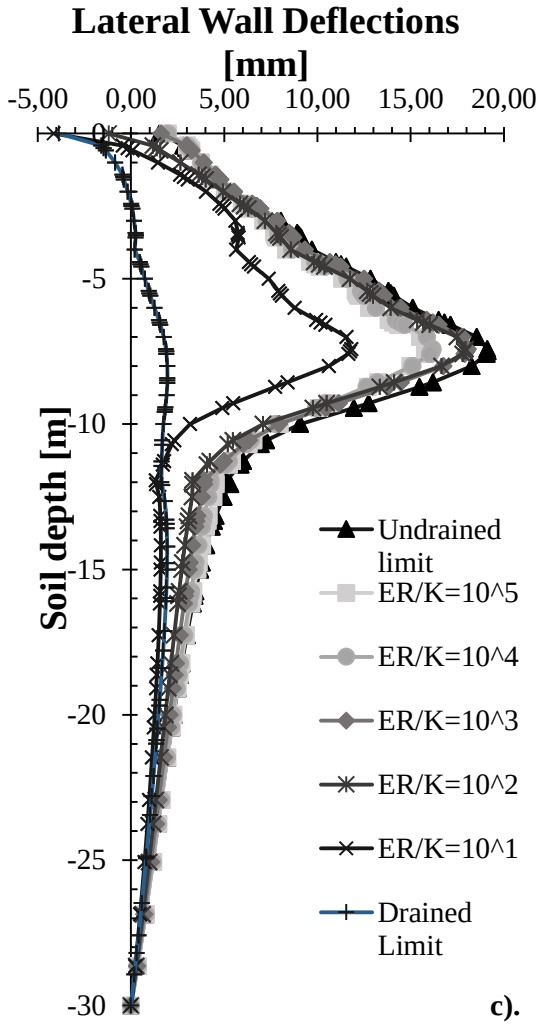

Figure 4-8 Lateral wall movements: (s) excavation width 10.0m; (b) excavation width 20.0m; (c) excavation width 30.0m

4.1.3. Ratio of excavation rate to soil permeability

Figure 4-9 presents ground surface settlements at the final excavation stage versus wall distance for four different ratios of ER/k and for a 20-m-wide excavation. Each graph includes 5 different curves representing different values of hydraulic conductivity varying from 1 m/day (1.16×10^{-3}cm/s) to 10^{-4} m/day (1.16×10^{-7}cm/s). Each graph presents the settlement response for constant ER/k ratios varying from 10^1 to 10^4. Note that by maintaining a constant ER/k ratio, the vertical deformations obtained for different values of the soil hydraulic conductivity are basically the same. It is worth noting that only results for excavation widths of 20.0m are presented as the results obtained for excavation widths of 10 and 30 m yielded similar behavior.

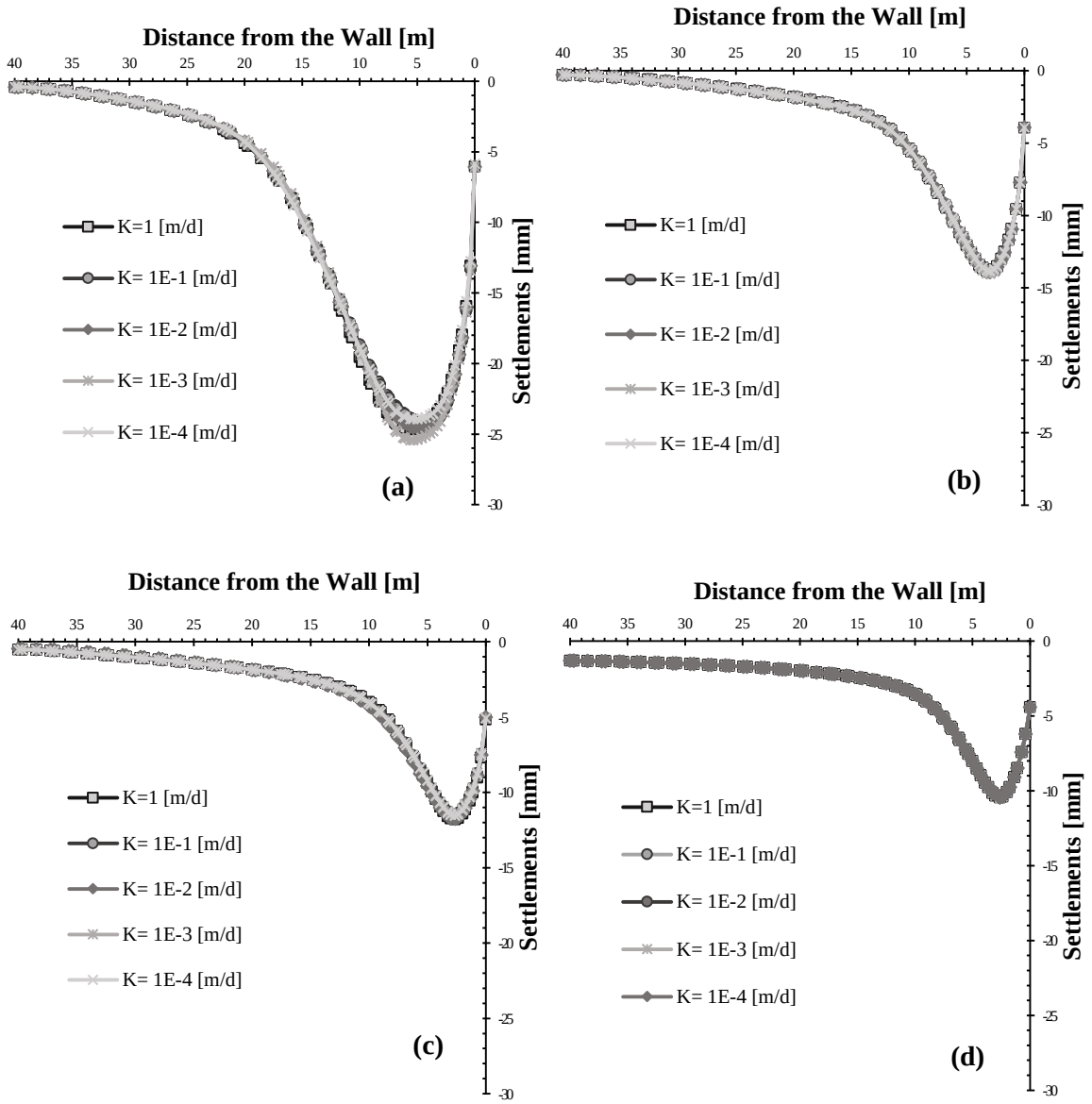

Figure 4-9 Ground surface settlements for an excavation width of 20.0 m: (a) ER/k=10^1; (b) ER/k=10^2; (c) ER/k=10^3; (d) ER/k=10^4

4.1.4. Maximum lateral deformation versus maximum ground settlement

Figure 4-10 shows the relation between the maximum ground surface settlement and lateral wall movement normalized against the excavation height for different ratios of ER/k. Also included in the figure are the cases where fully undrained and drained conditions were modeled. The data presented in the figure represents maximum ground movements at the final excavation stage. It can be seen that for fully undrained conditions and ER/k ratios larger than 10^2, the ratio between the

maximum ground surface settlements and the maximum lateral wall deflections is about 0.6. For ER/k ratios lower than 10^2, the $\delta v_{(max)}/\delta h_{(max)}$ ratio increases until reaching a value 2.0 for fully drained conditions, indicating that the ER/k ratio is an important factor, along with soil type and support system stiffness, that directly affects the excavation induced ground movements. Note also that the range obtained for the $\delta v_{(max)}/\delta h_{(max)}$ ratio (between 0.6 and 2.0) is in agreement with previous works (Wang et al. 2010) (Moorman 2004) (Liu et al. 2005).

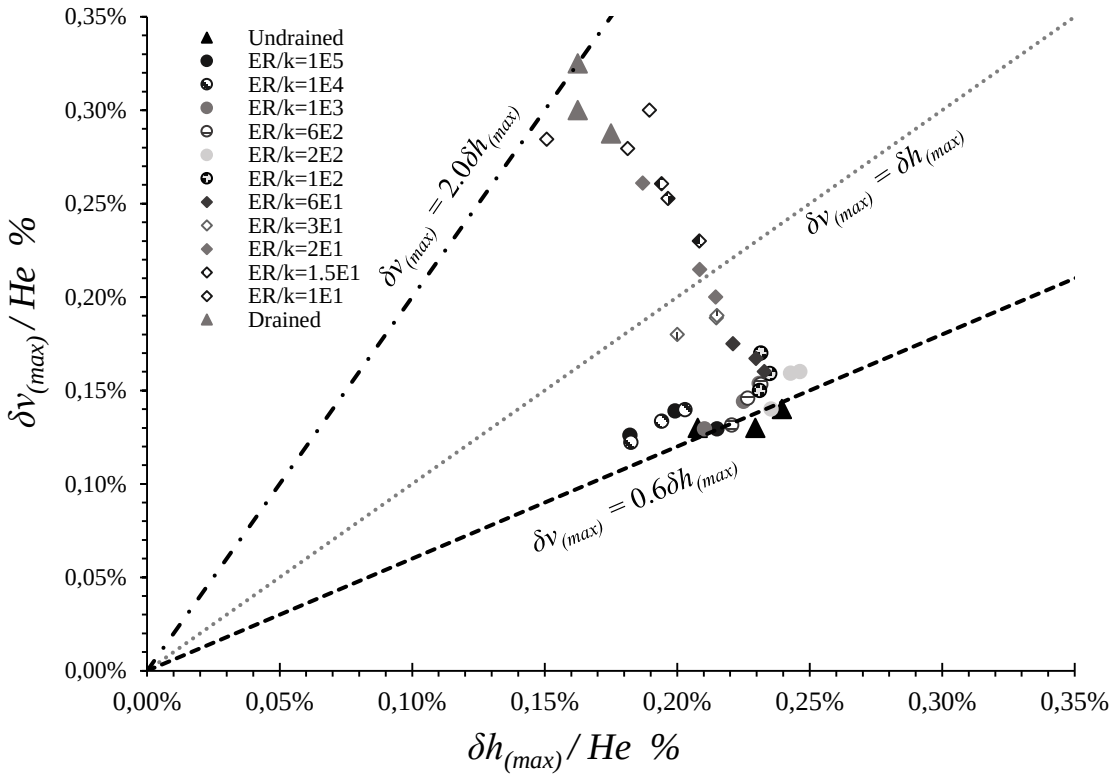

Figure 4-10 Normalized maximum lateral deformation vs Normalized maximum vertical surface

4.2 Excess pore water pressure ratio (alpha)

In this section, the excess pore water pressure ratio proposed by Ng, 1992 and subsequently rewritten by Callisto et al., 2006 as the Alpha parameter is calculated at each excavation stage. The Alpha parameter is defined as the ratio between the change in excess pore water pressure to the vertical stress relief inside the site of the excavation. Values of Alpha were calculated below the excavation bottom, where maximum values of excess pore water pressure are developed (Ng, 1992; Callisto et al., 2006), and at 0.5 m behind the retaining wall for each of the 8 excavation stages modeled (see **Figure 4-11**).

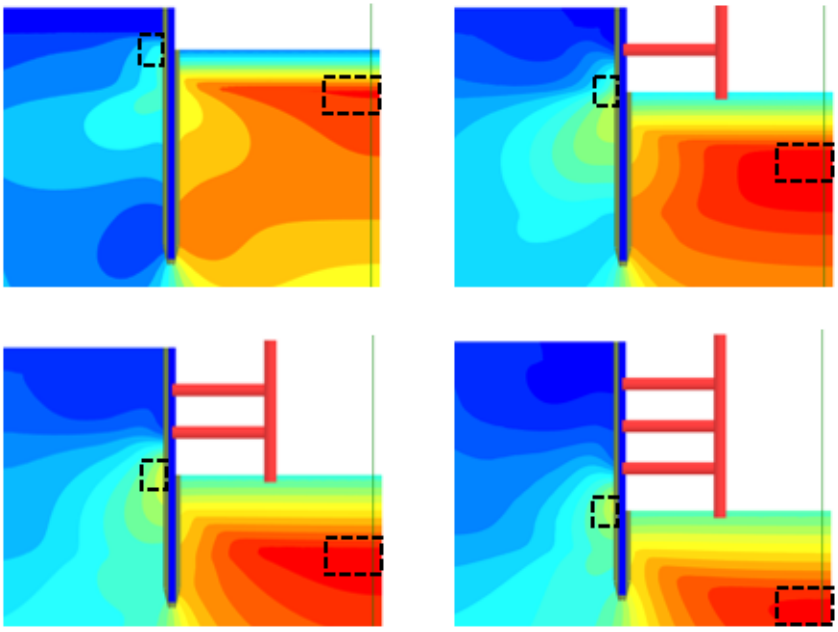

Figure 4-11 Zones of excess pore water pressure used in the alpha values computed for all the numerical models.

Figure 4-12, Figure 4-13 and **Figure 4-14** presents α-values calculated at the bottom of the excavation and behind the retaining wall as a function of the ratio B/H_e, where B is the width of the excavation and H_e is the excavation height. Values of α were calculated for all the ratios between the excavation and the hydraulic conductivity presented in **Table 4-2**. Note that a unique relationship between α and B/H_e is obtained. For the soil mass located at the excavation bottom, α-values increase with B/H_e towards an asymptotic behavior after B/H_e is about 10. On the other hand, the soil mass located behind the retaining wall shows α-values basically constant as B/H_e increases. Also it can be noticed that the change in the pore water pressure due to the vertical stress relief inside the excavation is greater at the bottom location than at the location behind the retaining wall. For the cases with a faster excavation rate, values of alpha at the bottom of the excavation reached a magnitude higher than 0.6, while for the location behind the retaining wall, the effects of the vertical stress reduction were very small and values of α less than 0.2 were obtained. As expected, the parameter alpha decreases as the ER/k ratio decreases (i.e. reaching a fully drained conditions). These results are in accordance with previous works (Nogueira et al. 2009) (Holt and Griffiths (1992) that reported that for excavations conducted under a ratio of ER/k lower than 10^2, α-values become negligible and a transition process start to take place from a partially drained condition to a fully drained condition.

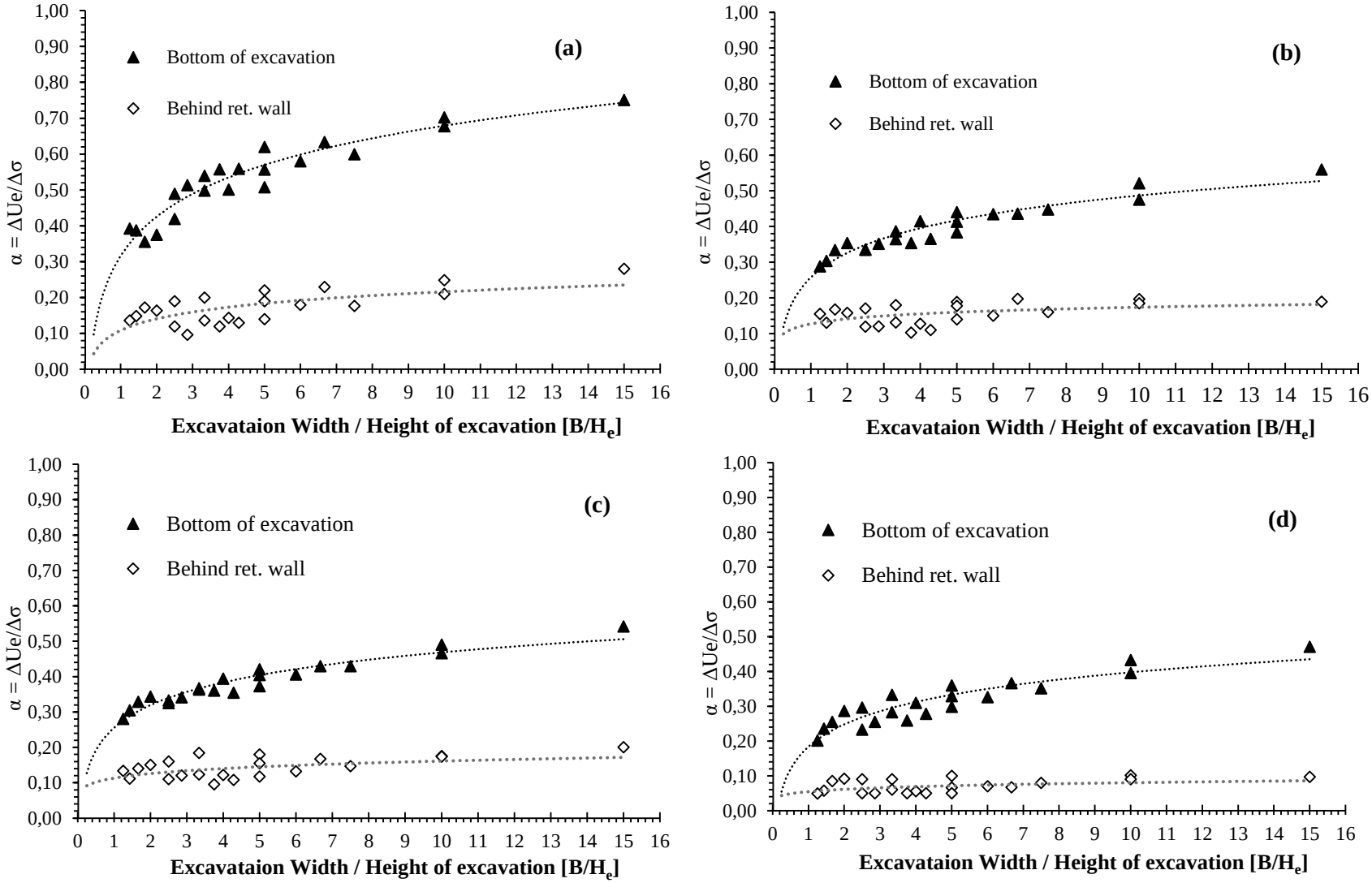

Figure 4-12 values of α versus the ratio b/h: (a) fully undrained; (b) ER/k=10^5; (c) ER/k=10^4; (d) ER/k=10^3

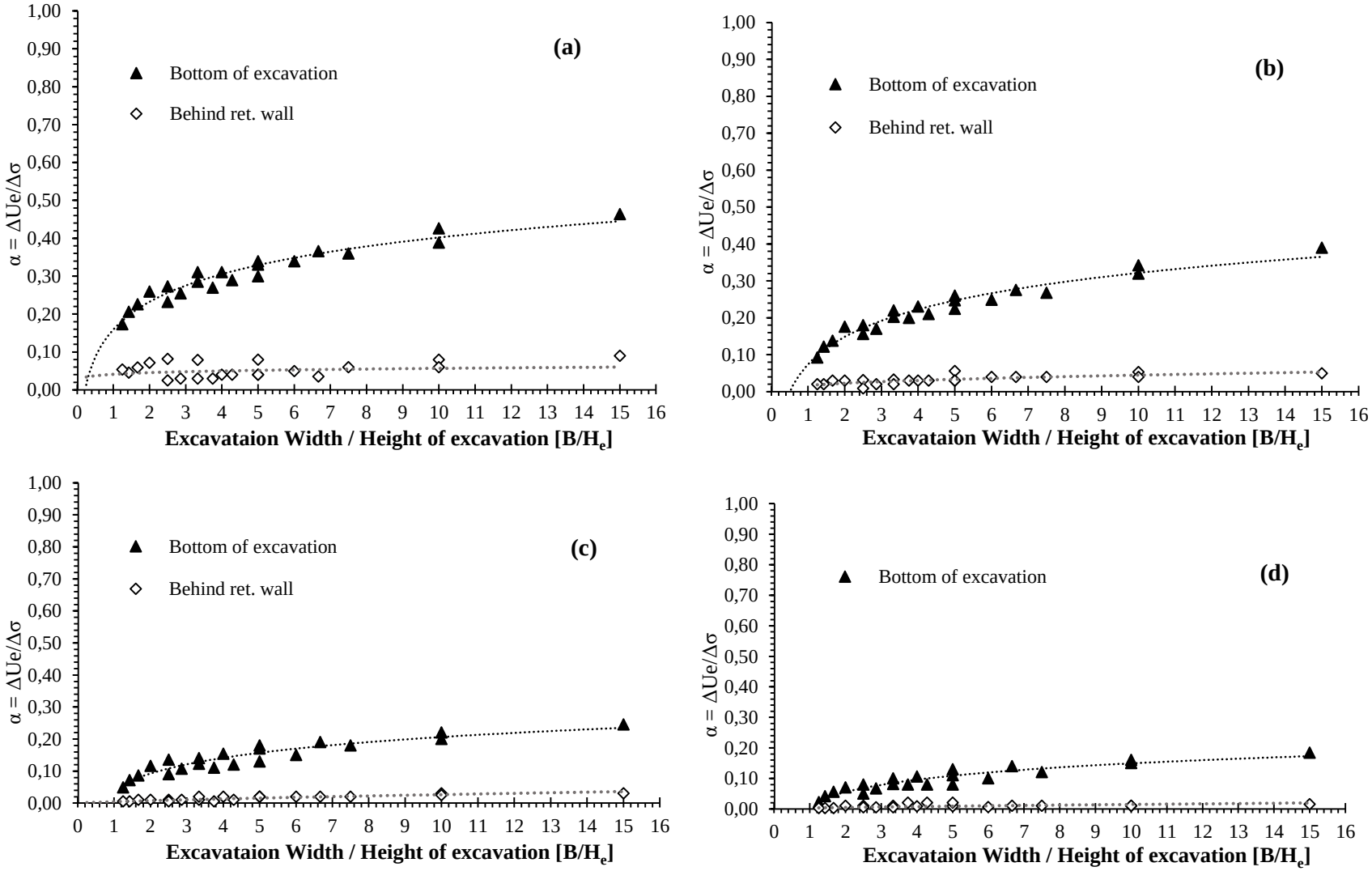

Figure 4-13 values of α versus the ratio b/h: (a) ER/k=600; (b); ER/k=200 (c) ER/k=100; (d) ER/k=60

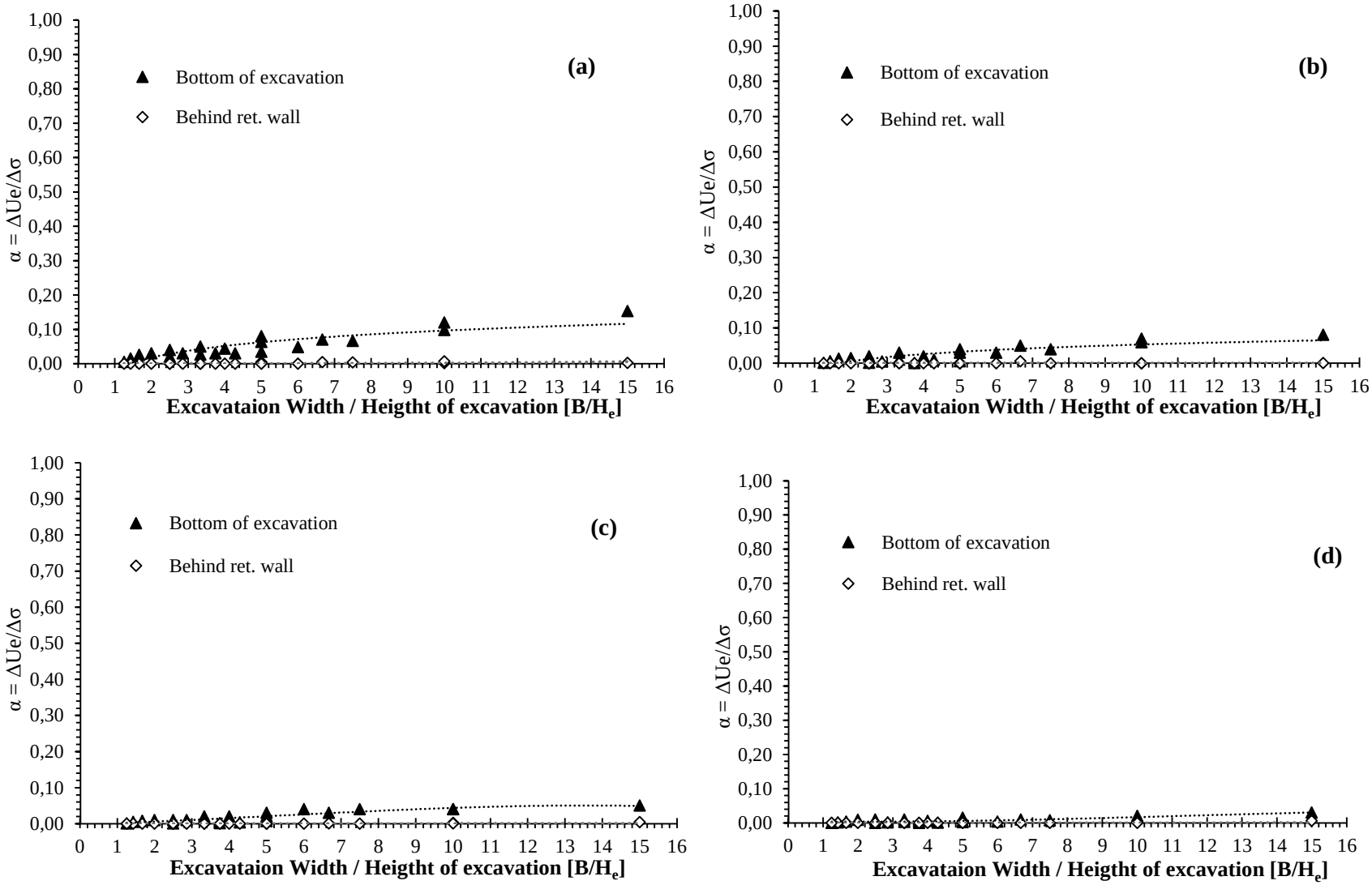

Figure 4-14 values of α versus the ratio b/h: (a) ER/k=30; (b); ER/k=20 (c) ER/k=15; (d) ER/k=10

4.3 Influence of wall stiffness

Currently, the philosophy for designing deep urban excavations is based on deformation control. Final excavation-induced ground movements (horizontal and vertical) must be controlled to assure the safety of the nearby infrastructure. Especial focus is on ground surface settlements and their distribution as it is directly related to distortions and structural damaged. **Figure 4-15** presents the maximum ground surface settlement computed behind the retaining wall against the alpha values calculated at the bottom of the excavation. The ground settlements are normalized by the height of the excavation and the horizontal axis (α-values) are presented in both arithmetic and logarithmic scales. **Figure 4-15** includes the results of all the previous models at the final stage of the excavation and for 2 different stiffness of the retaining wall system representing flexible sheet pile walls and stiffer tangent pile walls. Note that for α-values larger than 0.2, the normalized maximum ground settlement stays constant converging to the value obtained for the fully undrained condition. These α-values correspond to excavation rates of two order of magnitude larger than the hydraulic conductivity of the soil, indicating that for these conditions (i.e., $\alpha > 0.2$) it is not necessary to perform a fully coupled flow deformation analysis in order to assess the maximum settlement behind the wall. Although some dissipation is excess pore water pressure occur, one can just simulate the excavation as fully undrained, and in terms of ground deformations, the results would be practically the same. Observed also that the stiffness of the retaining system has an important role in the magnitude of the arising settlements. As expected, this variable does not have an impact in the generation of excess pore water pressure therefore the shape of the curve is maintained but shifting it down.

For values of alpha less than 0.2, the implementation of fully coupled flow deformation analyses is essential to correctly predict excavation-induced ground movements as partially drained conditions predominate. Note in **Figure 4-15** that the limit fully drained and undrained conditions would lead to very conservative analysis (i.e. drained conditions) or in the worst of the scenarios sub estimating the dissipation process of excess pore water pressure that can result in larger ground deformations than the ones calculated.

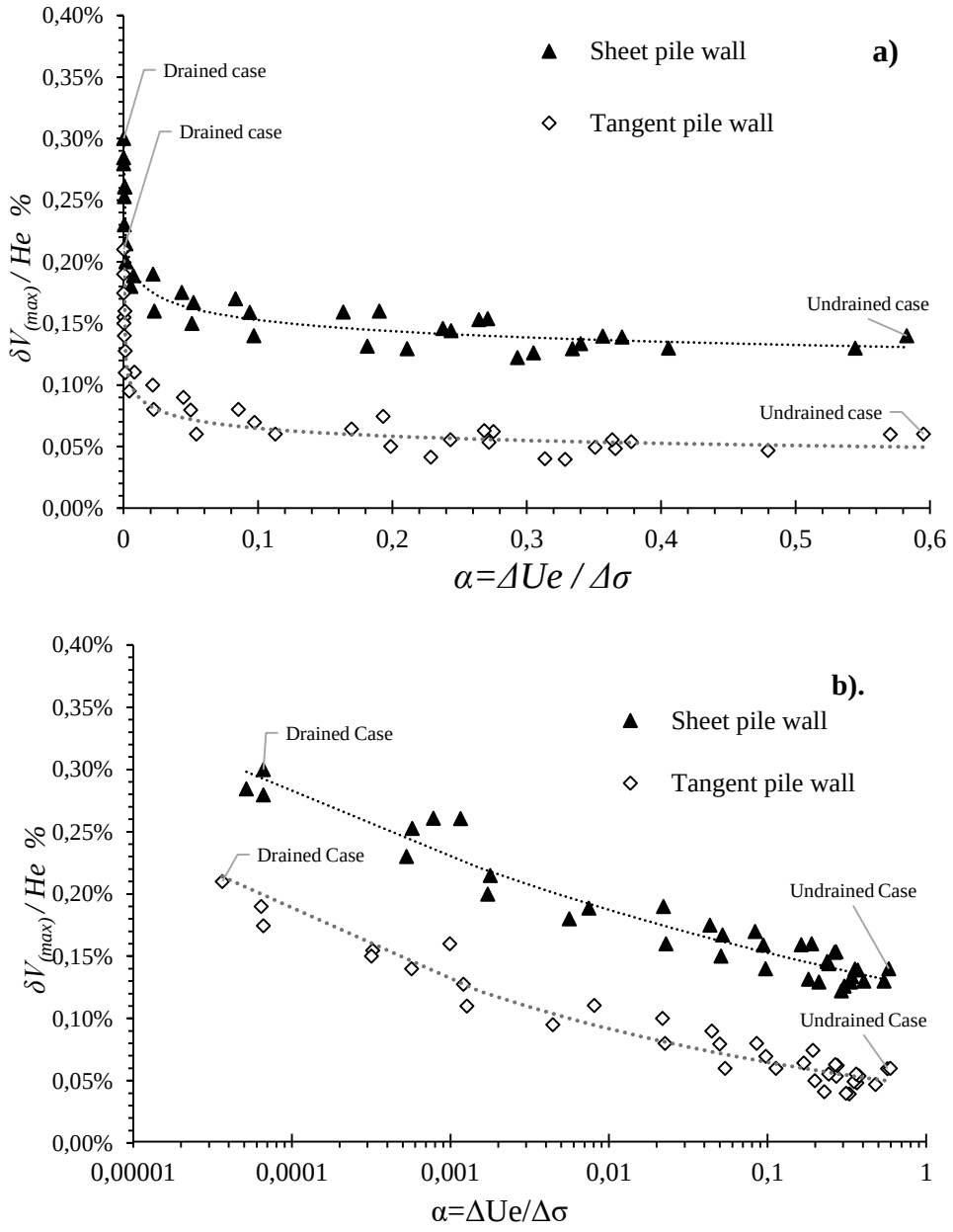

Figure 4-15 Normalized maximum vertical surface settlement vs alpha (α) parameter: (a) normal scale; (b); logarithmic scale

4.4 Data synthesis and proposed method

The results of the parametric study presented in this chapter are synthetized **in Figure 4-16.** The figure presents a flow chart that allows the designer to define under which drainage conditions the excavation should be modeled to accurately predict excavation-induced deformations. It especially focusses on stablishing when a fully coupled flow deformation analysis is required. The method uses

as input data the hydraulic conductivity of the soil, excavation rates and support system stiffness to predict excess pore water pressures at the bottom of the excavation and behind the retaining wall system, which are related to the ER/k ratios and to ground movements.

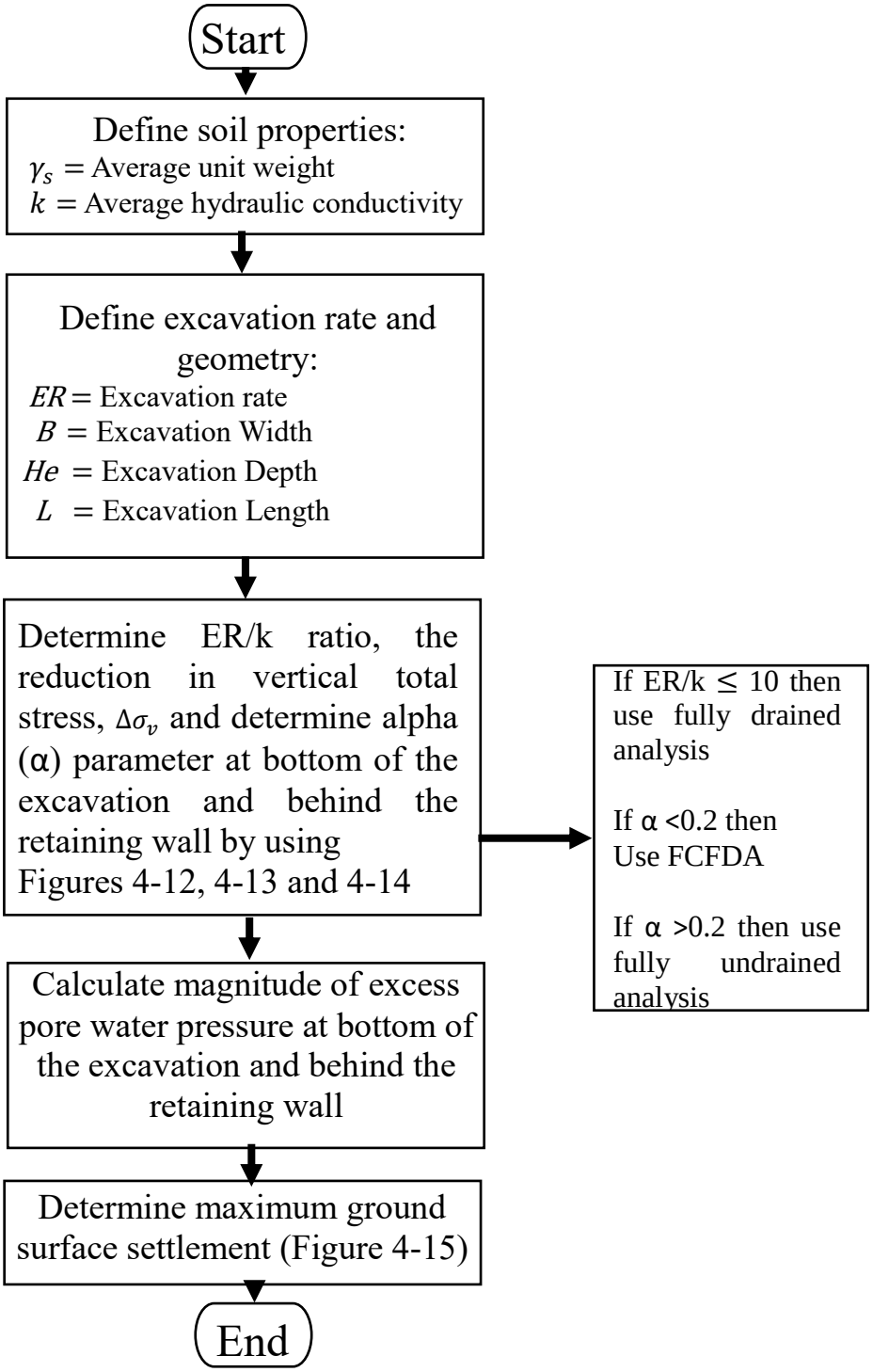

Figure 4-16 Flow chart for prediction excess pore water pressures at bottom of the excavation, behind the retaining wall, maximum surface ground settlements and selection for correct drainage analysis

The following steps, as illustrated in **Figure 4-16**, are proposed to guide the designer in the definition of the drainage conditions under which the excavation must be modeled. The method is intended to predict the magnitude of excess pore water pressure generated at the bottom of the excavation and behind the retaining wall, as well as to yield expected ground surface settlements related to the unloading process:

Step 1. Define basic soil properties: For each of the soil strata, determine the unit weight, γs, and hydraulic conductivity, *k*. for stratified soils, perform a weighted average using the thickness of each stratum in the area of influence in the excavation.

Step 2. Define the geometry of the excavation: Define the final excavation depth, H_e, and plan dimensions, i.e., width, B, and length, L.

Step 3. Define the rate of excavation, ER: Based on the experience of the local excavation contractors, estimate the average progress rate that the work will have until reaching the final level of the excavation.

Step 4. Determine the ER/k ratio, the reduction in the vertical total stress associated with the entire excavation depth, $\Delta\sigma_v$; and use **Figure 4-12**, **Figure 4-13** or **Figure 4-14** to calculate the alpha parameter based on the B/H_e geometry ratio of your excavation.

Step 5. Based on the alpha parameter calculated and/or the ER/k ratio, defined the drainage conditions under which the excavation is executed.

Step 6. Based on the alpha value and the reduction in the vertical total stress associated to the entire soil depth excavated, calculate the magnitude of the excess pore pressure generated in each of the locations (i.e. below the excavation bottom and behind the retaining wall system).

Step 7. Once the value of alpha (at the bottom of the excavation) is determined, use **Figure 4-15** to calculate the expected maximum ground surface settlement taking into account the stiffness of the retaining wall (i.e. very flexible walls such us sheet pile walls or medium stiff walls like tangent pile walls).

The proposed method is intended to be used as a first approach to determine the appropriate drainage condition under which an excavation process must be simulated (i.e. fully drained, partially drained or fully undrained). It also helps to stablish the necessary conditions for a correct implementation of the fully coupled flow-deformation method or under which circumstances a simplified analysis for

limit drainage conditions (i.e. fully drained or fully undrained analysis) is reliable for accurate numerical predictions.

It is important to mention the assumptions and limitations of the proposed method, specifically, those related to the numerical models used for the parametric analysis, in order to clarify the necessary conditions for its correct implementation. The most important assumption or limitations to consider are:

- Fully saturated soils are considered in all the numerical models. Unsaturated soil conditions were not evaluated herein.
- The entire subsurface stratigraphy was modeled as a soft to medium, over consolidated clay deposit. Different soil types and clay consistencies are not included in the proposed method.
- Load surcharges inside the influence zone of the excavation were not taken into account in the numerical models.
- The stiffness of the excavation support system was limited to only two types of typical retaining walls (i.e. sheet pile walls and tangent pile walls).
- The numerical models assumed the installation of the retaining wall system as "wish into place." Deformations due to this construction activity were not considered.
- Site specific geotechnical problems and construction incidents significantly influence the performance of an excavation. This features as mention before are very specific and were not addressed in the parametric study.

5. VALIDATION WITH EXCAVATION CASE HISTORIES

This chapter presents the validation of the proposed charts and method against 11 worldwide projects including urban excavations and physical scale models (i.e. geotechnical centrifuge models) reported in the technical literature. The case histories are located mainly in Boston, Taipei, Shanghai, Cambridge, and Chicago. **Table 5-1** lists the cases histories used, the parameters necessary (hydraulic conductivity, *k*, soil unit weight,γ_s, rates of excavation, ER, excavation depth, H_e, excavation width, *B*, and type of retaining wall system) to estimate the excess pore water pressures and settlements based on the proposed method. Each case history included a monitoring program composed of piezometers at the bottom of the excavation and/or behind the retaining wall system, inclinometers and surface settlement points. **Table 5-2** lists the calculated parameters, i.e., the excavation rate to permeability ratio, ER/k, the reduction in the vertical total stress associated with the entire excavation depth, $\Delta\sigma_v$, and the alpha values estimated based on the reported data. **Table 5-3** lists the measured excess pore water pressures at both locations according to the available data for each case (i.e. below the bottom of the excavation and behind the retaining wall system), and the maximum ground surface settlement normalized against the excavation depth reported in the literature technical. Also included in the table are the excess pore water pressures and the normalized settlements predicted from the proposed charts. A general description of each case history is presented in Appendix A.

Table 5-1. Excavation case histories: geometry, soil properties, support system and excavation characteristics

#	Case History	Input Data						
		Reference	**Wall type**	**k [m/day]**	**ER [m/day]**	**B [m]**	**He [m]**	**γ_s [kN/m3]**
1	ASC	Rounainia et al 2017	TPW	2.59×10^{-5}	0.51	100	14	19.0
2	NECP	Liao et al. 1997	TPW	9.50×10^{-5}	0.21	43	19.7	18.0

3	BL-12	Hsiung 2002	TPW	9.50×10^{-5}	0.59	20	19.2	15.2
4	POS	Whittle et al. 1993	TPW	1.80×10^{-2}	0.08	61	21	19.6
5	LYP	Ng 1992	TPW	2.60×10^{-5}	0.18	45	9.34	20.0
6	NEMCS	Jaworsky 1973	TPW	4.32×10^{-5}	0.35	21.4	15.7	19.0
7	YRS	Liu et al. 2005	TPW	8.64×10^{-4}	2.58	17.4	15.5	15.0
8	HDR-4	Finno et al. 1991	SPW	1.00×10^{-5}	0.37	12.2	12.2	19.0
9a	CATP – N	Whelan 1995	TPW	2.00×10^{-3}	1.19	61.0	12.3	17.4
9b	CATP – S	Whelan 1995	SPW	2.00×10^{-3}	0.87	61.0	11.1	17.6
10	GCM – UK	Lam et al. 2014	TPW	1.00×10^{-5}	0.12	7.20	5.40	16.5
11	GCM-TK	Takemura et al. 1999	SPW	1.73×10^{-4}	0.17	14.0	5.0	17.0

Table 5-2. Excavation case histories: estimated parameters for the implementation of the proposed method

#	Case History	Estimated Parameters			
		ER/k	$\Delta\sigma_v$[kPa]	**Alpha parameter (α)**	
				Bottom	Behind
1	ASC	1.95×10^{4}	277.4	0.50	-
2	NECP	2.29×10^{3}	354.6	0.32	0.05
3	BL-12	6.24×10^{3}	291.6	0.26	0.05
4	POS	4.31	411.6	-	1×10^{-4}
5	LYP	6.80×10^{3}	186.80	0.48	0.13
6	NEMCS	8.12×10^{3}	299.04	0.34	0.12
7	YRS	2.99×10^{3}	232.5	0.20	-
8	HDR-4	4.5×10^{4}	231.80	-	0.12
9a	CATP – N	4.94×10^{2}	214.5	0.4	0.04
9b	CATP – S	3.59×10^{2}	195.18	0.36	0.04
10	GCM – UK	1.21×10^{4}	89.0	0.36	0.12
11	GCM-TK	9.65×10^{2}	85.0	0.34	0.06

Table 5-3. Excavation case histories: measured and predicted excess pore water pressures and settlements

#	Case History	E.P.W.P bottom [kPa]		E.P.W.P behind wall [kPa]		% $\delta v_{(max)}$ / He	
		Predicted	**Measured**	**Predicted**	**Measured**	**Predicted**	**Measured**
1	ASC	138,7	133,3	-	-	0,14	0,2
2	NECP	113,47	110	17,73	13	0,14	0,4
3	BL-12	75,8	78,4	14,58	19,6	0,15	0,52
4	POS	-	-	4,11	4,9	0,19	0,2
5	LYP	89,7	93,1	24,3	29,4	0,11	0,06
6	NEMCS	101,7	107,8	35,88	39,2	0,06	0,076
7	YRS	46,5	49	-	-	0,06	0,07
8	HDR-4	-	-	27,81	24	0,14	2,1
9a	CATP -N	85,8	93,1	8,6	9,8	0,05	1,14

9b	CATP -S	70,3	78,4	7,81	14,7	0,14	0,9
10	GCM-UK	32	40	10,68	10	0,14	0,56
11	GCM-TK	28,9	37	5,1	10	0,14	3

Figure 5-1 shows predicted versus measured excess pore water pressures at the bottom of the excavation and behind the retaining wall for each excavation case history. The figure also includes the bounds for 95% prediction intervals. A good correlation between predicted and observed responses is noted in the figure with all of the case histories falling inside the 95% prediction band interval. The standard error, SE, was just 5.25 kPa and the coefficient of determination, R^2, calculated as the square of the Pearson correlation coefficient and the coefficient of Multiple-R-squared , ${R_o}^2$ (= 0.944), was equal to 0.988, indicating a very good correlation of proposed method with the measure data. Appendix B presents the statistical analysis performed to evaluate the predicting performance of the proposed method.

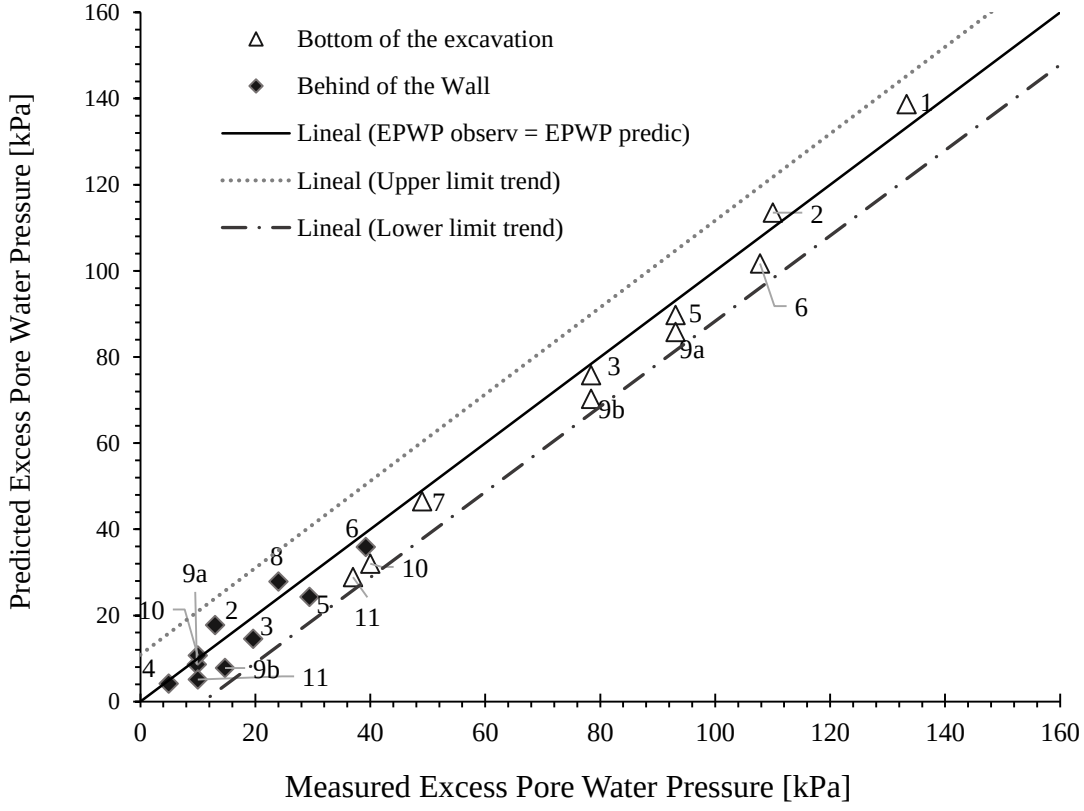

Figure 5-1 Performance of the proposed method for the Excess pore water pressures prediction, and bounds of 95% prediction interval.

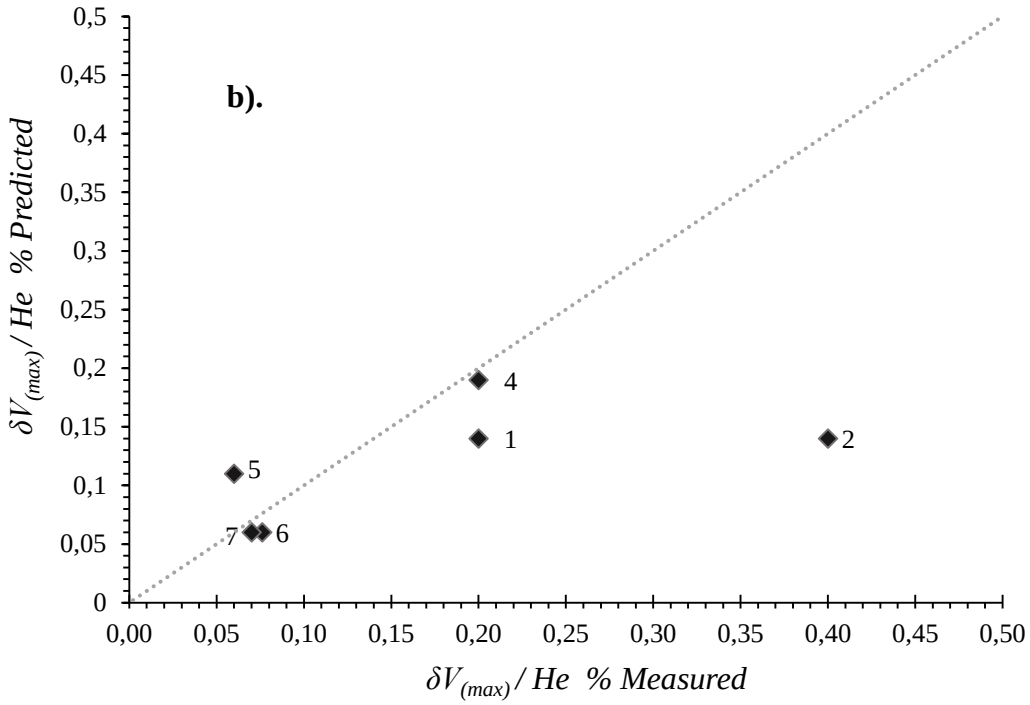

Figure 5-2 Performance of the proposed method for the maximum ground surface settlements prediction a). All case histories. b). Similar conditions cases histories

presents predicted versus measured maximum ground settlements at the end of excavation for each cases history. The ground settlement values are normalized with respect to the height of the excavation. Unlike the predictions for excess pore pressures, settlement predictions, approximately 60% of the data (cases, 3, 8, 9a, 9b, 10 and 11), highly underestimate the field measurements. The major discrepancy between the predicted ground surface settlements against the measured in the cases histories mention above can be explained due to the major differences found between each specific case history and the conditions assumed in the numerical models made in the performed parametric analysis. The most important differences in the presented cases histories, regarding the conditions under which the numerical models were executed can be summarized as: A). Although the soil profile in all of the cases present similar conditions to those assumed in the parametric analysis and the water table was found around the same depth from the assumed, it should noticed that for cases 8 and 9, the first soil stratum (i.e. strata of fill layers) on which the excavation is executed (i.e. around 40 to 50% of the excavation height) presented a completely different behavior from the assumed soil in the parametric analysis. B).All of the cases, with the exception of the physical scale models, presented nearby infrastructure that can be considered as a load surcharges inside the influence zone of the excavation that was not taken into account in the modeling process

C). Finally in the majority of the cases (60%) the depth of the excavation is considerably deeper than the assumed in the models, also in case 3 a specific site condition was founded that was not assumed in the numerical models, the pore pressure before the excavation was not initially hydrostatic due to previous pumping process from deep aquifers in the area of interest. Note also that the values with larger dispersion were obtained from cases 10 and 11 corresponding to physical scale models, which are known to be susceptible to errors in the measuring instruments (Takemura et al.1999). Due to the large number of numerical models performed (138 in total), a complete parametric study taking into account the above mentioned variables in a fully couple flow deformation analysis was not possible.

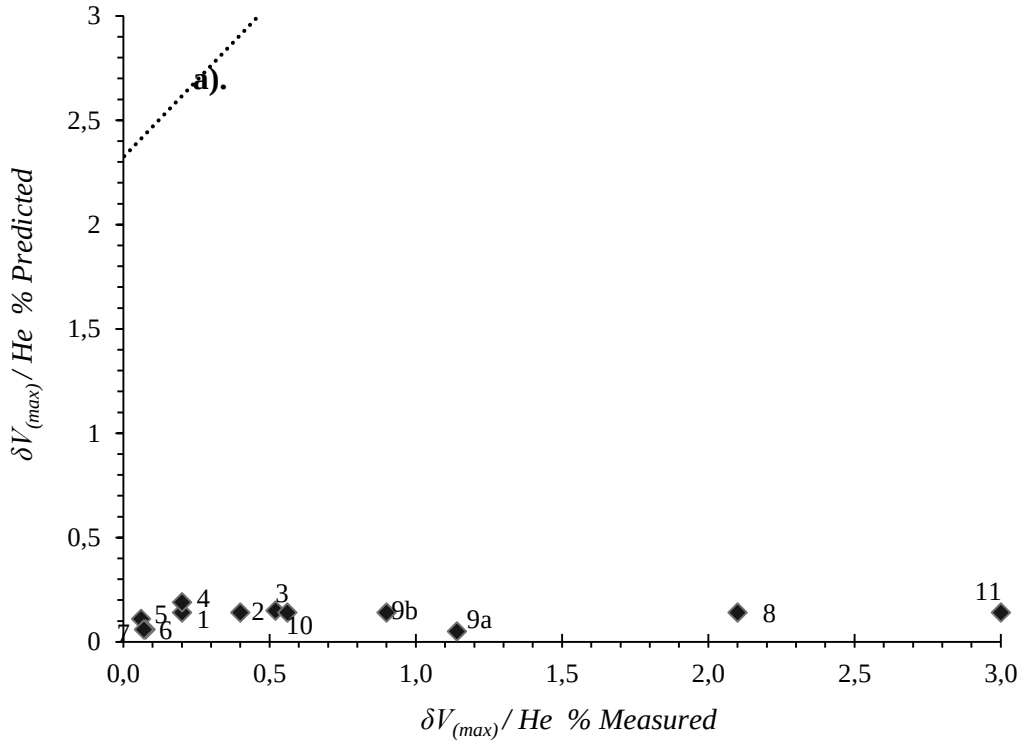

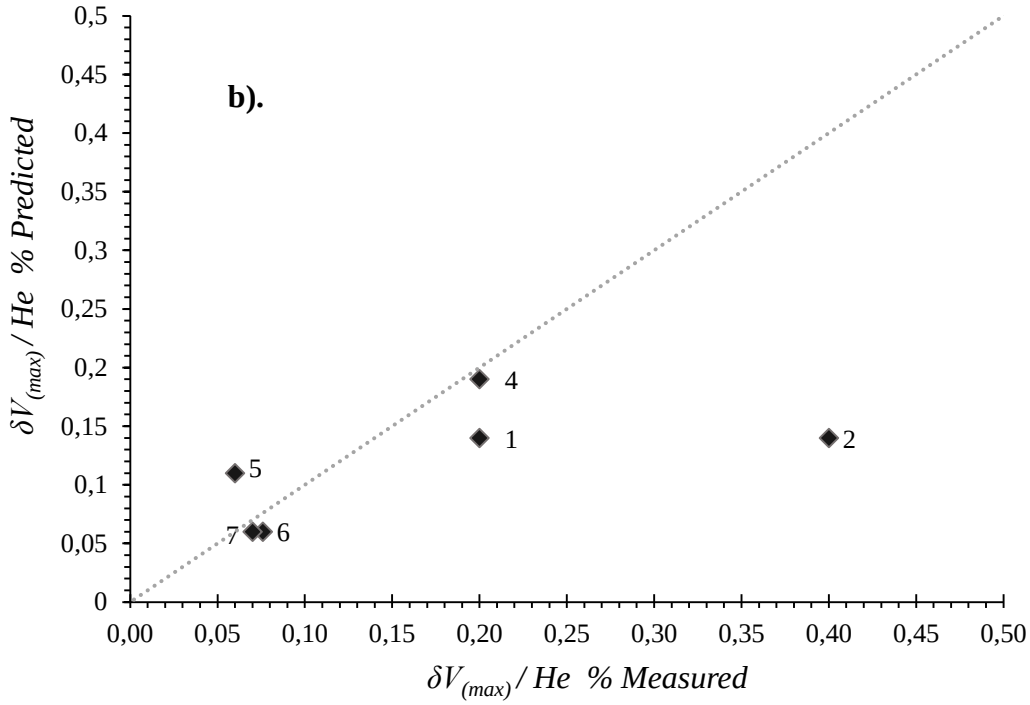

Figure 5-2 Performance of the proposed method for the maximum ground surface settlements prediction a). All case histories. b). Similar conditions cases histories

6. CONCLUSIONS AND RECOMMENDATIONS

6.1 Summary

This research work presented a method to define the drainage condition that most likely will take place during an excavation process. Guidelines to define the applicability of fully drained and undrained cases were given. Special focus was given to define the cases were the implementation of fully coupled flow-deformation analyses was essential for an accurate modeling of excavation in soft to medium clays. This research work is believed to be the first attempt to employed advanced finite element modeling of a generalized excavation where soil consolidation and non-linear soil behavior were simulated via fully couple flow-deformations analyses along with the advanced hypoplasticity clay model that accounts for stress history and small strain behavior. The proposed design charts were based on a parametric study conducted to evaluate the effects on excess pore pressures and ground surface settlements of variations in excavation rates, hydraulic conductivity of the soil, excavation geometry and support system stiffness. The proposed method was validated against field performance data (i.e. ground surface settlements and excess pore water pressures) collected from 11 different excavation case histories around the world.

6.2 Conclusions

Based on the parametric study, the validation process against excavation cases histories, and a detailed review of the technical literature, the main conclusions of this research work are:

- The drainage conditions that take place during excavation activities are mainly function of the hydraulic conductivity of the soil and the excavation rate. Two parameters that can be easily measured and defined. When the excavation rate is 4 orders of magnitude larger than

the hydraulic conductivity of the soil, an undrained condition is reached. In contrast, drained conditions are achieved for excavation rates at least 1 order of magnitude larger than the hydraulic conductivity of the soil. For excavation projects conducted in soft to medium fully saturated clays where the hydraulic conductivity of the soil is in the range of $1.16x10^{-3}$ cm/s to $1.16x10^{-7}$ cm/s, the excavation rates required to reach fully drained and undrained conditions for the lowest permeability are unrealistic ($1x10^{-3}$m/day and 1m/day, respectively) and consequently, partially drained conditions prevailed. It emphasizes the importance of implementing fully coupled flow deformation analyses to properly estimate excavation-induced ground deformations.

- For the range of soil hydraulic conductivities evaluated ($1.16x10^{-3}$ to $1.16x10^{-7}$ cm/s), it was found that by maintaining a constant ratio of excavation rate to hydraulic conductivity (ER/k), the magnitude and distribution of excavation-induced surface settlements is very similar. Additionally, for ER/k ratios larger than 10^2, very similar results, in terms of ground surface settlements, are obtained in comparison to the fully undrained case. This finding indicates that a simplified fully undrained analysis will suffice to correctly estimate excavation-induced ground movements as long as the expected ER/k ratio stays larger than 10^2. The same behavior is observed in terms of the pore water pressure parameter alpha. Although some excess pore water dissipation is expected for values of alpha larger tan 0.2 (i.e., ER/k ratios larger than 200), a fully undrained simulation would yield essentially the same ground settlements as a fully couple flow deformation model.

- The proposed model is accurate to estimate the magnitude of excess pore water pressures arising from excavation activities in soft to medium clays. The validation procedures against case history data showed that the design charts predict well excess pore pressures at the excavation bottom and behind the retaining wall during the several stages of the excavation process. Larger discrepancies were obtained for the predictions of ground surface settlements, with the proposed method highly underestimating the observed case history settlements. The differences are attributed to the fact that ground movements around excavations are affected by specific construction techniques, specific geotechnical site conditions, wall installation, concrete time-dependent effects, support system stiffness and other features no considered in this research effort.

Additionally, this research work confirmed tendencies or findings already reported in the technical literature. Among them are:

- The alpha parameter describes a unique relationship with the geometry of the excavation (i.e., ratio between width and height of the excavation). For the soil mass located below the excavation bottom, α increases for values of B/H_e lower than 10. For larger ratios, alpha does not increase. On the other hand, for the soil mass located behind the retaining wall, α is less variable. It basically remains constant as the excavation geometry changes.

- The change in the pore water pressure due to the vertical stress relief inside the excavation is larger at the excavation bottom than behind the retaining wall. For the cases with a faster excavation rate, values of alpha at the bottom of the excavation were larger than 0.6, while for the location behind the retaining wall, the effects of the vertical stress reduction were very small and values of α less than 0.2 were obtained.

6.3 Recommendations

- The proposed design charts should be used only in the preliminary stages of the excavation design to define the required drainage conditions of the analysis and to roughly estimate excavation-induced pore water pressures. If ground movements around the excavation site are a concern, a proper soil exploration and testing program should be implemented to feed detailed numerical simulations of the specific project geometry, construction sequence and workmanship.

- Future research is required to assess the behavior of unsaturated soils under the conditions studied in this work and to establish the conditions for the implementation of fully couple flow deformations analyses under these circumstances.

- The implementation of a geotechnical monitoring system that allows to measure pore water pressures in real time must become standard practice in excavation projects and other geotechnical applications. Excess pore water pressure is closely related to soil strength and can yield valuable information related to soil failure and excessive ground deformations.

APPENDIX A

This chapter contains a general description of each one of the 13 historical cases studied for the validation process, that is, name and city of the project, geometry of the excavation (i.e. large, width and depth), the stratigraphic soil profile, the retaining wall system, the geotechnical monitoring system, the significant differences of one each of these projects with the assumptions made in the numerical models and the input values required for the implementation of the method

A.1 Allston Science Complex, Boston (Rouainia et al., 2017) – Case 1

The site of the Allston Science Complex is located in Boston, Massachusetts at Harvard University in Western Avenue, it is a project composed by four buildings containing up to eight storeys that currently is under construction however the excavation for the projected two story basement was already executed. The case study is a 14.6 m deep, and 100 m wide basement, a major in situ test program including SPT, SCPTU, SBPT and field vane testing was executed for collecting data of the ground conditions. The groundwater table was encountered at 2.0 m below ground surface, the stratified sequence of the soil profile is composed by successive strata of made ground, alluvium deposits, sandy gravel, the Boston Blue Clay (BBC) marine clay, glacial till and the Cambridge argillite bedrock. The excavation retaining system is composed by two different types of wall, a diaphragm wall and a soldier pile tremie concrete wall, both of them were designed to resist the soil and water pressure with four rows of tiebacks, **Figure A-1** shows the soil profile, the support system and the excavation stages. The geotechnical monitoring system was composed by vibrating wire piezometers installed with depth across the site, surface settlement markers and inclinometers embedded within the retaining wall.

The most important differences presented in the presented case history, regarding the conditions under which the numerical models were executed can be summarized as: A). Although the behavior of the excavation will be controlled by the stratum BBC due to its significant thickness, more of the 30% of the total depth of the excavation (about 5.0 m below ground level) are in soils that will

present a completely different behavior from the used soils in the numerical models. B) The excavation retaining system is expected to have a greater stiffness than the modeled ones due to the implementation of four rows of tiebacks. C). It should be noted that the depth of the excavation is greater than assumed in the models, however the difference is not of excessive magnitude, then it could be assumed that the case history under study is an excavation of similar characteristics from the numerical models performed. **Table A-1** shows the resume of the input parameters obtain from the data analysis of the case history necessary in the implementation of the method, additionally present the results of all the essential parameters in order to obtain the method predictions and the results obtained from geotechnical instrumentation.

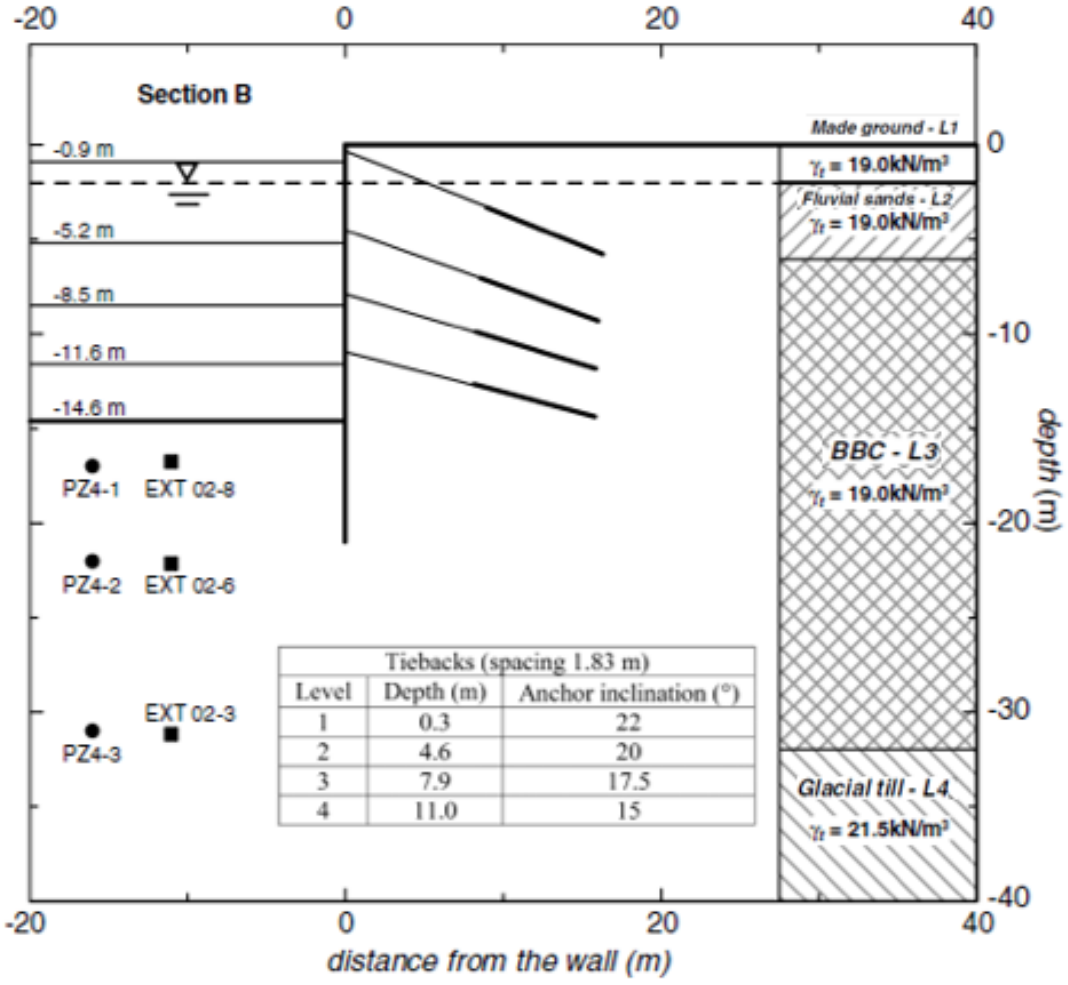

Figure A-1 Characteristics of the excavation support system, soil profile and excavation stages for the Allston Science Complex (Rouainia et al., 2017)

It is worth to mention that there are no data available of excess pore water pressures behind the retaining wall because piezometers were not installed at these locations. So no predictions were made for these variable.

Table A-1. Resume of input data and results for the proposed method at the ASC case

Input Data		Parameter Estimated		Output Data		Measured Data	
He [m]	14.6	ER/k	$1.95x10^4$	Ue [kPa]	138.7	Ue [kPa]	133.3
B [m]	100.0						
γ_s [kN/m3]	19.0	α_{bottom}	0.50				
k [m/day]	$2.59x10^{-5}$						
ER [m/day]	0.506	σ_v[kPa]	277.4	% $\delta v_{(max)}$./He	0.14	% $\delta v_{(max)}$./He	0.20
Wall Type	TPW						

A.2 Enterprise Center Project, Taipei (Liao and Ou, 1997) – Case 2

The site of the enterprise center project is located in Taipei, at the intersection on Nanking Eats Road and San – Ming Road, Sun Shan district of Taipei city, it's an eighteen storeys building with five levels for the basement. The excavation studied have the following dimensions, 19.7 m depth, 43.0 m wide and a varying length between 60.0 m and 105.0 m. Is important to mention that the method of excavation implemented was ¨Top-Down¨ (i.e. the superstructure and the underground structure is constructed simultaneously). In order to establish the soil profile and properties field tests as Standard penetration tests (SPT), Piezo cone penetration tests (PCPT) and Vane tests (VT) combined with laboratory tests were executed. The major soil strata at the site is the Sung – Shan formation, essentially the stratified sequence is composed by a thicker clay with a thinner sand layer, the ground water level was found at 2 m below the ground surface. The excavation retaining system is composed by a perimeter diaphragm wall of 90cm thick and 35 m deep, two levels of temporary steel props and five levels of concrete slabs were established to provide the lateral support before the end of the excavation. The geotechnical monitoring system was composed by piezometers (it can be seen that the pore pressure in this case at both excavated and retaining side were monitored), inclinometers, extensometers and settlement points. **Figure A-2** shows the soil profile, the support system, the excavation stages and the location of the geotechnical monitoring system.

The most important differences presented in the presented case history, regarding the conditions under which the numerical models were executed can be summarized as: A). It should be noted that the depth of the excavation is considerably deeper than the assumed in the models, its more than double the maximum depth modeled, nevertheless the soil profile present similar conditions to those assumed in the parametric analysis, additionally its worth to mention that the excavation method adopted in the case under study (Top-down excavation method) is very similar to the excavation

process assumed in the performed parametric analysis, then it could be assumed that the case history under study is an excavation of similar characteristics from the numerical models performed.

Table A-2 shows the resume of the input parameters obtain from the data analysis of the case history necessary in the implementation of the method, additionally present the results of all the essential parameters in order to obtain the method predictions and the results obtained from geotechnical instrumentation.

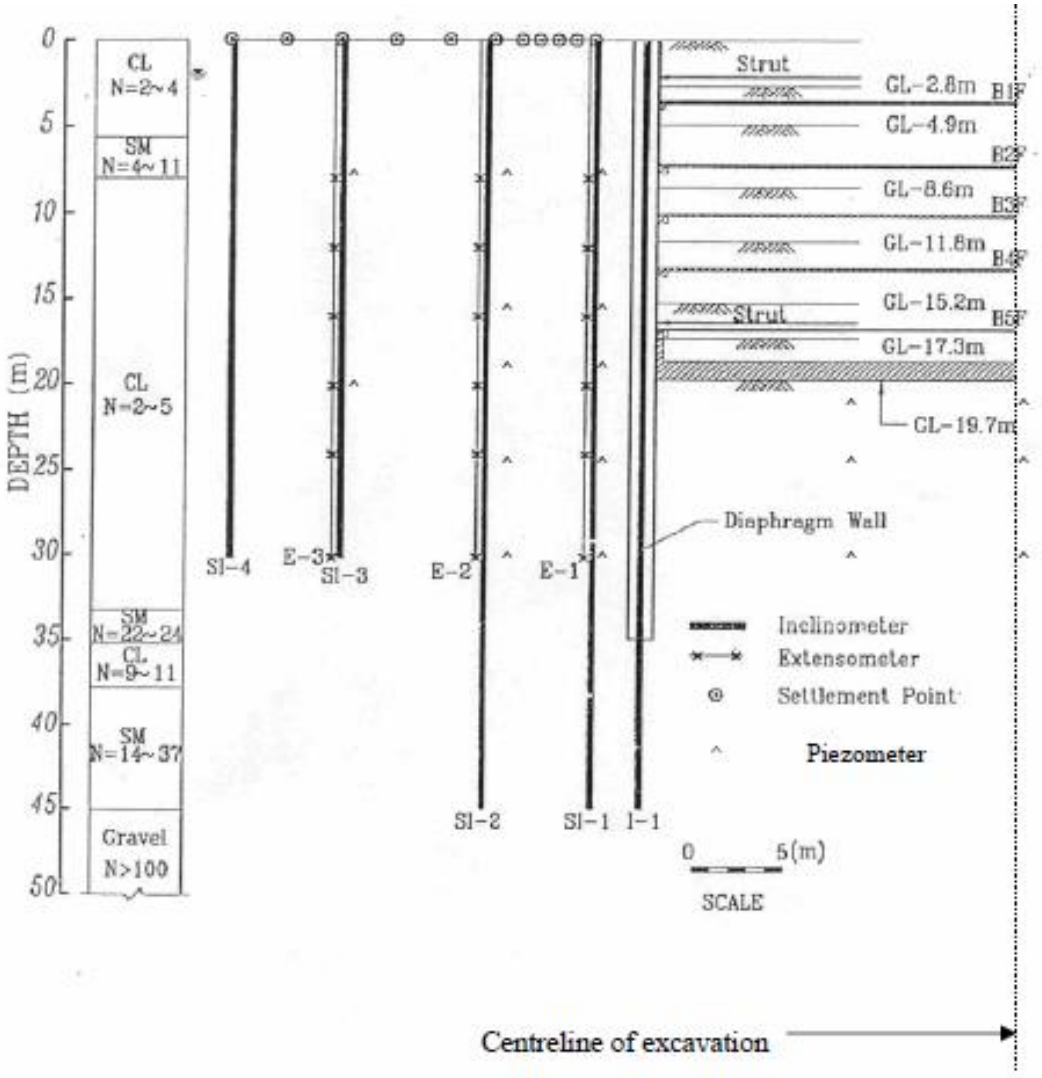

Figure A-2 Characteristics of the excavation support system, soil profile, monitoring system and excavation stages for the National Enterprise Center Project (Liao and Ou, 1997).

Table A-2. Resume of input data and results for the proposed method at the NECP case

Input Data		Parameter Estimated		Output Data		Measured Data	
He [m]	19.7	ER/k	$2.29x10^3$	Ue bottom[kPa]	113.5	Ue bottom[kPa]	110.0
B [m]	43.0						
γ_s [kN/m3]	18.0	α_{bottom}	0.32	Ue behind [kPa]	17.73	Ue behind [kPa]	13.0
k [m/d]	$9.50*10^{-5}$	α_{behind}	0.05				
ER [m/d]	0.21	σ_v[kPa]	354.6	% $\delta v_{(max)}$./He	0.14	% $\delta v_{(max)}$./He	0.40
Wall Type	TPW						

A.3 Sun Yat-Sen Memorial Hall Station, Taipei (Hsiung, 2002) – Case 3

The site of the Dr. Sun Yat-Sen Memorial Hall (BL12) Station is located in Taipei, at the junction of the Chung – Hsiao East Road and Kung – Fu South Road and is part of the phase 1 of the rapid transit system in Taipei, Taiwan. The length and width for the excavation studied are 256.0 m and 20.0 m respectively and 16.2 m of depth, and its structure is composed by a two level reinforced concrete box. Is important to mention that the method of excavation implemented was ¨semi – bottom - up¨. Due to the major strata in the area was the well-known Sung-Shan Formation, in order to establish the soil profile and properties only Standard penetration tests (SPT) were executed in the field soil investigation program, however a more detail laboratory test program was realized in order to obtain an accuracy profile of the undrained shear strength. A perched water level was encountered between 1.0 – 2.0 m below the ground surface level. The excavation retaining system is composed by a perimeter diaphragm wall of 1.0 m thick and 33 m deep, excavation was first made to reach the level of the 1.5 m. thick roof slab which provides permanent support to the diaphragm walls preventing cantilever movements, then the excavation was continued to full depth, with five levels of steels props that provide temporary lateral support, before the station box was completed, The geotechnical monitoring system was composed by open stand pipes and electrical piezometers (it can be seen that the pore pressure in this case at both excavated and retaining side were monitored), inclinometers, permanent bench markers, vibrating wire strain gauges and load cells. **Figure A-3** shows, the support system, the excavation stages and the location of the geotechnical monitoring system.

The most important differences presented in the presented case history, regarding the conditions under which the numerical models were executed can be summarized as: A). Using the site data obtain it can be noticed that the pore pressure before the excavation was not initially hydrostatic due

to previous pumping process from deep aquifers in the area of interest. B). the project present several nearby buildings causing surcharge loads that were not considered in the numerical modeling process. C). It should be noted that the depth of the excavation is considerably deeper than the assumed in the models, its more than double the maximum depth modeled, nevertheless the soil profile present similar conditions to those assumed in the parametric analysis, additionally its worth to mention that the excavation method adopted in the case under study (semi bottom-up excavation method) is in good agreement with the excavation process assumed in the performed parametric analysis, then it could be assumed that the case history under study is an excavation of similar characteristics from the numerical models performed.

Table A-3 shows the resume of the input parameters obtain from the data analysis of the case history necessary in the implementation of the method, additionally present the results of all the essential parameters in order to obtain the method predictions and the results obtained from geotechnical instrumentation.

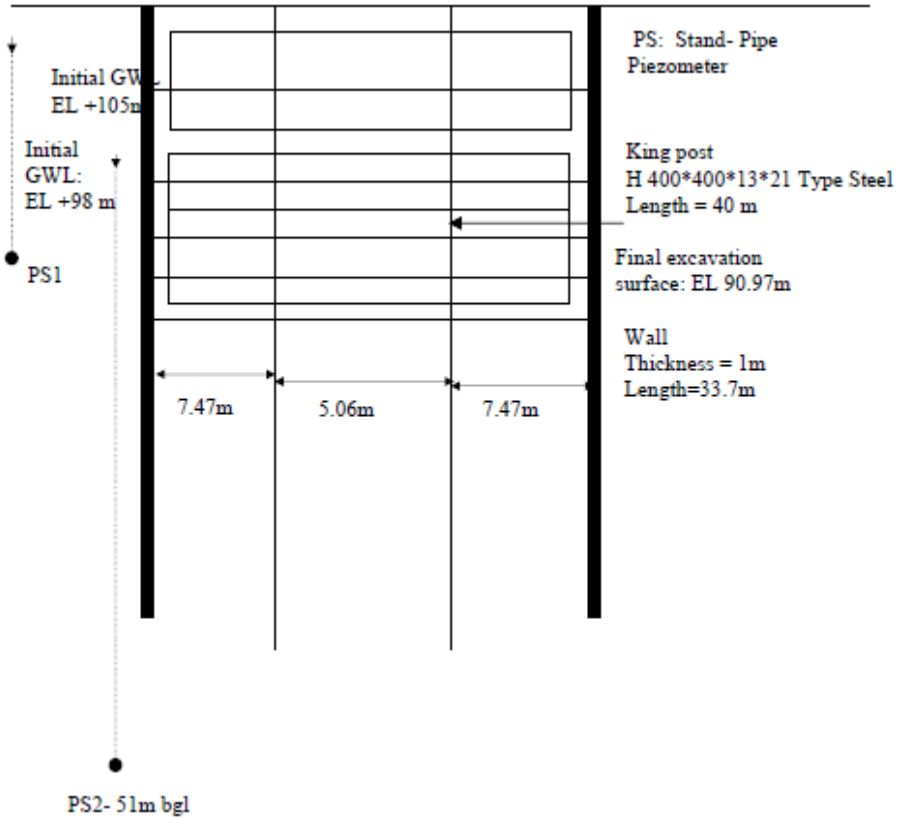

Figure A-3 Characteristics of the excavation support system, monitoring system and excavation stages for the Sun Yat-Sen Memorial Hall Station (Chin et al., 1994)

Table A-3. Resume of input data and results for the proposed method at the BL-12 case

Input Data		Parameter Estimated		Output Data		Measured Data	
He [m]	19.2	ER/k	$6.24x10^3$	Ue bottom[kPa]	75.8	Ue bottom[kPa]	78.4
B [m]	20.0						
γ_s [kN/m3]	15.2	α_{bottom}	0.26	Ue behind [kPa]	14.58	Ue behind [kPa]	19.60
k [m/d]	$9.50x10^{-5}$	α_{behind}	0.05				
ER [m/d]	0.59	σ_v[kPa]	291.6	% $\delta v_{(max)}$./He	0.15	% $\delta v_{(max)}$./He	0.52
Wall Type	TPW						

A.4 Post Office Square Garage, Boston (Whittle et al., 1993) – Case 4

The site of the parking garage at post office square (POS) is located in Boston, Massachusetts at the intersections of Pearl, Congress, Milk and Franklin Streets, the excavation was made for a seven storeys, underground parking garage for the POS. The length and width for the excavation studied are 116.0 m and 61.0 m respectively and 21.0 m of depth. Is important to mention that the method of excavation implemented was ¨Top-Down¨ (i.e. the superstructure and the underground structure is constructed simultaneously).The subsurface stratigraphy was interpreted from a field test program composed by 15 borings as well as a detail laboratory test program, the groundwater table was encountered at 2.5 m below ground surface, the stratified sequence of the soil is in agreement with the typical weathering profiles of the glacial geology in the Boston area, composed by successive strata of fill layers, the Boston Blue Clay (BBC) marine clay, dense sand, glacial till and the Cambridge argillite bedrock. The excavation retaining system is composed by a perimeter diaphragm wall of 0.9 m thick and 25.6 m deep, excavation was made using the ¨Top-Down¨ method, the perimeter wall was internally braced by the floors slabs, dewatering was accomplished using deep wells located at the excavation side area. The field monitoring program was composed by open stand pipes piezometers installed one year prior construction, inclinometers cast within the wall and located close to the adjacent buildings, boreholes extensometers, optical survey monitoring surface settlements. **Figure A-4** shows, the support system, the excavation stages and the stratified soil profile.

The most important differences presented in the presented case history, regarding the conditions under which the numerical models were executed can be summarized as: A). Using the site data obtain it can be noticed that the pore pressure before the excavation was not initially hydrostatic due to previous pumping process from deep aquifers in the area of interest. B). The project present several nearby buildings up to 40 storeys causing significant surcharge loads that were not

considered in the numerical modeling process. C). It should be noted that the depth of the excavation is considerably deeper than the assumed in the models, its more than double the maximum depth modeled, nevertheless the soil profile present similar conditions to those assumed in the parametric analysis, additionally its worth to mention that the excavation method adopted in the case under study (Top-Down method) is in good agreement with the excavation process assumed in the performed parametric analysis, then it could be assumed that the case history under study is an excavation of similar characteristics from the numerical models performed. It is worth to mention that there are no data available of excess pore water pressures at the bottom of the excavation because piezometers were not installed at these locations. So no predictions were made for these variable.

Table A-4 shows the resume of the input parameters obtain from the data analysis of the case history necessary in the implementation of the method, additionally present the results of all the essential parameters in order to obtain the method predictions and the results obtained from geotechnical instrumentation.

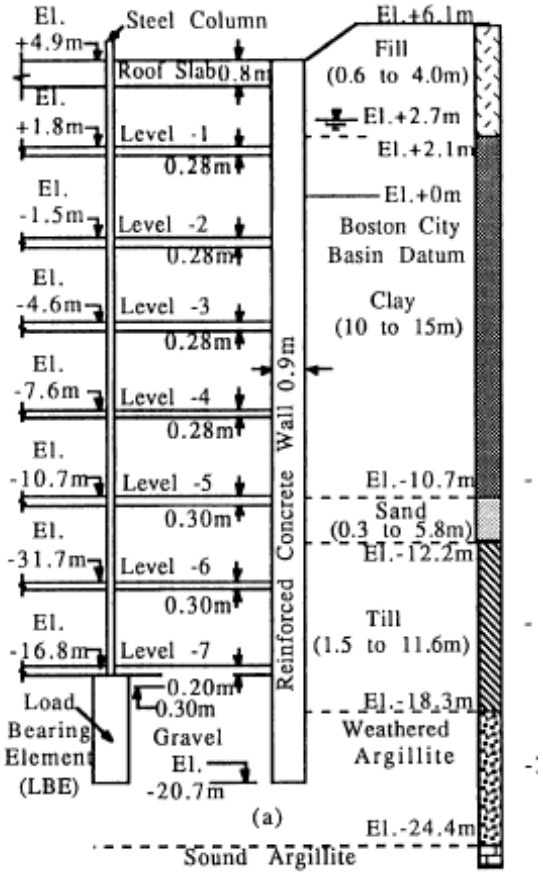

Figure A-4 Characteristics of the excavation support system, excavation stages and the stratified soil profile for the Post Office Square (Whittle et al., 1993)

Table A-4. Resume of input data and results for the proposed method at the POS case

Input Data		Parameter Estimated		Output Data		Measured Data	
He [m]	21.0	ER/k	4.31	Ue behind [kPa]	0.041	Ue behind [kPa]	19.60
B [m]	61.0						
γ_s [kN/m3]	19.6	α_{behind}	$1.0x10^{-4}$				
k [m/d]	$1.80x10^{-2}$						
ER [m/d]	0.08	σ_v[kPa]	411.6	% $\delta v_{(max)}$./He	0.19	% $\delta v_{(max)}$./He	0.20
Wall Type	TPW						

A.5 Lion Yard Development, Cambridge (Ng, 1992) – Case 5

The site of the Lion Yard Project (LYP) is located in Cambridge, London at the intersections of Downing Street, St Tibbs Row and Corn Exchange Street, the structure consists of a three level underground parking beneath a five storeys hotel. The length and width for the excavation studied are 65.0 m and 45.0 m respectively and 9.35 m of depth. Is important to mention that the method of excavation implemented was ¨Top-Down¨ (i.e. the superstructure and the underground structure is constructed simultaneously).The subsurface stratigraphy was interpreted from a field test program composed by SPT and self-boring pressuremeter tests SBPT, besides a detail laboratory test program, the groundwater table was encountered about 3.0 to 3.5 m below the existing ground surface, the stratified sequence is composed by successive strata of 3.0 m to 4.0 m of made ground above 38.0 m of Gault clay which overlays the lower Greensand. The excavation retaining system is composed by a perimeter diaphragm wall of 0.6 m thick and 17.0 m deep, excavation was made using the ¨Top-Down¨ method, the perimeter wall was internally braced by the floors slabs. A very extensive and detail field monitoring program was implemented in the project and was composed by earth pressure cells, electro level system (measure the rotation on the diaphragm wall), tape measurements (measured movement at the top of the wall), vibrating wire struts loads, rebar load cells (measured temperature in struts), extensometer system, settlement monitoring system, and a pneumatic piezometer system **Figure A-5** shows, the support system, the location of some of the monitoring instruments installed and the stratified soil profile.

The most important differences presented in the presented case history, regarding the conditions under which the numerical models were executed can be summarized as: A). The project present several nearby buildings causing surcharge loads that were not considered in the numerical modeling process. B). Although the behavior of the excavation will be controlled by the Gault clay stratum due to its significant thickness, more of the 40% of the total depth of the excavation (about 4.0 m below ground level) are in soils (made ground soils) that will present a completely different behavior

from the used soils in the numerical models , nevertheless the soil profile present similar conditions to those assumed in the parametric analysis, additionally its worth to mention that the excavation method adopted in the case under study (Top-Down method) is in good agreement with the excavation process assumed in the performed parametric analysis, then it could be assumed that the case history under study is an excavation of similar characteristics from the numerical models performed.

Table A-5 shows the resume of the input parameters obtain from the data analysis of the case history necessary in the implementation of the method, additionally present the results of all the essential parameters in order to obtain the method predictions and the results obtained from geotechnical instrumentation.

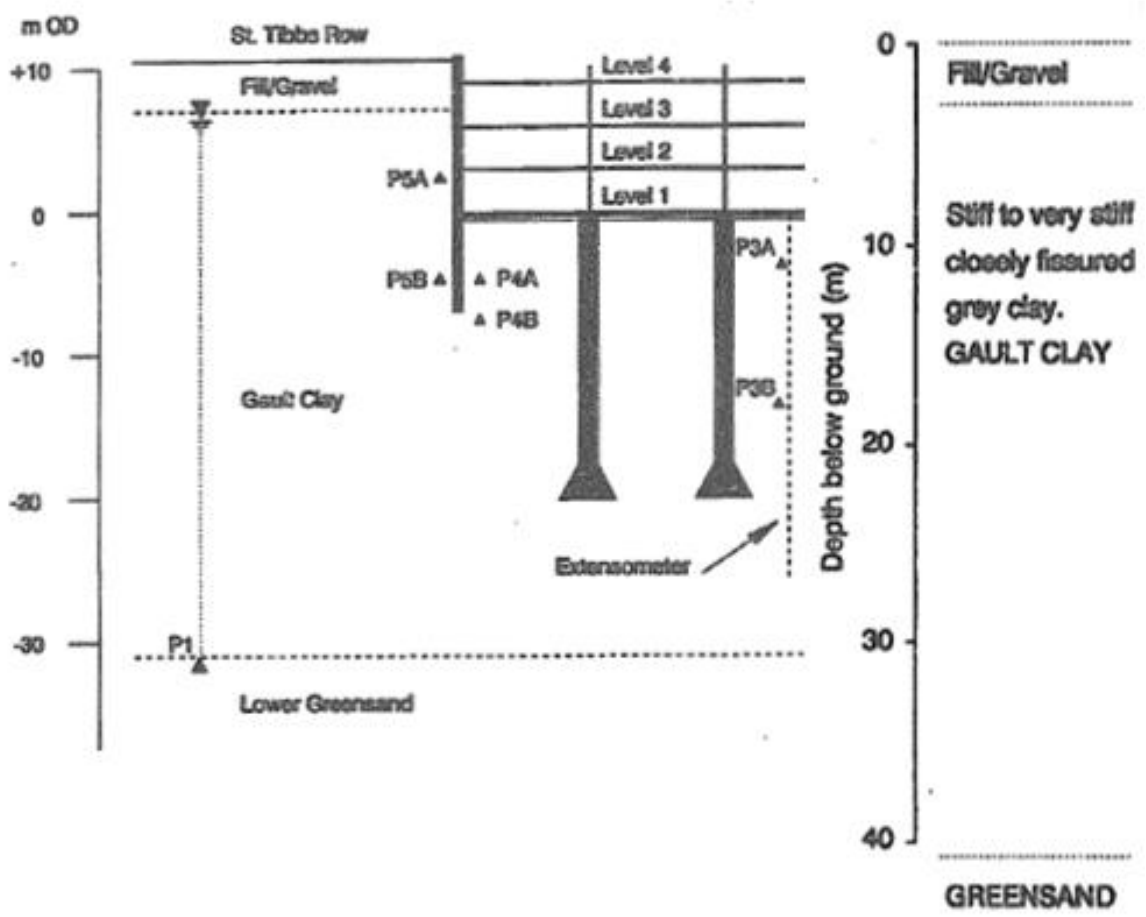

Figure A-5 Characteristics of the excavation support system, excavation levels and the stratified soil profile for the Lion Yard Project (Ng, 1992)

Table A-5. Resume of input data and results for the proposed method at the LYP case

Input Data		Parameter Estimated		Output Data		Measured Data	
He [m]	9.34	ER/k	$6.80*10^3$	Ue bottom[kPa]	89.7	Ue bottom[kPa]	93.1
B [m]	45.0						
γ_s [kN/m3]	20.0	α_{bottom}	0.48	Ue behind [kPa]	24.3	Ue behind [kPa]	29.4
k [m/d]	$2.60x10^{-5}$	α_{behind}	0.13				
ER [m/d]	0.18	σ_v[kPa]	186.80	% $\delta v_{(max)}$./He	0.11	% $\delta v_{(max)}$./He	0.06
Wall Type	TPW						

A.6 New England Medical Center Subway Station, Boston (Jaworsky, 1973) – Case 6

The site of the New England Medical Center Subway Station (NEMCS) is located in Boston, Massachusetts at South of the Downtown and is part of the Orange Line of the rapid transit system of the City, the station (the underground structure) has an overall length of 183.0 m, average excavation depth of 15.0 m and ranges in width between 18.0 to 24.0 m. Is important to mention that the method of excavation implemented was ¨semi – bottom - up¨ (i.e. removal of soil followed by the installation of struts). The subsurface stratigraphy was interpreted from a field test program composed essentially by field vane tests, besides a detail laboratory test program, the groundwater table was encountered about 5.2 m below the existing ground surface and a perched water table was detected within the fill at 1.5m, the subsurface profile is composed by 4 major layers: 2.5 m of fill (mainly cider ash) above 4.6 m of hard yellow clay overlaying the main deposit of Boston Blue clay which overlays the lower glacial till at depth of 32.0 m. The excavation retaining system was divided in two sections, the side near a school building is composed by a 60.0 m long diaphragm wall of 0.9 m thick and 24.4 m deep with three level of cross lot bracing, the remainder of the excavation, also supported by three levels of bracing, uses sheet pile walls. A very extensive and detail field monitoring program was implemented at the north east corner of the infrastructure in close proximity (less than 1.5m) composed by inclinometers (Wilson Slope indicators), a series of heave roads (monitoring soil deformation within the excavation zone), vibrating wire strain gauges and vibrating wire piezometers installed prior the construction of the retaining wall system at both locations, inside the excavation and behind the wall. **Figure A-6** shows, the support system, the location of some of the monitoring instruments installed and the stratified soil profile.

The most important differences presented in the presented case history, regarding the conditions under which the numerical models were executed can be summarized as: A). The project present

several nearby buildings up to seven storeys (Don Bosco Scholl Building) causing surcharge loads that were not considered in the numerical modeling process. B). Although the behavior of the excavation will be controlled by the Boston Blue Clay stratum due to its significant thickness, more of the 15% of the total depth of the excavation (about 3.0 m below ground level) are in soils (mainly cider ash) that will present a completely different behavior from the used soils in the numerical models, nevertheless the soil profile present similar conditions to those assumed in the parametric analysis. C). It should be noted that the depth of the excavation is considerably deeper than the assumed in the models, it's about the double the maximum depth modeled, nevertheless the soil profile present similar conditions to those assumed in the parametric analysis and the excavation method adopted in the case under study is in good agreement with the excavation process assumed in the performed parametric analysis, then it could be assumed that the case history under study is an excavation of similar characteristics from the numerical models performed

Table A-6 shows the resume of the input parameters obtain from the data analysis of the case history necessary in the implementation of the method, additionally present the results of all the essential parameters in order to obtain the method predictions and the results obtained from geotechnical instrumentation.

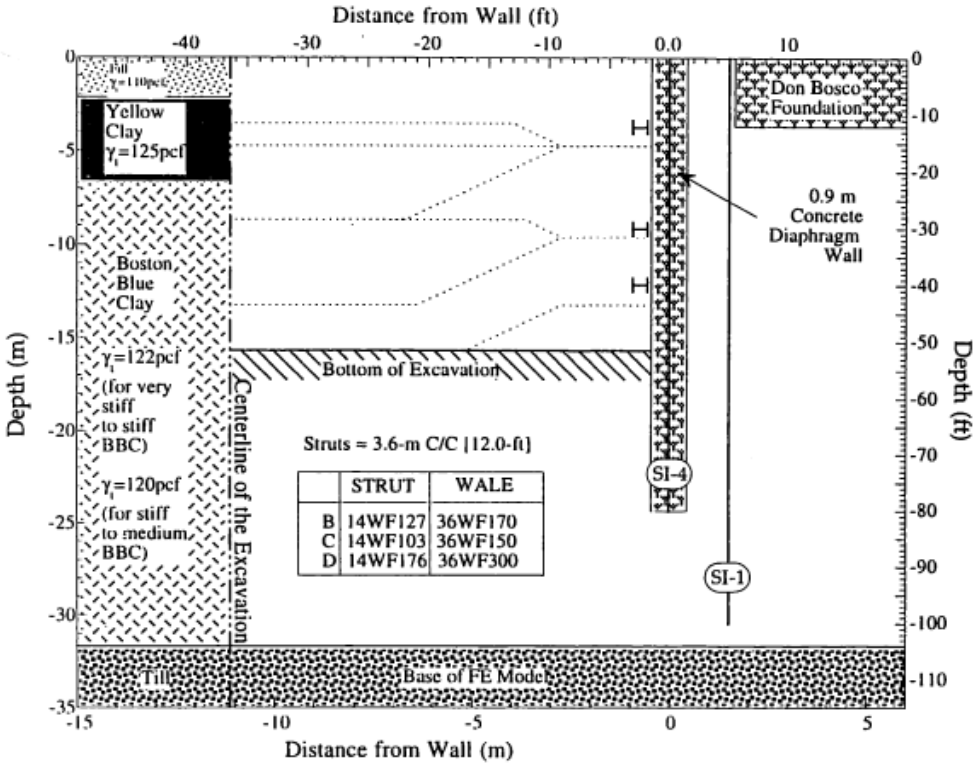

Figure A-6 Characteristics of the excavation support system, excavation levels and the stratified soil profile for the New England Medical Center Subway Station (Jaworsky, 1973)

Table A-6. Resume of input data and results for the proposed method at the NEMCS case

Input Data		Parameter Estimated		Output Data		Measured Data	
He [m]	15.70	ER/k	$8.12x10^3$	Ue bottom[kPa]	101.7	Ue bottom[kPa]	107.8
B [m]	21.40						
γ_s [kN/m3]	19.0	α_{bottom}	0.34	Ue behind [kPa]	35.88	Ue behind [kPa]	39.2
k [m/d]	$4.32x10^{-5}$	α_{behind}	0.12				
ER [m/d]	0.35	σ_v[kPa]	299.04	% $\delta v_{(max)}$./He	0.06	% $\delta v_{(max)}$./He	0.076
Wall Type	TPW						

A.7 Yishan Road Station, Shanghai (Liu et al., 2005) – Case 7

The site of the Yishan Road Subway Station (YRS) is located in Shanghai, China and is located in the southwest and is part of the Pearl Metro Line (rapid transit system in Shanghai), the station (the underground structure) has an overall length of 335.0 m, average excavation depth of 15.5 m and with 17.4 m of width. Is important to mention that the method of excavation implemented was ¨semi – bottom - up¨ (i.e. removal of soil followed by the installation of pre-stressed struts) besides the soil was improved by compacting grouting at passive zones of the excavation subsequent the construction of the retaining wall. The subsurface stratigraphy was interpreted from a field test program composed essentially by in situ vane shear tests, besides a detail laboratory test program, the groundwater table was encountered about 1.0 m below the existing ground surface, the subsurface profile is composed by 3 major layers: 2.5 m of fill, above a medium clay deposit of 2.5m, underlain by a thick, relatively soft to medium soft marine clay deposits between 5 and 18.0 m depth. The excavation retaining system was composed by of 0.6 m thick diaphragm wall and ranges in depth between 28.0 to 34.0 m depending in the vulnerability of the infrastructure nearby, in addition with five level of pre-stressed struts. A very extensive and detail field monitoring program was implemented composed by inclinometers casts within the retaining wall, surface markers, earth pressure cells and vibrating wire piezometers. **Figure A-7** shows, the support system, the location of some of the monitoring instruments installed and the stratified soil profile.

The most important differences presented in the presented case history, regarding the conditions under which the numerical models were executed can be summarized as: A). The project present several multistory residential houses founded on shallow foundations besides an adjacent light-rail line running parallel to the wall causing surcharge loads that were not considered in the numerical modeling process. B). Although the behavior of the excavation will be controlled by the soft to medium clay marine deposits stratum due to its significant thickness, more of the 15% of the total depth of the excavation (about 3.0 m below ground level) are in soils that will present a completely

different behavior from the used soils in the numerical models, nevertheless the soil profile present similar conditions to those assumed in the parametric analysis. C). It should be noted that the depth of the excavation is considerably deeper than the assumed in the models, it's about the double the maximum depth modeled, nevertheless the soil profile present similar conditions to those assumed in the parametric analysis and the excavation method adopted in the case under study is in good agreement with the excavation process assumed in the performed parametric analysis, then it could be assumed that the case history under study is an excavation of similar characteristics from the numerical models performed.

Table A-7 shows the resume of the input parameters obtain from the data analysis of the case history necessary in the implementation of the method, additionally present the results of all the essential parameters in order to obtain the method predictions and the results obtained from geotechnical instrumentation.

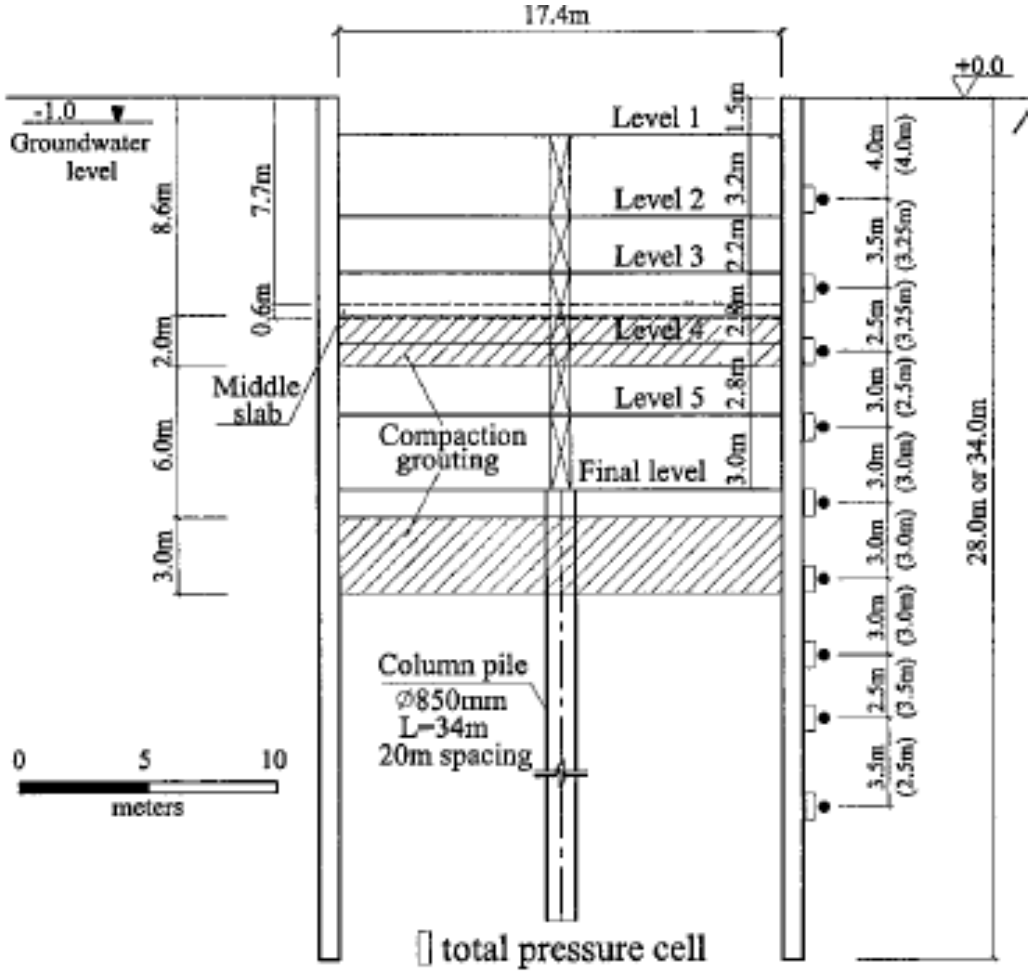

Figure A-7 Characteristics of the excavation support system, excavation levels and the stratified soil profile for the Yishan Road Station, Shanghai (Liu et al., 2005)

Table A-7. Resume of input data and results for the proposed method at the YRS case

Input Data		Parameter Estimated		Output Data		Measured Data	
He [m]	15.5	ER/k	$2.99x10^3$	Ue bottom [kPa]	46.5	Ue bottom [kPa]	49.0
B [m]	17.4						
γ_s [kN/m3]	15.0	α_{bottom}	0.20				
k [m/d]	$8.64x10^{-4}$						
ER [m/d]	2.58	σ_v[kPa]	232.5	% $\delta v_{(max)}$./He	0.06	% $\delta v_{(max)}$./He	0.07
Wall Type	TPW						

A.8 HDR-4 Subway Project, Chicago (Finno et al., 1991) – Case 8

The site of the HDR-4 Subway Station (HDR-4) is located in Chicago, Illinois, the station (the underground structure) has an overall average excavation depth of 12.2 m and with 12.2 m of width. Is important to mention that the method of excavation implemented was ¨semi – bottom - up¨ (i.e. removal of soil followed by the installation of pre-stressed struts) The groundwater table was encountered about 4.0 m below the existing ground surface, the subsurface profile is composed by a rubble fill overlaying a sequence of glacial clayey tills, in descending order they are Blodgett till (Soft clay), and Deerfield Till (medium to stiff clay) beneath a thin dense granular deposit overlaying the Niagaran limestone, the excavation was made thorough the fill, the soft and medium to stiff clay tills. The excavation retaining system was composed by 19.2 m depth sheet pile wall supported by four levels of bracing. A very extensive and detail field monitoring program was implemented composed by inclinometers casts within the retaining wall and behind the wall, settlement surface markers, earth and vibrating wire piezometers. **Figure A-8** shows, the support system, the location of some of the monitoring instruments installed and the stratified soil profile.

The most important differences presented in the presented case history, regarding the conditions under which the numerical models were executed can be summarized as A). Although the behavior of the excavation will be controlled by the soft to medium clay marine deposits stratum due to its significant thickness, more of the 40% of the total depth of the excavation (about 5.0 m below ground level) are in soils that will present a completely different behavior from the used soils in the numerical models, nevertheless the soil profile present similar conditions to those assumed in the parametric analysis. B). It should be noted that the depth of the excavation is considerably deeper than the assumed in the models, it's about 50% deeper than the maximum depth modeled, nevertheless the soil profile present similar conditions to those assumed in the parametric analysis and the excavation method adopted in the case under study is in good agreement with the excavation

process assumed in the performed parametric analysis, then it could be assumed that the case history under study is an excavation of similar characteristics from the numerical models performed. It is worth to mention that there are no data available of excess pore water pressures at bottom of the excavation because piezometers were not installed at these locations. So no predictions were made for these variable.

Table A-8 shows the resume of the input parameters obtain from the data analysis of the case history necessary in the implementation of the method, additionally present the results of all the essential parameters in order to obtain the method predictions and the results obtained from geotechnical instrumentation.

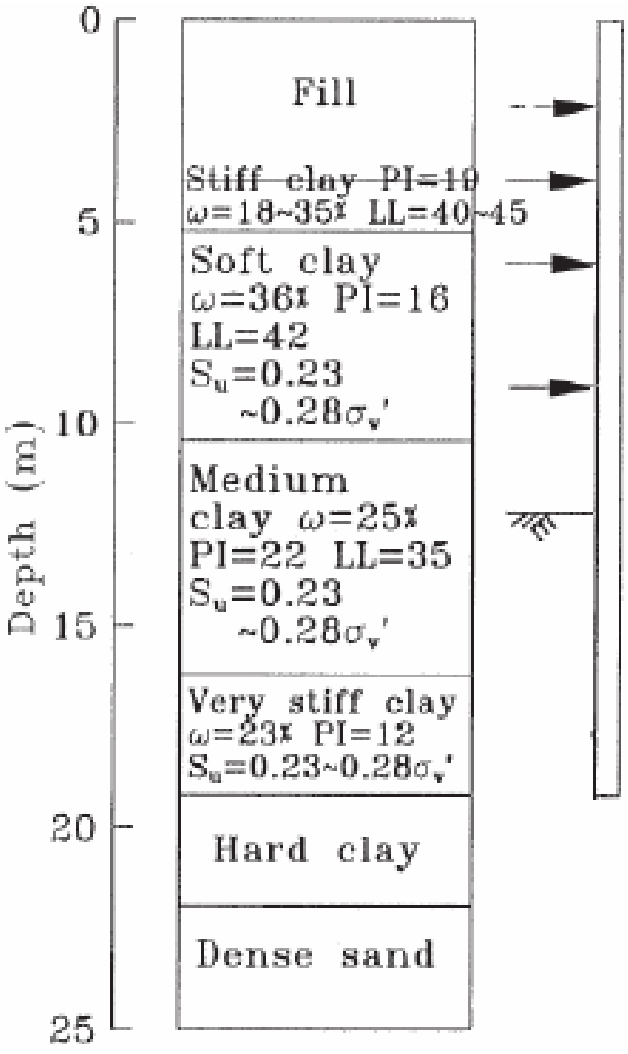

Figure A-8 Characteristics of the excavation support system, excavation levels and the stratified soil profile for the HDR-4 Subway Station, Chicago (Finno et al., 1989)

Table A-8. Resume of input data and results for the proposed method at the HDR-4 case

Input Data		Parameter Estimated		Output Data		Measured Data	
He [m]	12.2	ER/k	$4.5x10^4$	Ue behind [kPa]	27.81	Ue behind [kPa]	24
B [m]	12.2						
γ_s [kN/m3]	19.0	α_{behind}	0.12				
k [m/d]	$1.0x10^{-5}$						
ER [m/d]	0.37	σ_v[kPa]	231.8	% $\delta v_{(max)}$./He	0.14	% $\delta v_{(max)}$./He	2.1
Wall Type	SPW						

A.9 Central Artery Tunnel Project, Boston (Whelan, 1995) – Case 9a and 9b

The site of the Central Artery Tunnel Project (CATP) is located in Boston, Massachusetts at South of the Downtown and is part for a depressed roadway project, the excavation studied has an overall, excavation depth of 12.3 m and 11.1 m at North and South side respectively, and 61.0 m in width. The subsurface stratigraphy was interpreted from an extensive in situ investigation program which included 62 borings, besides a detail laboratory test program, the groundwater table was encountered about 3.0 m below the existing ground surface, the average soil profile consist of 31.4 m of superficial deposits founded on glacial deposits and bedrock, the subsurface profile is composed by 4 major layers: 2.6 m of granular fill, above 4.6 m of cohesive fill and 4.6 m of organic deposit overlaying the main deposit of Boston Blue clay which overlays the lower glacial till at depth of 31.5 m. The excavation retaining system was divided in two different sections, the North side near by an existing building is composed by 0.9 m thick diaphragm wall of and 31.2 m deep with three tiers of tiebacks grouted in the underlying glacial till and bedrock, the remainder of the excavation (i.e. South side), also supported by three levels of tiebacks grouted in the clay crust of the Boston Blue Clay stratum, but, using sheet pile walls extending 16.8 m below the ground surface, the excavation process consisted in the removal of the soil, followed by the installation and lock-off of the tiebacks, continued until reached final excavation level. A very extensive and detail field monitoring program was implemented at both sides, composed by inclinometers located near the two supported walls, surface settlements are measured at nine monitoring points, heave measurements were reported at 4 locations using multi point heave gauges, pore pressures are measured at 15 locations including two observation wells, one open stand pipe and 12 vibration wire piezometers, inside the excavation and behind the wall, besides the inclinometers, the remaining instruments were installed before any construction activities. **Figure A-9** and **Figure A-10** shows,

the support system, the location of some of the monitoring instruments installed and the stratified soil profile.

The most important differences presented in the presented case history, regarding the conditions under which the numerical models were executed can be summarized as: A). Although the behavior of the excavation will be controlled by the stratum BBC due to its significant thickness, more of the 50% of the total depth of the excavation (about 6.0 m below ground level) are in soils that will present a completely different behavior from the used soils in the numerical models. B) The excavation retaining system is expected to have a greater stiffness than the modeled ones due to the implementation of three rows of tiebacks at both sides. C). It should be noted that the depth of the excavation is greater than assumed in the models, it's about 50% deeper than the maximum depth modeled, however the difference is not of excessive magnitude, then it could be assumed that the case history under study is an excavation of similar characteristics from the numerical models performed.

Table A-9 and **Table A-10** shows the resume of the input parameters obtain from the data analysis of the case history necessary for both sides (i.e. North and South) in the implementation of the method, additionally present the results of all the essential parameters in order to obtain the method predictions and the results obtained from geotechnical instrumentation.

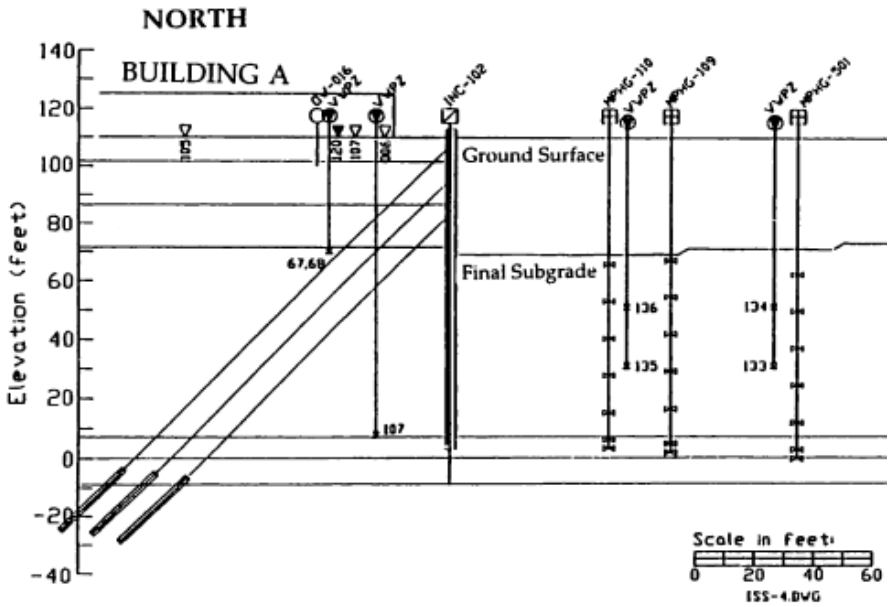

Figure A-9 Characteristics of the excavation support system, excavation levels and the stratified soil profile for the Central Artery Tunnel Project North Side, Boston (Whelan, 1995)

Table A-9. Resume of input data and results for the proposed method at the North side of the CATP case

Input Data		Parameter Estimated		Output Data		Measured Data	
He [m]	12.3	ER/k	$4.94x10^2$	Ue bottom[kPa]	85.8	Ue bottom[kPa]	93.1
B [m]	61.0						
γ_s [kN/m3]	17.4	α_{bottom}	0.4	Ue behind [kPa]	8.6	Ue behind [kPa]	9.8
k [m/d]	$2.0x10^{-3}$	α_{behind}	0.04				
ER [m/d]	1.19	σ_v[kPa]	214.5	% $\delta v_{(max)}$./He	0.05	% $\delta v_{(max)}$./He	1.14
Wall Type	TPW						

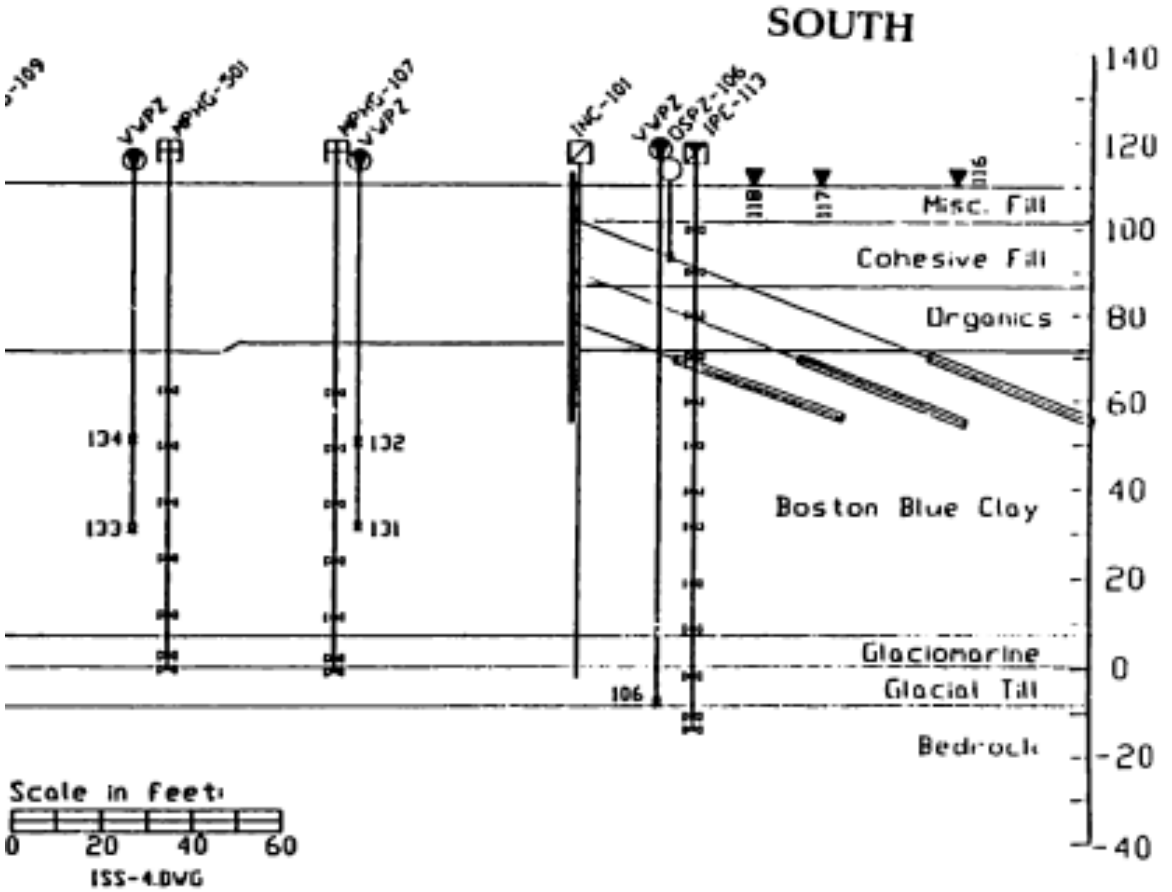

Figure A-10 Characteristics of the excavation support system, excavation levels and the stratified soil profile for the HDR-4 Subway Station, Chicago (Finno et al., 1989)

Table A-10. Resume of input data and results for the proposed method at the South side of the CATP case

Input Data		Parameter Estimated		Output Data		Measured Data	
He [m]	11.1	ER/k	$3.59x10^2$	Ue bottom[kPa]	70.3	Ue bottom[kPa]	78.4
B [m]	61.0						
γ_s [kN/m3]	17.6	α_{bottom}	0.36	Ue behind [kPa]	7.81	Ue behind [kPa]	14.7
k [m/d]	$2.0x10^{-3}$	α_{behind}	0.04				
ER [m/d]	0.87	σ_v[kPa]	195.18	% $\delta v_{(max)}$./He	0.14	% $\delta v_{(max)}$./He	0.90
Wall Type	SPW						

A.10 Geotechnical centrifuge model, Cambridge (Lam et al., 2014) – Case 10

A small scale centrifuge model was made intended to simulate a prototype behavior of an excavation in soft soil, a centrifugal acceleration field of 60g was used to match the stressed induced by gravity, and the parameters of the model were adopted to simulate a floating rigid wall internally braced with stiffs props, the model subsurface stratigraphy consists of a layer of lightly over consolidated kaolin clay above a base layer of dense sand, the ground water table was simulated at the ground surface by permitting overflow from a stand pipe, the excavation retaining system was modeled by a 6 mm thick aluminum, these wall simulate a 0.9m diaphragm wall in the field, the excavation process was modeled by installing the wall at a depth of 160 mm (9.6 m at the prototype scale), then trimmed the clay to a height cut for installation of the prop system (3 rows of props) of the retaining wall until reached the final excavation level 90 mm (5.2 m at the prototype scale), the width of the excavation modeled was 120 mm (7.2 m at the prototype scale), the geotechnical monitoring system was composed by LVDTs that were placed to measure the settlements behind the retaining wall, a laser sensor was used to monitor the lateral displacement and 9 pore pressure gauges were installed at different locations in order to evaluate the developed an dissipation of the water pore pressure. **Figure A-11** shows a schematic diagram of the experimental set up and the positions of the instruments.

The most important differences presented in the presented case history, regarding the conditions under which the numerical models were executed can be summarized as: A). The cases history under study is a small scale centrifuge model and the results obtain must be treated with special care, because the magnitude of the results (small variation ranges) are very susceptible to the sensitive of the instruments used. B) The excavation retaining system is a floating rigid wall (i.e. doesn't have a fixed wall toe condition), however the excavation method adopted in the case under study is in

good agreement with the excavation process assumed in the performed parametric analysis, then it could be assumed that the case history under study is an excavation of similar characteristics from the numerical models performed

Table A-11 shows the resume of the input parameters obtain from the data analysis of the case history necessary in the implementation of the method, additionally present the results of all the essential parameters in order to obtain the method predictions and the results obtained from geotechnical instrumentation.

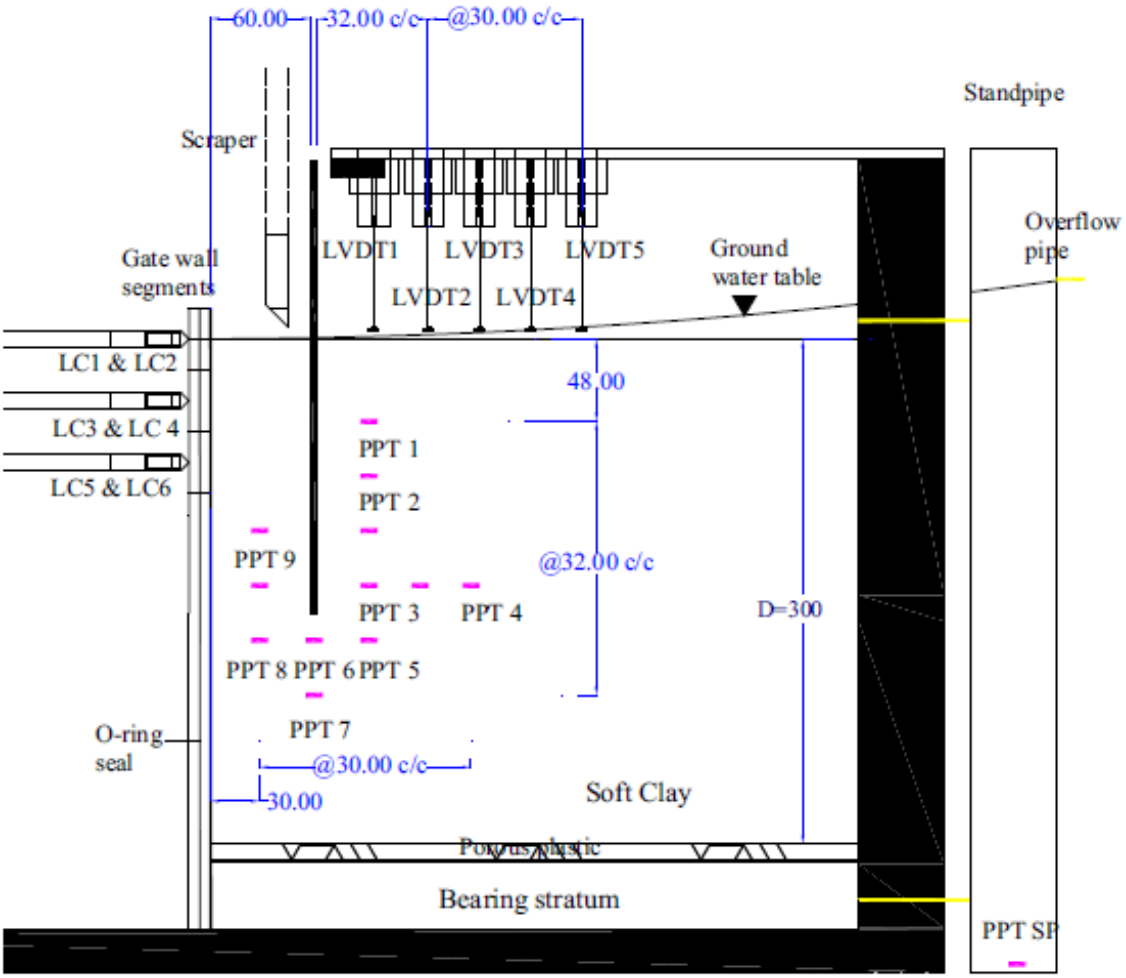

Figure A-11 Characteristics of the excavation support system, excavation levels and the stratified soil profile for the centrifuge model, Cambridge (Lam et al., 2014)

Table A-11. Resume of input data and results for the proposed method at the South side of the centrifuge model in Cambridge

Input Data		Parameter Estimated		Output Data		Measured Data	
He [m]	5.40	ER/k	$1.21x10^4$	Ue bottom[kPa]	32.0	Ue bottom[kPa]	40.0
B [m]	7.20						
γ_s [kN/m3]	16.5	α_{bottom}	0.36	Ue behind [kPa]	10.68	Ue behind [kPa]	10.0
k [m/d]	$1.0x10^{-5}$	α_{behind}	0.12				
ER [m/d]	0.12	σ_v[kPa]	89.0	% $\delta v_{(max)}$./He	0.07	% $\delta v_{(max)}$./He	0.56
Wall Type	TPW						

A.11 Geotechnical centrifuge model, Tokyo (Takemura et al., 1999) – Case 11

A small scale centrifuge model was made intended to simulate a prototype behavior of an excavation in soft soil, a centrifugal acceleration field of 50g was used to match the stressed induced by gravity, and the parameters of the model were adopted to simulate a fixed base flexible wall internally braced with stiffs props, the model subsurface stratigraphy consists of 3 major layers: top and bottom Toyoura sands and normally consolidated Kaolin clay in between the two sand layers, the ground water table was simulated at the ground surface by permitting overflow from a stand pipe, the excavation retaining system was modeled by a 3 mm thick aluminum, these wall simulate sheet pile wall with a flexural rigidity of 20 MPa×m4/m in the field, the excavation process was modeled by installing the wall at a depth of 195 mm (9.75 m at the prototype scale), then trimmed the clay to a height cut for installation of the prop system (2 rows of props) of the retaining wall until reached the final excavation level 100 mm (5.0 m at the prototype scale), the width of the excavation modeled was 280 mm (14.0 m at the prototype scale), the geotechnical monitoring system was composed by 8 LVDTs that were placed to measure the settlements behind the retaining wall, 2 laser displacement transducer were used to monitor the lateral displacement, the sheet pile wall was instrumented with 12 strain gauges and 4 earth pressure cells at each side of the wall and 5 pore pressure transducers were installed at different locations in order to evaluate the developed an dissipation of the water pore pressure. **Figure A-12** shows a schematic diagram of the experimental set up and the positions of the instruments.

The most important differences presented in the presented case history, regarding the conditions under which the numerical models were executed can be summarized as: A). The cases history under study is a small scale centrifuge model and the results obtain must be treated with special care,

because the magnitude of the results (small variation ranges) are very susceptible to the sensitive of the instruments used. B) Although the behavior of the excavation will be controlled by the stratum Kaolin clay due to its significant thickness, more of the 25% of the total depth of the excavation (about 1.25 m below ground level) are in soils that will present a completely different behavior from the used soils in the numerical models, however the excavation method adopted in the case under study is in good agreement with the excavation process assumed in the performed parametric analysis, then it could be assumed that the case history under study is an excavation of similar characteristics from the numerical models performed.

Table A-12 shows the resume of the input parameters obtain from the data analysis of the case history necessary in the implementation of the method, additionally present the results of all the essential parameters in order to obtain the method predictions and the results obtained from geotechnical instrumentation.

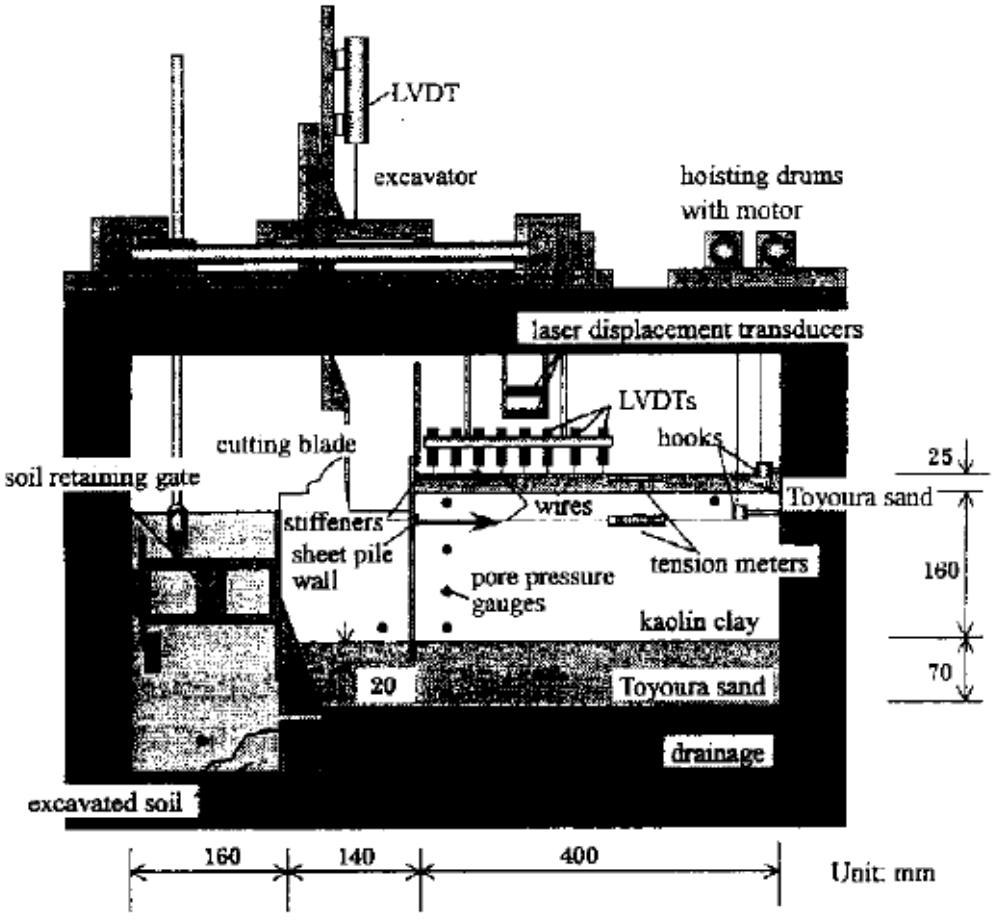

Figure A-12 Characteristics of the excavation support system, excavation levels and the stratified soil profile for the centrifuge model, Tokyo (Takemura et al., 1999)

Table A-12. Resume of input data and results for the proposed method at the South side of the centrifuge model in Tokyo.

Input Data		**Parameter Estimated**		**Output Data**		**Measured Data**	
He [m]	5.0	ER/k	9.65×10^{2}	Ue bottom[kPa]	28.9	Ue bottom[kPa]	37.0
B [m]	14.0						
γ_s [kN/m3]	17.0	α_{bottom}	0.34	Ue behind [kPa]	5.1	Ue behind [kPa]	10.0
k [m/d]	1.73×10^{-4}	α_{behind}	0.06				
ER [m/d]	0.17	σ_v[kPa]	85.0	% $\delta v_{(max)}$./He	0.14	% $\delta v_{(max)}$./He	3.0
Wall Type	SPW						

APPENDIX B

A statistic analysis is presented to evaluate the uncertainty of the method proposed, the statistical treatment was implemented only for the predictions of the excess pore water pressure parameter, for the ground surface settlements predictions, the uncertainty is not necessary to evaluate due to as see in the method clearly underestimated the results of the measurements made in the field.

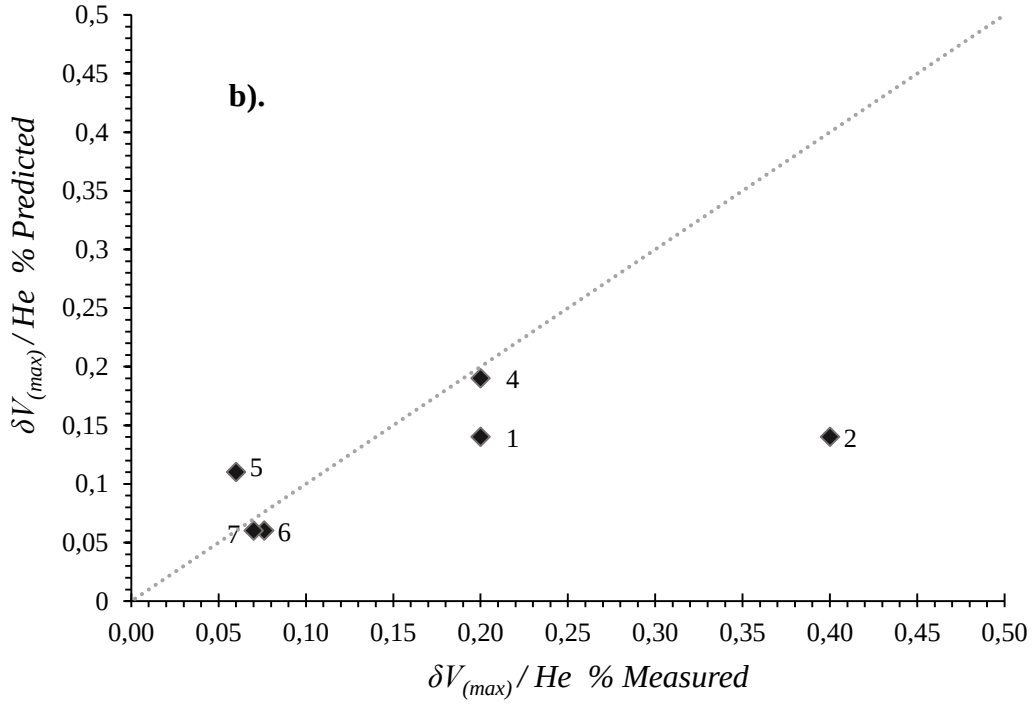

Figure 5-2 Performance of the proposed method for the maximum ground surface settlements prediction a). All case histories. b). Similar conditions cases histories

The statistical analysis of the performance for the proposed method was performed through graphical and analytical methods according to Montgomery et al. (2006), the verification of the adequacy of the model was made through the analysis of standardized residuals, where normal distribution was verified by means of the Shapiro-Wilk test, homogeneity of variance and T-student test.

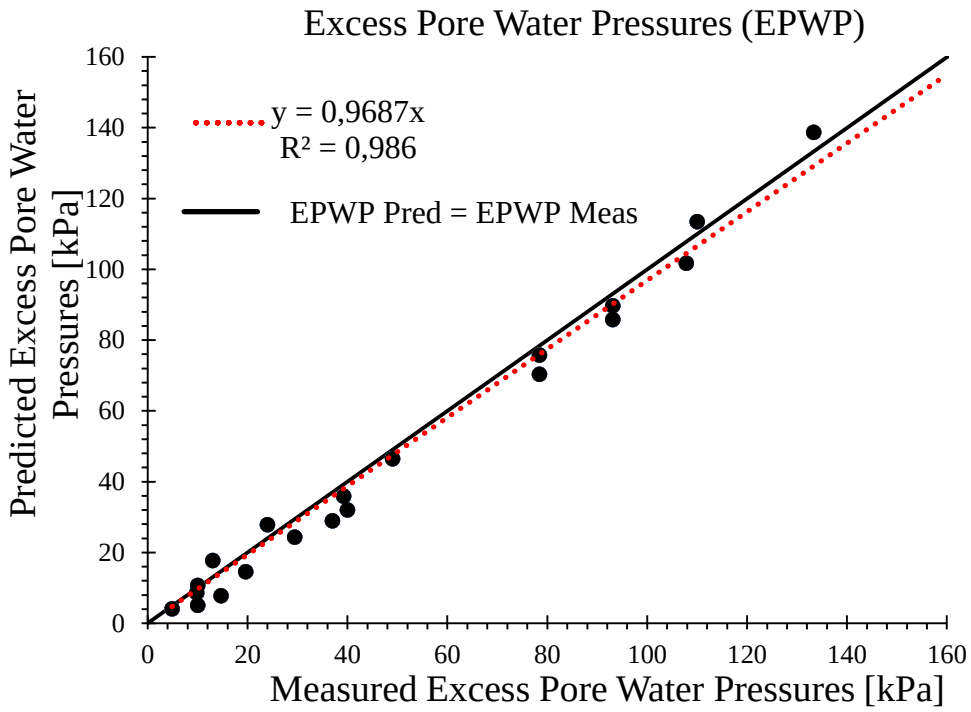

Figure B-1 Linear fit between the observed and predicted Excess pore water pressures

Figure B-1 shows the linear relationship between the observed and predicted excess pore water pressures for both locations (i.e. below the excavation bottom and behind the retaining wall) and for all the cases considered for the statistical analysis. As mention before it can be seen that the adjustment has a very close approximation to the line 1:1, where $EPWP_{Predited}$ = $EPWP_{Measured}$, because of this, the significance test was performed considering the regression by the origin, line 1: 1, and it was executed by means of the F test, according to Eq. (39), assuming the null hypothesis, Ho, with slope of the line equal to zero, Ho:$\hat{\beta}_1 = 0$. Additionally, the P value is calculated by taking as a reference a level of significance, α = 0.05, to corroborate or reject the hypothesis Ho.

$$F_o = \frac{MS_R}{MS_{Res}} \tag{39}$$

$$MS_R = \hat{\beta}_1 \sum_{i=1}^{n} y_i x_i \tag{40}$$

$$MS_{Res} = \frac{\sum_{i=1}^{n} (y_i - \hat{y}_i)^2}{n-1} \tag{41}$$

Where MS_R in the source of variation from the regression, MS_{Res} is the residual mean squared, $\hat{\beta}_1$ is the slope of the curve, $\hat{\beta}_1 = 1$, y_i and x_i are the predicted and measured values of excess pore water pressures respectively, $\hat{y}_i$ is the adjusted value and n is the number of data considered in the

statistical analysis. As a result, the calculated P value is equal to $3.91x10^{-22}$, and since is minor than the assuming level of significance, $\alpha = 0.05$, Ho is rejected, meaning, $\hat{\beta}_1 \neq 0$ and the model assume $\hat{y} = x$ is significant.

B.1 Homoscedasticity and test for normality

The variance of homogeneity or homoscedasticity was calculated through the analysis of residuals, also the normal distribution of the residuals was verified. Residuals were calculated as $e_i = y_i - \hat{y}_i$ and normalized residuals, as $d_i = {e_i}/{\sqrt{MS_{Res}}}$. **Figure B-2** shows the normalized residuals as a function of the adjusted values $\hat{y} = x$, which represent the measured excess pore water pressures. Also can be observed that the residuals tend to a horizontal band, and that there are no outliers (i.e. no value d_i>3).

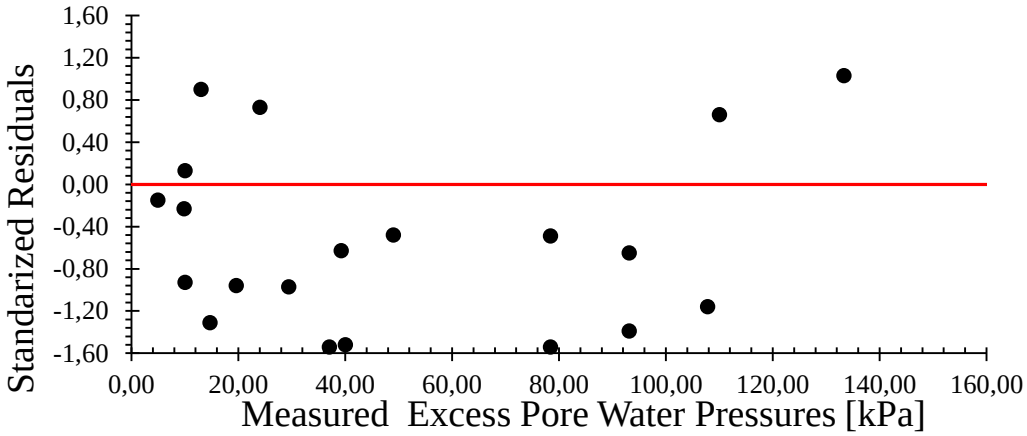

Figure B-2 Standardized Residuals according to the adjusted values, $\hat{y} = x$

Once the homoscedasticity is verified by means of the standardized residuals, the normal distribution is verified graphically and by means of the Shapiro-Wilk test, where Ho states that the standardized residuals come from a normal distribution. **Figure B-3** shows the normal probability graphs and the results for the Shapiro-Wilk test. It can be seen that the standardized residuals are adjusted to the theoretical line and are within the confidence bands, in addition the calculated P value of the Shapiro-Wilks test is 0.074, higher than the level of significance, assumed as, $\alpha = 0.05$. Therefore the Ho is accepted and it is concluded that the data through which the residuals are obtained come from a normal distribution. Verified the significance of the regression $\hat{y} = x$, the homogenity and normality

of the results, it can be establish that the model presents a good fit between the observed and predicted deformations

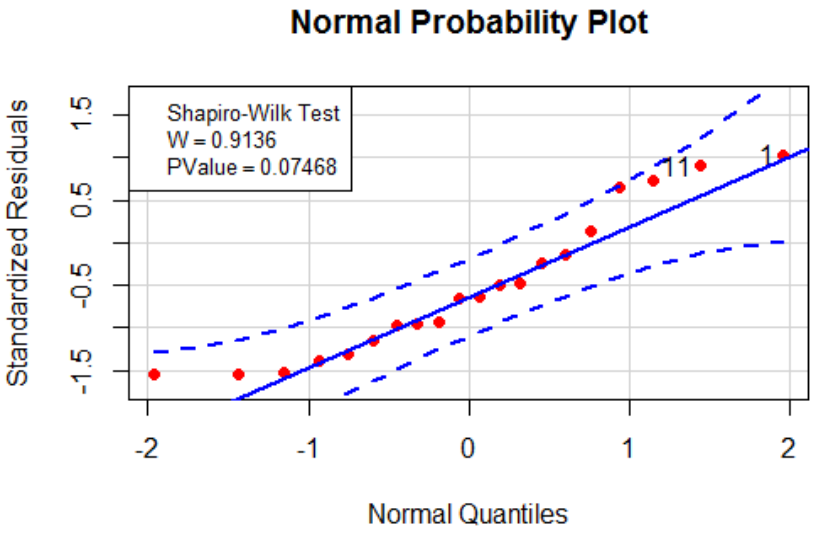

Figure B-3 Normal probability graph and Shapiro-Wilk test results

B.2 Confidence interval

A confidence interval (CI) is usually interpreted as the range of values that encompass the 'true' value, estimated by a certain statistic, with a given probability, according to equation (42), the confidence interval is calculated for 95% of β_1 slope, considering $\hat{\beta}_1$=1. **Table B-1** shows the results of the 95% confidence interval. A ratio of $EPWP_{Pred}/EPWP_{Meas}$ between 0.96 and 1.04 can be expected for future validations with a sample size at least equal of 20 data.

$$\hat{\beta}_1 - t_{\frac{\alpha}{2},n-1}\sqrt{\frac{MS_{Res}}{\sum_{i=1}^{n} x_i^2}} \leq \beta_1 \leq \hat{\beta}_1 + t_{\frac{\alpha}{2},n-1}\sqrt{\frac{MS_{Res}}{\sum_{i=1}^{n} x_i^2}} \quad (42)$$

Where, $t_{\frac{\alpha}{2},n-1}$ is the T-student distribution for α/2 and n-1.

Table B-1. Values for Confidence Interval of 95%

Parameter	**2.5%**	$\boldsymbol{\beta_1}$:	**97.5%**
EPWP	0.96	$\leq \frac{Pred}{Meas} \leq$	1.04

The prediction interval of 95% for a future observation is calculated by means of Eq. (43). Considering the linear regression at the origin $\hat{y} = x$. **Figure B-4** presents the results of the

prediction intervals, the points in black are the data considered in the statistical analysis, and it is observed that all the data obtained are within the 95% confidence bands of prediction.

$$\hat{y}_o - t_{\frac{\alpha}{2},n-1}\sqrt{MS_{Res}\left(1+\frac{{x_o}^2}{\sum_{i=1}^{n}{x_i}^2}\right)} \leq y_o \leq \hat{y}_o + t_{\frac{\alpha}{2},n-1}\sqrt{MS_{Res}\left(1+\frac{{x_o}^2}{\sum_{i=1}^{n}{x_i}^2}\right)} \quad (43)$$

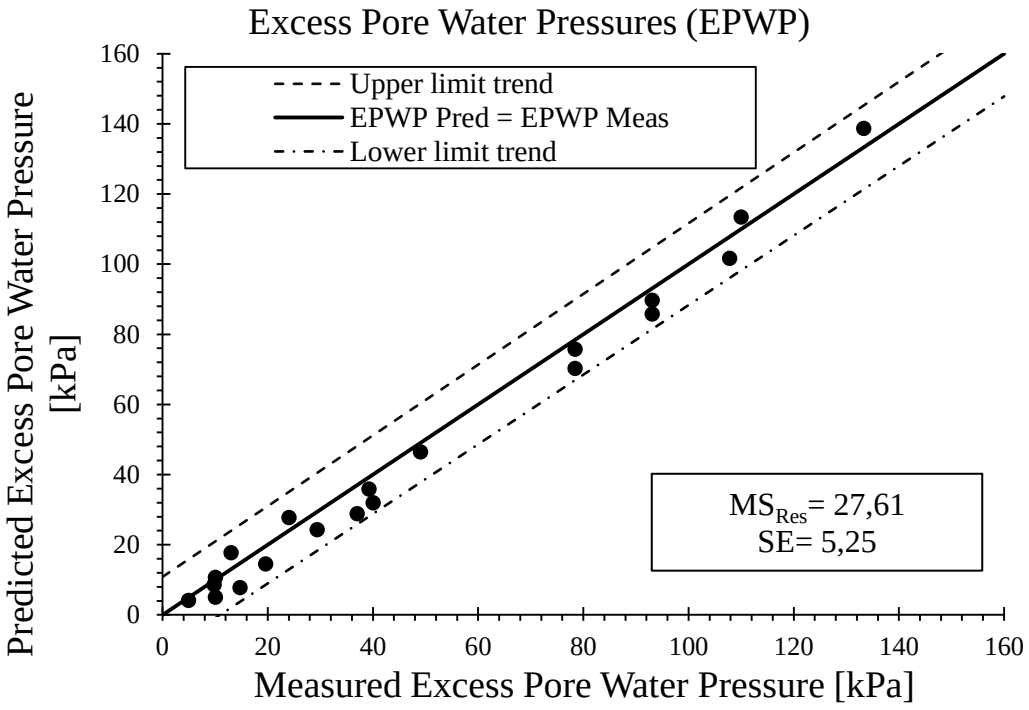

Figure B-4 prediction confidence bands of 95% level of confidence

In addition to all the previous verifications, the coefficient of determination R^2 and coefficient of variation CV are calculated. The statisticR^2, was determined as the square of the Pearson correlation coefficient, by equation (44). Also the multiple R-squared,${R_o}^2$ by the equation. (45).

$$R^2 = \frac{{\sigma^2}_{xy}}{{\sigma^2}_x{\sigma^2}_y} \quad (44)$$

$${R_o}^2 = \frac{\sum {\delta_{Predicted}}^2}{\sum {\delta_{observed}}^2} \quad (45)$$

Where σ_{xy} is the covariance of (x,y), ${\sigma^2}_x$ and ${\sigma^2}_y$ are the variance of the measured and predicted excess pore water pressures respectively. Similar to Kung et al. (2007), the uncertainty of the model

is estimated by means of the Bias Factor, $BF = EPWP_{Pred}/EPWP_{Meas}$ the closer the BF to 1, the more accurate the model will be. **Table B-2** shows the BF results for all the data considered in the validation and statistical analysis, as well as the average, the standard deviation, and the coefficient of variation.

Table B-2. Uncertainty of the model expressed by the Bias factor "BF"

E.P.W.P [kPa]		BIAS FACTOR
Measured	**Predicted**	
133.3	138.7	0.96
110	113.47	0.97
78.4	75.8	1.03
93.1	89.7	1.04
107.8	101.7	1.06
49	46.5	1.05
93.1	85.8	1.09
78.4	70.3	1.12
40	32	1.25
37	28.9	1.28
13	17.73	0.73
19.6	14.58	1.34
4.9	4.11	1.19
29.4	24.3	1.21
39.2	35.88	1.09
24	27.81	0.86
9.8	8.6	1.14
14.7	7.81	1.88
10	10.68	0.94
10	5.1	1.96
	Average	1.16
	Standard Deviation	0.30
	CV %	25.7

From the validation of the model for the excess pore water pressures prediction, R^2= 0.988, ${R_o}^2 =$ 0.944 and CV_{BF} == 25.7% were obtained. Obtaining very good coefficients of determination for the model, which is reflected in the adjustment of the results with the continuous black curve from **Figure 5-1** , which represents $EPWP_{Pred}/EPWP_{Meas}$ (1: 1)., as for the BF, the values are close to 1 and the CV_{BF} calculated is less than 30% that represent a moderate variability in the Bias coefficient.

7.-REFERENCES

Arboleda-Monsalve, L. G. (2014a). "Performance, Instrumentation and Numerical Simulation of One Museum Park West Excavation." *Ph.d Thesis*, Northwestern University.

Bae, S., and Martinez, A. F. (2016). *Fully Coupled vs Consolidation Analysis Project Overview (Fully Coupled vs Consolidation Analysis)*.

Biot, M. A. (1941). "General Theory Of Three-Dimensional Consolidation." *Journal of Applied Pysics*, 12(2), 155–164.

Borges, J. L., and Guerra, G. T. (2014). "Cylindrical excavations in clayey soils retained by jet grout walls: Numerical analysis and parametric study considering the influence of consolidation." *Computers and Geotechnics*, 55, 42–56.

Brinkgreve, R. B. J., Swolfs, W. M., and Engin, E. (2011). "Reference Manual Plaxis." *Plaxis*.

Callisto, L., Maltese, F., and Bertoldo, F. (2014). "Design of deep excavations in fine-grained soils accounting for changes in pore water pressures." *Geotechnical Aspects of Underground Construction in Soft Ground*, 161–166.

Chen, J. J., Lei, H., and Wang, J. H. (2013). "Numerical analysis of the installation effect of diaphragm walls in saturated soft clay." *Acta Geotechnica*, 9(6), 981–991.

"Engineering Performance of a Deep Excavation of Taipei National Enterprise Centre." (1997). *Research Report GT 96008*, National Taiwan Universityof Science and Technology.

Finno, B. R. J., and Chung, C. (1993). "Stress-strain-strength responses of compressible chicago glacial clays." 118(10), 1607–1625.

Finno, R. J., Harahap, I. S., and Sabatini, P. J. (1991). "Analysis of braced excavations with coupled finite element formulations." *Computers and Geotechnics*, 12(2), 91–114.

Galavi, V. (2010). *Groundwater flow, fully coupled flow deformation and undrained analyses in PLAXIS 2D and 3D*. *Plaxis Internal Report*.

Herle, I., and Kolymbas, D. (2004). "Hypoplasticity for soils with low friction angles." *Computers and Geotechnics*, 31(5), 365–373.

Holt, D. A., and Griffiths, D. V. (1992). "Transient analysis of excavations in soil." *Computers and Geotechnics*, 13(3), 159–174.

Hsie, J. P., and Small, J. C. (1992). "Simulation of excavation in a poro-elastic material." *International Journal for Numerical and Analytical Methods in Geomechanics*, 16(1), 25–43.

Hsie, J. P., and Small, J. C. (1993). "Application Of a Fully Coupled Method To The Analyisis Of An Excavation." *Soils and Foundations*, 33(4), 36–48.

Hsieh, P. G., and Ou, C. Y. (1998). "Shape of ground surface settlement profiles caused by excavation." *Canadian Geotechnical Journal*, 35(6), 1004–1017.

Hsiung, B. C. (2002). "Engineering Performance of Deep Excavations in Taipei." *Ph.d Thesis*, University of Bristol.

Jaworsk, W. E. (1973). "An evaluation of the performance of a braced excavation." *Sc.D Thesis*, Massachusets Institute of Technology.

Jen, L. C. (1998). "The Design and Performance of Deep Excavations in Clay." *Ph.d Thesis*, Massachusetts Institute of Technology.

Kim, T., and Finno, R. J. (2012). "Anisotropy Evolution and Irrecoverable Deformation in Triaxial Stress Probes." *Journal of Geotechnical and Geoenvironmental Engineering*, 138(2), 155–165.

Kolymbas, D., Wu, W., and Bauer, E. (1996). "Hypoplastic constitutive model with critical state for granular materials." *Mechanics of Materials*, 23(1), 45–69.

Kung, G. T., Juang, C. H., Hsiao, E. C., and Hashash, Y. M. (2007). "Simplified Model for Wall Deflection and Ground-Surface Settlement Caused by Braced Excavation in Clays." *Journal of Geotechnical and Geoenvironmental Engineering*, 133(6), 731–747.

Lam, S. Y., Haigh, S. K., and Bolton, M. D. (2014). "Understanding ground deformation mechanisms for multi-propped excavation in soft clay." *Soils and Foundations*, Elsevier, 54(3), 296–312.

Liu, G. B., Ng, C. W. W., and Wang, Z. W. (2005a). "Observed Performance of a Deep Multistrutted Excavation in Shanghai Soft Clays." *Journal of Geotechnical and Geoenvironmental Engineering*, 131(8), 1004–1013.

Liu, G. B., Ng, C. W., and Wang, Z. W. (2005b). "Observed Performance of a Deep Multistrutted Excavation in Shanghai Soft Clays." *Journal of Geotechnical and Geoenvironmental Engineering*, 131(8), 1004–1013.

Mašín, D. (2005). "A hypoplastic constitutive model for clays." *International Journal for Numerical and Analytical Methods in Geomechanics*, 29(4), 311–336.

Mašín, D. (2012). "Clay hypoplasticity with explicitly defined asymptotic states." *Acta Geotechnica*, 8(5), 481–496.

Mašín, D. (2014). "Clay hypoplasticity model including stiffness anisotropy."

Mašín, D. (2015). "Hypoplasticity for Practical Applications." (June), 1–26.

Montgomery, D. C., Peck, E. A., and Geoffrey, V. (2006). *Introduccion al Analisis de Regresion Lineal*. CONTINENTAL, Mexico.

Moorman, C. (2004). "ANALYSIS OF WALL AND GROUND MOVEMENTS DUE TO DEEP EXCAVATIONS IN SOFT SOIL BASED ON A NEW WORLWIDEDATABASE." *Soils and Foundations*, 44(1), 87–98.

Ng, C. W. W. (1992). "An Evaluation of Soil-structure Interaction Associated with a Multi-propped Excavation." *Ph.d Thesis*, University of Bristol, UK.

Niemunis, A. (2002). “Extended hypoplastic models.” (January), 191.

Niemunis, A. (2003). “Anisotropic effects in hypoplasticity.” *Deformation Characteristics of Geomaterials*.

Niemunis, A., and Herle, I. (1997). “Hypoplastic model for cohesionless soils with elastic strain range.” *Mechanics of Cohesive-Frictional Materials*, 2(4), 279–299.

Niemunis, A., and Krieg, S. (1996). “Viscous behaviour of soils under oedometric conditions.” *Canadian Geotechnical Journal*, 33, 159–168.

Nogueira, C. de L., Azevedo, R. F., and Zornberg, J. G. (2009). “Coupled Analyses of Excavations in Saturated Soil.” *International Journal of Geomechanics*, 9(2), 73–81.

Osaimi, E., and Clough, W. (1979). “Pore-Pressure Dissipation During Excavation.” *journal of geotechnical engineering*, 105, 481–498.

Rouainia, M., Elia, G., Panayides, S., and Scott, P. (2017). “Nonlinear Finite-Element Prediction of the Performance of a Deep Excavation in Boston Blue Clay.” *Journal of Geotechnical and Geoenvironmental Engineering*, 143(5), 1–12.

Sarabia, F. (2012). “Hypoplastic constitutive law adapted to simulate excavations in Chicago glacial clays.” Northwestern University.

Takemura, J., Kondoh, M., Esaki, T., Kouda, M., and Kusakabe, O. (1999). “Centrifuge model tests on double propped wall excavation in soft clay.” *Soils and Foundations*, 39(3), 75–87.

United Nations. (2007). “World Urbanization Prospects The 2007 Revision Highlights.” *Desa*, ESA/P/WP/2(4), 883.

Wang, J. H., Xu, Z. H., and Wang, W. D. (2009). “Wall and Ground Movements due to Deep Excavations in Shanghai Soft Soils.” *Journal of Geotechnical and Geoenvironmental Engineering*, 136(7), 985–994.

Whelan, M. P. (1995). “Performance of Deep Excavations in Boston.” *M.S Thesis*, Massachusets Institute of Technology.

Whittle, A. j, Hashash, Y., and Whitman, R. (1993). “Analysis Of Deep Excavation In Boston.” *journal of geotechnical engineering*, 119(1), 69–90.

Wolffersdorff, P. A. (1996). “Hypoplastic relation for granular materials with a predefined limit state surface.” *Mechanics of Cohesive-Frictional Materials*, 1(3), 251–271.

Wroth, C. P. (1984). “The interpretation of in situ soil tests.” *Géotechnique*, 34(4), 449–489.

Yong, K., Lee, F., Parnploy, U., and Lee, S. (1989). “Elasto-Plastic Consolidation Analysis For Strutted Excavation In Clay.” *Computers and Geotechnics*, 8, 311–328.

Zapata-Medina, D. G. (2007). “Semi-empirical method for designing excavation support systems based on deformation control.” *Masters Thesis*, University of Kentucky.